This is to certify that the
dissertation entitled

SOLID STATE NUCLEAR MAGNETIC RESONANCE OF THE HIV-1 AND INFLUENZA FUSION PEPTIDES ASSOCIATED WITH MEMBRANES

presented by

Michele L Bodner

has been accepted towards fulfillment
of the requirements for the

Ph.D degree in Chemistry

David A. Weliky
Major Professor's Signature

4/25/06
Date

SOLID STATE NUCLEAR MAGNETIC RESONANCE OF THE HIV-1 AND INFLUENZA FUSION PEPTIDES ASSOCIATED WITH MEMBRANES

By

Michele L. Bodner

A DISSERTATION

Submitted to
Michigan State University
in partial fulfillment of the requirements
for the degree of

DOCTOR OF PHILOSOPHY

Department Of Chemistry

2006

ABSTRACT

SOLID STATE NUCLEAR MAGNETIC RESONANCE OF THE HIV-1 AND INFLUENZA FUSION PEPTIDES ASSOCIATED WITH MEMBRANES

By

Michele L. Bodner

The HIV-1 viral fusion peptide serves as a biologically relevant model for viral/target cell membrane fusion and in my work, the structure of the membrane-associated peptide was probed by solid state NMR MAS ^{13}C chemical shift measurements. Solution NMR studies have shown that the peptide is predominantly helical in detergent micelles and this was correlated with solid state NMR ^{13}C chemical shifts in frozen detergent. Large shift changes (2-4 ppm) were observed for the peptide in a mixture whose lipid headgroup and cholesterol composition reflects the membranes of host cells of the virus. In this more biologically relevant composition, the chemical shifts are consistent with predominant non-helical structure. NMR spectra were compared at –50 °C and at 20 °C. Similar peak chemical shifts were observed at both temperatures, which indicates that cooling the sample does not significantly change the peptide structure. Relative to -50 °C, the 20 °C signals were narrower and had lower intensity, which is consistent with greater motion at higher temperature. $^{13}C/^{13}C$ correlation experiments were performed on a sample in which the peptide was U-$^{13}C/^{15}N$ labeled over three or twelve sequential residues. The resulting 2D spectra were used to assign the ^{13}C chemical shifts in the labeled residues and the shifts were consistent with beta strand structure. $^{15}N/^{13}C$ 2D correlation experiments were also performed on the samples, and the resulting data allowed for an assignment of the ^{15}N chemical shifts. 2D $^{13}C/^{13}C$ and

$^{15}N/^{13}C$ correlation experiments were also carried out on an influenza fusion peptide, which allowed for a ^{15}N and ^{13}C chemical shift assignment.

In the previous samples, an increase in the number of uniformly labeled residues gave rise to ambiguity in the chemical shift assignment. Because of ^{13}C linewidths and the amino acid multiplicity, scatter-uniform rather than complete-uniform labeling is necessary for unambiguous chemical shift assignment of individual residues with 2D solid state NMR. The scatter-uniform labeling method only uniformly labels one residue of each amino acid type per sample. Using scatter-uniform labeling, five HFP samples associated with lipids were used to determine an unambiguous chemical shift assignment. Across the five samples, residues 1-16 and residue 21 were uniformly ^{13}C, ^{15}N labeled. 2D $^{13}C/^{13}C$ correlation experiments were used to determine the complete unambiguous chemical shift assignment over the labeled residues. The computer program TALOS was used to calculate the ϕ,ψ angles based on the inputted ^{13}C chemical shifts. Both the ^{13}C chemical shifts and ϕ,ψ angles were consistent with β-strand secondary structure.

To Tim, Sara, Jennifer, Jayda, Mom and Dale

Acknowledgements

I would like to thank my advisor, Dr. David Weliky, and the Weliky group for their help and support during my time here at MSU. I also want to thank my family and friends for all their support. This research would not have been possible with out the Max T Rogers NMR Facility and the Mass Spectrometry Facility in the chemistry and biochemistry departments respectively.

TABLE OF CONTENTS

LIST OF TABLES

Pages

LIST OF FIGURES

Pages

LIST OF ABBREVIATIONS

AIDS	Acquired Immune Deficiency Syndrome
ATR-FTIR	Attenuated Total Reflectance Fourier Transform InfraRed
CD	Circular Dichroism
CP	Cross Polarization
CS	Chemical Shift
CW	Continuous Wave
DC	Dipolar Coupling
DPC	Dodecylphosphocholine
ESR	Electron Spin Resonance
EPR	Electron Paramagnetic Resonance
FMOC	9-Fluorenylmethoxycarbonyl
FP	Fusion Peptide
FTIR	Fourier Transform InfraRed
FWHM	Full-Width-at-Half-Maximum
HA	Influenza Hemagglutinin Protein
HEPES	N-2-Hydroxyethylpiperazine-N'-2-Ethanesulfonic acid
HFP	HIV Fusion Peptide
HFIP	HexaFluoroIsoPropanol
HIV	Human Immunodeficiency Virus
HPLC	High Performance Liquid Chromatography
IFP	Influenza Fusion Peptide
IR	InfraRed

LM	Lipid Mixture
LSNMR	Liquid State Nuclear Magnetic Resonance
LUV	Large Unilamellar Vesicles
MALDI	Matrix Assisted Laser Desorption Ionization
MAS	Magic Angle Spinning
MES	MorpholineEthaneSulfonic Acid
NAL	N-Acetyl-Leucine
NMR	Nuclear Magnetic Resonance
NOE	Nuclear Overhauser Effect
PDSD	Proton Driven Spin Diffusion
PI	Phosphatidylinositol
POPC	1-Palmitoyl-2-Oleoyl-sn-glycero-3-Phosphocholine
POPE	1-Palmitoyl-2-Oleoyl-sn-glycero-3-Phosphoethanolamine
POPG	1-Palmitoyl-2-Oleoyl-sn-glycero-3-[Phospho-rac-(1-Glycerol)]
POPS	1-Palmitoyl-2-Oleoyl-sn-glycero-3-[Phospho-L-Serine]
PPM	parts per million
REDOR	Rotational Echo Double Resonance
RF	Radio Frequency
RFDR	Radio Frequency Driven Recoupling
SDS	Sodium Dodecyl Sulphate
SH3	α-spectrin Src-Homology domain
SSB	Spinning Side Band
SSNMR	Solid State Nuclear Magnetic Resonance

SUL	Scatter Uniform Labeling
TALOS	Torsion Angle Likelihood Obtained from Shift and sequence similarity
TFA	TriFluoroacetic Acid
TFE	TriFluoroEthanol
TPPM	Two Pulse Phase Modulation
UNAL	Uniformly labeled N-Acetyl-Leucine

Chapter 1

Introduction

Fusion between cells and cellular components plays an important role in such significant physiological processes as egg fertilization and synaptic transmission in the nervous system. Membrane fusion is also an important step in viral infection for widespread and serious diseases including measles, influenza and AIDS.[1-3] Understanding viral fusion is important as a key step in the viral life cycle and as a possible target for anti-viral therapeutics.

Enveloped viruses such as human immunodeficiency virus (HIV) and influenza are surrounded by a membrane and infection of target cells begins with fusion of the viral and target cell membranes. After the fusion process the viral nucleocapsid is now inside the target cell and can begin viral replication. HIV fuses directly with the plasma membrane whereas influenza is first endocytosed and fusion occurs between the viral and endosomal membranes.[3, 4] Figure 1[5] illustrates the three sequential steps of fusion in HIV: binding of two membranes, mixing of lipid membranes, and formation of a large pore through which the contents of both the virus and the host cell mix.[4] Influenza fusion is pH mediated (figure 2[4]). The virus first binds to the receptors on the host cell surface and enters through endocytosis.[6] Fusion of the viral membrane with the endosomal membrane is required to release the virus into the cytoplasm and to allow insertion of the viral genetic material into the host cell.

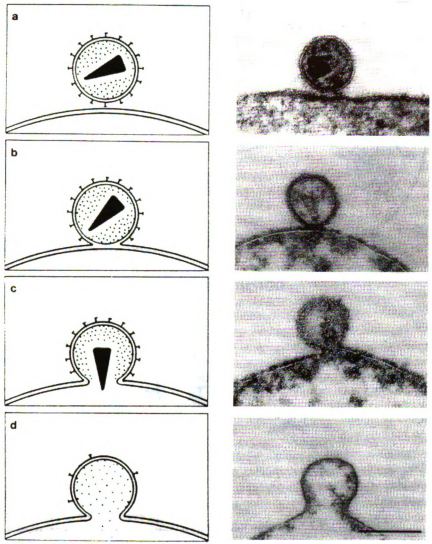

Figure 1. Model (left) and Electron Microscopy (right) of the HIV virus (a) binding to host cell (b) fusion of viral and host cell membranes (c,d) formation of large pore and infection of host cell. The triangle represents the viral RNA that enters the host cell.

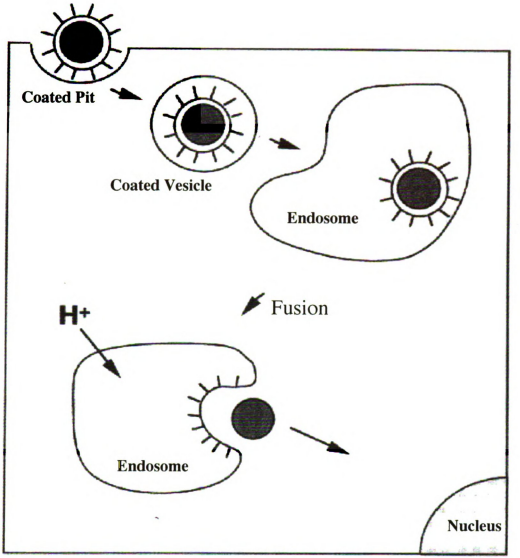

Figure 2. The first half of the influenza viral life cycle. The virus enters the cell by endocytosis. The pH drops in the endosome, initiating conformational changes of the hemagglutinin protein on the viral membrane surface. These conformation changes ultimately lead to fusion of the viral and endosomal membranes and release of the viral contents into the cell.

There is a high kinetic barrier to membrane fusion and both the HIV and influenza virus have a "fusion peptide" (FP) catalyst which increases the fusion rate.[7, 8] The FP is the 20-residue apolar domain at the N-terminus of the gp41 protein (HIV) or HA2 subunit of the humagglutinin protein (influenza). The sequences are different for the FPs of the two viruses. The FPs are hidden within the envelope protein until a conformational change is triggered which exposes the FPs, and allows them to interact with the membranes of the target cell.[9-11] The triggering event for influenza is the reduction of the endosomal pH to ~5 while in HIV the event is binding of the protein to the target cell protein receptors. Even in the absence of the rest of the fusion protein, the free fusion peptide catalyzes fusion between liposomes, which are lipid-bilayers bounded vesicles and serves as a good model system for understanding some aspects of HIV and influenza viral fusion. Mutational studies have shown strong correlations between FP-induced fusion and viral/host cell fusion.[7, 8, 12, 13]

Current models of HIV-1/host cell infection include interaction of the fusion peptide with the host cell membrane as displayed in figures 3[14] and 4[15]. Fusion and infection are initiated by strong interactions of two viral enveloped proteins (gp41 and gp120) with the CD4 and chemokine (e.g. CXCR4) receptors of the human T and macrophage cells.[16, 17] The gp41 protein traverses the HIV-1 membrane and the fusion peptide region is located at the N-terminus of the gp41 extraviral ectodomain.

There have been structural studies on peptides composed of the HIV FP (HFP) or influenza FP (IFP) in a variety of environments using a wide array of techniques including circular dichroism (CD), IR, ESR, liquid state NMR (LSNMR), and solid-state NMR (SSNMR) methods. CD spectra of HFPs show helical character for samples in

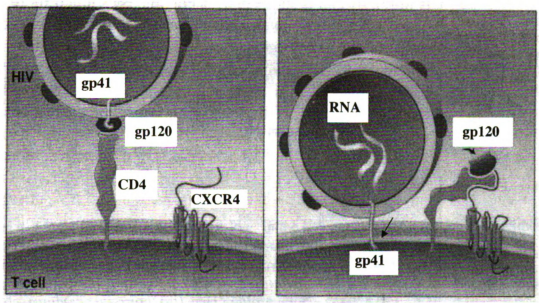

Figure 3. Model of HIV Infection. FP= Fusion Peptide. Time Sequence: Left to Right

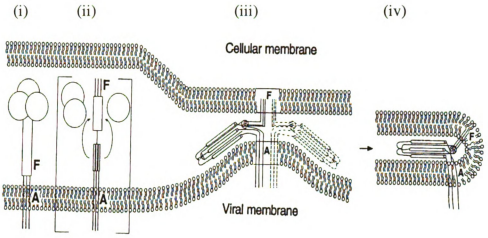

Figure 4. Model for HIV-1/Host cell fusion. In the left-most figure, a gp120/gp41 trimer is displayed with the balls representing gp120 and rods representing gp41. F represents the fusion peptide and A represents the transmembrane anchorage of gp41. Fusion proceeds temporally from left to right with (i) initial state, (ii) receptor binding and fusion peptide membrane insertion, (iii) gp41 conformational change, and (iv) membrane fusion.

50% trifluoroethanol (TFE)[18-20], or 70% hexafluoroisopropanol (HFIP)[20], in 20 mM Sodium Dodecyl Sulphate (SDS) with a HFP: SDS ratio of ~ 0.005 [18, 19, 21], and in 1-palmitoyl-2-oleoyl-sn-glycero-3-[phospho-rac-(1-glycerol)] (PG) or 1-palmitoyl-2-oleoyl-sn-glycero-3-phosphocholine (PC) lipid vesicles with a HFP:lipid ratio of ~0.005.[22, 23] These results seem reasonable because both TFE and HFIP are helix promoting solvents. β structure is observed when the HFP:SDS ratio is ~0.1[19] or HFP:PG or HFP:PC ~0.03.[22] Greater β structure at higher HFP:SDS or HFP:lipid is consistent with correlations of β structure with oligomer formation. ESR studies have also been done on HFPs where spin labels at individual residues provide information about mobility and environment of the residues. The studies show that the N-terminus is located in the hydrophobic core of the membrane and the C-terminus is near the aqueous/membrane interface.[19, 21, 23] ESR studies have also been done on IFP in PC/PG membranes at both pH 5 and 7.4 and were consistent with a pH-dependent change in the angle between the N-terminal helix and the bilayer normal.[24]

Both LSNMR and SSNMR studies have been done on HFP and IFP samples. LSNMR requires rapid molecular tumbling so the samples are in micellar environments rather than lipid bilayers. Secondary and tertiary structural information is obtained by chemical shifts (CS) and nuclear Overhauser effect (NOE) crosspeaks. At HFP:detergent ~ 0.01, LSNMR studies are consistent with helical structure over residues 4-12 in SDS or dodecylphosphocholine (DPC) micelles and some studies suggest that there may be additional C-terminal helical or β turn structure.[21, 25-28] There is some disagreement among the studies about insertion depth with different data supporting either a trans-micelle or a surface orientation.[21, 26, 27] LSNMR studies of IFP in detergent at pH 5

show that IFP forms a helix-turn-helix motif with the two helices extending from G1-I10 and W14 to I18.[24, 29, 30] Studies at pH 7.4 show a structure in detergent where the C-terminal helix is absent.[24]

SSNMR studies have been done on peptides in either membrane bilayer dispersions or in bilayers aligned between stacked glass plates. Measurements of CS and internuclear dipolar couplings (DCs) provide information about the peptide conformation, oligomerization, and insertion angle and depth relative to the membrane. ^{31}P SSNMR studies on HFP/lipid samples suggest that the FP perturbs the bilayer and causes increased lipid mobility in the presence of FPs.[23, 31, 32] ^{13}C SSNMR of HFP in aligned PC membranes with HFP:lipid ratio of ~0.05 was consistent with broad distributions of HFP orientation in the membrane.[23] The remaining SSNMR studies on HFP have been done by our group. Magic angle spinning (MAS) SSNMR has shown helical, β strand, and random coil structures at specific residues in HFP and the distribution of conformations at specific residues was shown to depend on the lipid headgroup and cholesterol composition of the membrane.[33-37] Measurements of DCs between HFPs showed that the β-strand structure is oligomeric and contains interpeptide hydrogen bonding and that there are approximately equal populations of parallel and anti-parallel strand alignments.[38]

Traditional SSNMR of peptides and proteins has relied on selective ^{13}C and ^{15}N labeling and by this approach the determination of a complete structure requires at least one selectively labeled sample per residue. Preparation of such a large number of samples is time consuming and backbone structures of two membrane-bound peptides have been reported with this methodology.[39, 40] There has been recent development

of SSNMR methods to solve the structures of U-^{13}C, ^{15}N labeled peptides and proteins analogous to solution NMR techniques [41-54]. There are a few examples of small microcrystalline protein and β amyloid fibril structures structures studies with these techniques. For the 61-residue α-spectrin Src-homology (SH3) domain in microcrystalline form, the samples were uniformly or extensively ^{13}C, ^{15}N labeled and a complete ^{13}C, ^{15}N assignment and 3D structure were obtained from a combination of 2D ^{13}C-^{13}C and ^{15}N-^{13}C experiments.[50, 55] For the forty-residue β-amyloid fibrils, the sample had "scatter-uniform labeling" (SUL) in which only one residue of each amino acid type was U-^{13}C, ^{15}N labeled. 2D ^{13}C-^{13}C and ^{13}C-^{15}N experiments were used for assignment and structure determination.[56, 57]

Unambiguous assignment is typically a prerequisite to NMR structure determination and spectral linewidths and dispersion play a large role in determining the number of uniformly labeled residues which can be unambiguously assigned. In this thesis, membrane-associated FP samples were studied with different number of uniformly labeled residues. One goal was assessment of the number of uniformly labeled residues which can be unambiguously assigned with 2D ^{13}C-^{13}C and ^{15}N-^{13}C experiments. In addition, the measured ^{13}C shifts were used to probe secondary structure of the membrane-bound peptides.

Multidimensional NMR techniques can be used to determine internuclear distance and angle constraints.[44, 49, 50, 54, 55, 58] A whole protein structure would then be developed through molecular dynamic simulations, which incorporate the constraints. The overall approach is analogous to the well-developed NMR methods for proteins and nucleic acids in aqueous solution and has the potential to provide high-resolution

structures for small proteins in intact biological membranes. The solid state NMR (SSNMR) approach will be complementary to solution NMR and crystallographic methods for membrane proteins, which are typically done in detergent environments. This thesis describes application of this type of SSNMR approach to the membrane associated HIV-1 and influenza fusion peptides.

References

1. Blumenthal, R. and D.S. Dimitrov, *Membrane Fusion*, in *Handbook of Physiology, Section 14: Cell Physiology*, J.F. Hoffman and J.C. Jamieson, Editors. 1997, Oxford: New York. p. 563-603.

2. Dimitrov, D.S., *Cell biology of virus entry*. Cell, 2000. 101(7): p. 697-702.

3. Eckert, D.M. and P.S. Kim, *Mechanisms of viral membrane fusion and its inhibition*. Annu Rev Biochem, 2001. 70: p. 777-810.

4. Hernandez, L.D., et al., *Virus-cell and cell-cell fusion*. Annu Rev Cell Dev Biol, 1996. 12: p. 627-61.

5. Grewe, C., A. Beck, and H.R. Gelderblom, *HIV: early virus-cell interactions*. J Acquir Immune Defic Syndr, 1990. 3(10): p. 965-74.

6. Murata, M., et al., *pH-Dependent Membrane Fusion Activity of a Synthetic Twenty Amino Acid Peptide with the Same Sequence as That of the Hydrophobic Segment of Influenza Virus Hemagglutinin*. Journal of Biochemistry, 1987. 102: p. 957-62.

7. Epand, R.M., *Fusion peptides and the mechanism of viral fusion*. Biochimica Et Biophysica Acta-Biomembranes, 2003. 1614(1): p. 116-121.

8. Durell, S.R., et al., *What studies of fusion peptides tell us about viral envelope glycoprotein-mediated membrane fusion (review)*. Mol Membr Biol, 1997. 14(3): p. 97-112.

9. Carr, C.M. and P.S. Kim, *A spring-loaded mechanism for the conformational change of influenza hemagglutinin*. Cell, 1993. 73(4): p. 823-32.

10. Bullough, P.A., et al., *Structure of influenza haemagglutinin at the pH of membrane fusion*. Nature, 1994. 371(6492): p. 37-43.

11. Wilson, I.A., J.J. Skehel, and D.C. Wiley, *Structure of the haemagglutinin membrane glycoprotein of influenza virus at 3 A resolution*. Nature, 1981. 289(5796): p. 366-73.

12. Pecheur, E., et al., *Peptides and Membrane Fusion: Towards an Understanding of the Molecular Mechanism of Protein-Induced Fusion*. J Membr Biol, 1999. 167(1): p. 1-17.

13. Nieva, J.L., Agirre, Aitziber, *Are fusion peptides a good model to study viral cell fusion?* Biochimica Et Biophyicica ACTA, 2003. 1614: p. 104-115.

14. *Breakthrough of the Year:New Hope in HIV Disease*. Science, New Series. 274: p. 1988-1991.

15. Weissenhorn, W., et al., *Atomic structure of the ectodomain from HIV-1 gp41*. Nature, 1997. 387(6631): p. 426-30.

16. Bleul, C.C., Farzan, M., Choe,H., Parolin, C., ClarkLewis, I., Sodroski, J., Springer, T.A, *The lymphocyte chemoattractant SDF-1 is a ligand for LESTR/fusin and blocks HIV-1 entry*. Nature, 1996. 382: p. 829-833.

17. Oberlin, E., Amara, A., Bachelerie, F., Bessia, C., Virelizier, J. L., ArenzanaSeisdedos, F., Schwartz, O., Heard, J.M., ClarkLewis, I., Legler, D.F.,Loetscher, M., Baggiolini,M., Moser, B., *The CXC chemokine SDF-1 is the ligand for LESTR/.Fusin and prevents infection by T-cell-line adapted HIV-1*. Nature, 1996. 382: p. 833-835.

18. Y. Kilger, A.A., D. Rapaport, P. Jones, R. Blumenthal, and Y. Shai, *Fusion peptides derived from the HIV type 1 glycoprotein 41 associate within phopholipid membranes and inhibit cell-cell Fusion. Strucutre-funciton Study*. Journal of Biological Chemistry, 1997. 272: p. 13496-505.

19. Gordon, L.M., et al., *The amino-terminal peptide of HIV-1 glycoprotein 41 interacts with human erythrocyte membranes: peptide conformation, orientation and aggregation*. Biochim Biophys Acta, 1992. 1139(4): p. 257-74.

20. Waring, A.J., P.W. Mobley, and L.M. Gordon, *Conformational mapping of a viral fusion peptide in structure-promoting solvents using circular dichroism and electrospray mass spectrometry*. Proteins, 1998. Suppl(2): p. 38-49.

21. Chang, D.K., S.F. Cheng, and W.J. Chien, *The amino-terminal fusion domain peptide of human immunodeficiency virus type 1 gp41 inserts into the sodium dodecyl sulfate micelle primarily as a helix with a conserved glycine at the micelle-water interface*. J Virol, 1997. 71(9): p. 6593-602.

22. Rafalski, M., J.D. Lear, and W.F. DeGrado, *Phospholipid interactions of synthetic peptides representing the N- terminus of HIV gp41*. Biochemistry, 1990. 29(34): p. 7917-22.

23. Curtain, C., et al., *The interactions of the N-terminal fusogenic peptide of HIV-1 gp41 with neutral phospholipids*. Eur Biophys J, 1999. 28(5): p. 427-36.

24. Han, X., et al., *Membrane structure and fusion-triggering conformational change of the fusion domain from influenza hemagglutinin*. Nat Struct Biol, 2001. 8(8): p. 715-20.

25. Vidal, P., Chaloin,L., Heitz,A., Van Mau, N., Mery, J., Divita, G., Heitz, F.,, *Interactinos of the N-terninal fusogenic peptide of HIV-1 gp41 inserts into the sodium dodecyl sulfate micelle primarily as a helix with a conserved glycine at the micelle-water interface.* Journal of Virology, 1998. 71: p. 6593-602.

26. Chang, D.K. and S.F. Cheng, *Determination of the equilibrium micelle-inserting position of the fusion peptide of gp41 of human immunodeficiency virus type 1 at amino acid resolution by exchange broadening of amide proton resonances.* J Biomol NMR, 1998. 12(4): p. 549-52.

27. Morris, K.F., Gao, X.F., Wong, T.C., *The interactions of the HIV gp41 fusion peptides with zwitterionic membrane mimics determined by NMR spectroscopy.* Biochimica Et Biophysica Acta-Biomembranes, 2004. 1667: p. 67-81.

28. Gabrys, C.M., Weliky, D.P., *unpublished experiments.*

29. Dubovskii, P.V., et al., *Structure of an analog of fusion peptide from hemagglutinin.* Protein Science, 2000. 9(4): p. 786-798.

30. Hsu, C.H., et al., *Structural characterizations of fusion peptide analogs of influenza virus hemagglutinin - Implication of the necessity of a helix-hinge-helix motif in fusion activity.* Journal of Biological Chemistry, 2002. 277(25): p. 22725-22733.

31. Schanck, A., J. Peuvot, and R. Brasseur, *Influence of the mode of insertion of SIV peptides into membranes on the structure of model membrane as studied by 31P NMR.* Biochem Biophys Res Commun, 1998. 250(1): p. 12-4.

32. Pereira, F.B., et al., *Interbilayer lipid mixing induced by the human immunodeficiency virus type-1 fusion peptide on large unilamellar vesicles: the nature of the nonlamellar intermediates.* Chem Phys Lipids, 1999. 103(1-2): p. 11-20.

33. Yang, J., et al., *Solid state NMR measurements of conformation and conformational distributions in the membrane-bound HIV-1 fusion peptide.* J Mol Graph Model, 2001. 19(1): p. 129-35.

34. Yang, R., Prorok, M., Castellino, F.J., Weliky, D.P., *A Trimeric HIV-1 Fusion Peptide Construct which does not Self-Associate in Aqueous Solution and which has 15-Fold Higher Membrane Fusion Rate.* Journal of the American Chemical Society, 2004. in press.

35. Yang, J., et al., *Application of REDOR Subtraction for Filtered MAS Observation of Labeled Backbone Carbons of Membrane-Bound Fusion Peptides.* Journal of Magnetic Resonance, 2002. 159(2): p. 101-110.

36. Bodner, M.L., et al., *Temperature Dependence and Resonance Assignment of 13C NMR Spectra of Selectively and Uniformly Labeled Fusion Peptides Associated with Membranes.* Magnetic Resonance in Chemistry, 2004. 42: p. 187-194.

37. Wasniewski, C.M., Parkanzky, Paul D., Bodner, Michele L., Weliky, David P., *Solid-state nuclear magnetic resonance studies of HIV and influenza fusion peptide orientations in membrane bilayers using stacked glass plate samples.* Chemistry and Physics of Lipids, 2004. 132: p. 89-100.

38. Yang, J. and D.P. Weliky, *Solid State Nuclear Magnetic Resonance Evidence for Parallel and Antiparallel Strand Arrangements in the Membrane-Associated HIV-1 Fusion Peptide.* Biochemistry, 2003. 42: p. 11879-11890.

39. Ketchem, R.R., W. Hu, and T.A. Cross, *High-resolution conformation of gramicidin A in a lipid bilayer by solid-state NMR.* Science, 1993. 261(5127): p. 1457-60.

40. Opella, S.J., et al., *Structures of the M2 channel-lining segments from nicotinic acetylcholine and NMDA receptors by NMR spectroscopy.* Nat Struct Biol, 1999. 6(4): p. 374-9.

41. Marassi, F.M., A. Ramamoorthy, and S.J. Opella, *Complete resolution of the solid-state NMR spectrum of a uniformly 15N- labeled membrane protein in phospholipid bilayers.* Proc Natl Acad Sci U S A, 1997. 94(16): p. 8551-6.

42. Marassi, F.M. and S.J. Opella, *Simultaneous assignment and structure determination of a membrane protein from NMR orientational restraints.* Protein Science, 2003. 12(3): p. 403-411.

43. Marassi, F.M. and S.J. Opella, *A solid-state NMR index of helical membrane protein structure and topology.* Journal of Magnetic Resonance, 2000. 144(1): p. 150-155.

44. McDermott, A., et al., *Partial NMR assignments for uniformly (C-13, N-15)-enriched BPTI in the solid state.* Journal of Biomolecular Nmr, 2000. 16(3): p. 209-219.

45. Mesleh, M.F., et al., *Dipolar waves as NMR maps of protein structure.* Journal of the American Chemical Society, 2002. 124(16): p. 4206-4207.

46. Straus, S.K., T. Bremi, and R.R. Ernst, *Experiments and strategies for the assignment of fully 13C/15N-labelled polypeptides by solid state NMR.* J Biomol NMR, 1998. 12(1): p. 39-50.

47. Hong, M. and K. Jakes, *Selective and extensive C-13 labeling of a membrane protein for solid-state NMR investigations.* Journal of Biomolecular Nmr, 1999. 14(1): p. 71-74.

48. Wang, J., et al., *Imaging membrane protein helical wheels.* Journal of Magnetic Resonance, 2000. 144(1): p. 162-167.

49. Detken, A., et al., *Methods for sequential resonance assignment in solid, uniformly C-13, N-15 labelled peptides: Quantification and application to antamanide.* Journal of Biomolecular Nmr, 2001. 20(3): p. 203-221.

50. Pauli, J., et al., *Backbone and side-chain C-13 and N-15 signal assignments of the alpha-spectrin SH3 domain by magic angle spinning solid-state NMR at 17.6 tesla.* Chembiochem, 2001. 2(4): p. 272-281.

51. Petkova, A.T., et al., *Backbone and side chain assignment strategies for multiply labeled membrane peptides and proteins in the solid state.* Journal of Magnetic Resonance, 2003. 160(1): p. 1-12.

52. Rienstra, C.M., et al., *De novo determination of peptide structure with solid-state magic-angle spinning NMR spectroscopy.* Proceedings of the National Academy of Sciences of the United States of America, 2002. 99(16): p. 10260-10265.

53. Lange, A., S. Luca, and M. Baldus, *Structural constraints from proton-mediated rare-spin correlation spectroscopy in rotating solids.* Journal of the American Chemical Society, 2002. 124(33): p. 9704-9705.

54. Egorova-Zachernyuk, T.A., et al., *Heteronuclear 2D-correlations in a uniformly [C-13, N-15] labeled membrane-protein complex at ultra-high magnetic fields.* Journal of Biomolecular Nmr, 2001. 19(3): p. 243-253.

55. Castellani, F., et al., *Structure of a protein determined by solid-state magic-angle-spinning NMR spectroscopy.* Nature, 2002. 420(6911): p. 98-102.

56. Petkova, A.T., et al., *A structural model for Alzheimer's beta-amyloid fibrils based on experimental constraints from solid state NMR.* Proceedings of the National Academy of Sciences of the United States of America, 2002. 99(26): p. 16742-16747.

57. Tycko, R. and Y. Ishii, *Constraints on Supramolecular Structure in Amyloid Fibrils from Two-Dimensional Solid State NMR Spectrosocpy with Uniform Isotopic Labeling.* Journal of the American Chemical Society, 2003. 125: p. 6606-6607.

58. Rienstra, C.M., et al., *2D and 3D N-15-C-13-C-13 NMR chemical shift correlation spectroscopy of solids: Assignment of MAS spectra of peptides.* Journal of the American Chemical Society, 2000. 122(44): p. 10979-10990.

Chapter 2

Experimental

Materials

Rink amide resin was purchased from Advanced Chemtech (Louisville, KY, USA) and 9-fluorenylmethoxycarbonyl(FMOC)-amino acids from Peptides International (Louisville, KY, USA). Isotopically labeled amino acids were purchased from Cambridge (Andover, MA, USA) and were FMOC-protected using literature procedures.[1, 2] 1-palmitoyl-2-oleoyl-sn-glycero-3-phosphocholine (POPC), 1-palmitoyl-2-oleoyl-sn-glycero-3-[phospho-L-serine] (POPS), 1-palmitoyl-2-oleoyl-sn-glycero-3-phosphoethanolamine (POPE), 1-palmitoyl-2-oleoyl-sn-glycero-3-[phospho-rac-(1-glycerol)] (POPG), phosphatidylinositol (PI), sphingomyelin, and dodecylphosphocholine (DPC) were purchased from Avanti Polar Lipids, Inc. (Alabaster, AL). N-2-hydroxyethylpiperazine-N'-2-ethanesulfonic acid (HEPES) and 4-Morpholineethanesulfonic acid (MES) was obtained from Sigma (St. Louis, MO). All other reagents were of analytical grade.

Peptides

HFP-U3 fusion peptide (sequence AVGIGALFLGFLGAAGSTMGARSKKK) (figure 5) was synthesized with the 23 N-terminal residues of the LAV_{1a} strain of the HIV-1 gp41 envelope protein followed by three additional lysines for improved solubility. HFP-U12 fusion peptide sequence

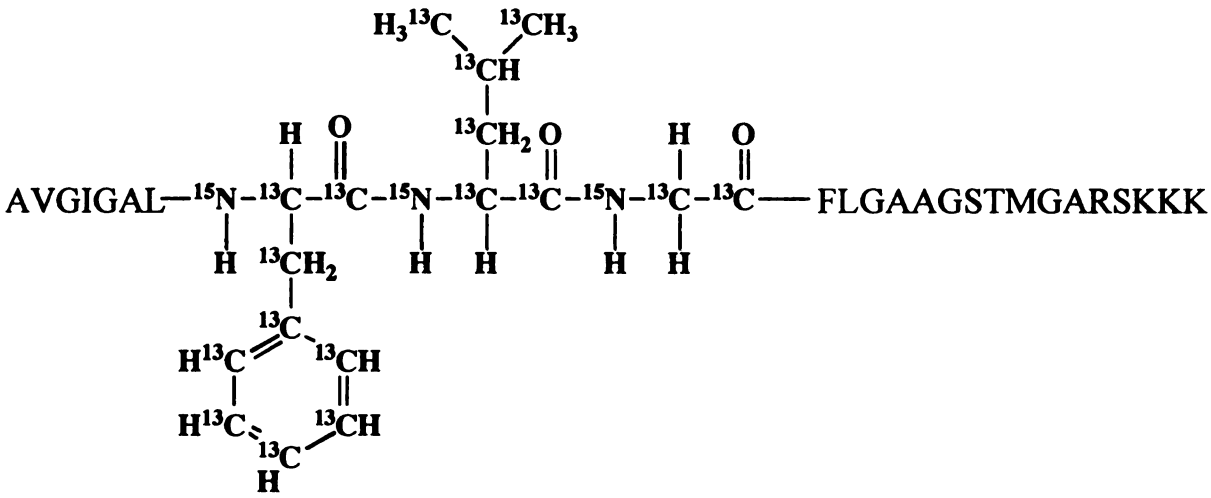

Figure 5. Chemical structure of HFP-U3 showing ^{13}C and ^{15}N labeling.

(AVGIGALFLGFLGAAGSTMGARSCKKKKKKW) was synthesized with the 23 N-terminal residues of the LAV_{1a} strain of the HIV-1 gp41 envelope protein followed by a cysteine to allow for cross-linking of the peptide. Cross-linking should create a FP topology similar to the one which likely exists in the fusogenic from of gp41 and there is functional evidence that this topology plays a significant role in enhancing membrane fusion rates.[3-6] There are high resolution structures of the gp41 "soluble ectodomain' which begins ~ 10 residues C-terminal of the FP.[6] Although the apolar FP is not part of the soluble ectodomain, the structures show trimeric oligomerization with the three N-termini in close proximity. These data suggest that during viral/target cell fusion, gp41 is trimeric with the C-termini of the three FPs close together. Thus the cysteine cross-linking is an effort to mimic the biologically relevant topology in a peptide model system. As in HFP-U3, the six C-terminal lysines enhance solubility.[7] A single tryptophan was added as a 280 nm chromophore for peptide quantitation. Similarly, the influenza peptide IFP-U10 (GLFGAIAGFIENGWEGMIDGGGKKKK) was synthesized with the 20 N-terminal residues of the HA2 domain of the influenza hemagglutinin fusion protein followed by a glycine and lysine sequence for improved solubility. All peptides were synthesized as their C-terminal amides using a peptide synthesizer (ABI 431A, Foster City, CA) equipped with FMOC chemistry. HFP-U3 had uniform ^{13}C, ^{15}N labeling at Phe-8, Leu-9, and Gly-10 and HFP-U12 had uniform ^{13}C, ^{15}N labeling over the twelve residues between Gly-5 and Gly-16. Five additional peptides with the same sequence as HFP-U12 were synthesized using different labeling schemes. HFP-A (**A**VGIGAL**F**LGF**L**GAAGSTMGARSCKKKKKKW), HFP-B (A**V**GIGA**L**FLG**F**LGA**A**GSTMGARSCKKKKKKW), HFP-C

(AVGIGALFLGFLGAAGSTMGARSCKKKKKW), HFP-D (AVGIGALFLGFLGAAGSTMGARSCKKKKKW), and HFP-E (AVGIGALFLGFLGAAGSTMGARSCKKKKKW) where the residues in bold are uniformly ^{13}C and ^{15}N labeled. IFP-U10 had uniform ^{13}C, ^{15}N labeling over the ten residues from Gly-1 to Ile-10. The peptides were cleaved from the resin in a three hour reaction using a mixture of trifluoroacetic acid (TFA):H_2O:phenol: thioanisole: ethanedithiol in a 33:2:2:2:1 volume ratio. Peptides were purified by reversed-phased HPLC using a preparative C_{18} column (Vydac, Hesperia, CA) and a water/acetonitrile gradient containing 0.1% TFA. Matrix assisted laser desorption ionization (MALDI) mass spectroscopy was used to confirm the identity of the peptide products.

Cross-Linking

HFP-U12, HFP-A, HFP-B, HFP-C, HFP-D, and HFP-E (0.002M) was cross-linked in 0.005 M dimethylaminopyridine buffer at pH 8.4. This solution was vortexed in air for 24 hours. Purification and characterization of the peptide dimer were carried out as described above for the monomeric peptides.

Solid State NMR Sample Preparation

HFP samples were prepared using a lipid/cholesterol mixture reflecting the approximate lipid headgroup and cholesterol content of host cells infected by the HIV virus.[8] This lipid mixture consists of POPC, POPE, POPS, PI, sphingomyelin, and cholesterol in a 10:5:2:1:2:10 molar ratio (LM3). The IFP sample was prepared with a 4:1 ratio of POPC:POPG (without cholesterol) (PC/PG). This lipid mixture was chosen because it has been used by other investigators studying FPs applying techniques other than solid state NMR.[9, 10] Lipid and cholesterol powders were dissolved together in

chloroform. The chloroform was removed under a stream of nitrogen followed by overnight vacuum pumping. Lipid dispersions were formed by addition of 5 mM HEPES buffer for the HFP samples and 5 mM HEPES/10 mM MES buffer for IFP followed by homogenization with ten freeze-thaw cycles. The buffer contained 0.01% NaN_3 as a preservative. Large unilamellar vesicles (LUVs) of ~100 nm diameter were prepared by extruding the lipid dispersions ~30 times through two stacked polycarbonate filters (Avestin, Inc., Ottawa, ON, Canada).

HFP and IFP peptides were dissolved in ~ 2 ml of 5 mM HEPES buffer (pH 7.0) or 5 mM HEPES/10 mM MES buffer (pH 5.0) respectively with 0.01% (w/v) NaN_3 preservative. The HFP-U3 sample contained 0.8 μmol peptide, 20 μmol total lipid, and 10 μmol cholesterol. The HFP-U12 sample contained 0.4 μmol peptide, 20 μmol total lipid, and 10 μmol cholesterol. The IFP sample contained 0.3 μmol peptide and 15 μmol total lipid. HFP-A thru HFP-E samples all contained 0.4 μmol peptide, 20 μmol total lipid, and 10 μmol cholesterol. Peptide/LUV solutions were then mixed and kept at room temperature overnight. The solution was then centrifuged at 100,000 – 130,000 * g for five hours to pellet down the LUV and associated bound peptide. Nearly all peptide bound to LUV under these conditions. The peptide/LUV pellet formed after ultracentrifugation was transferred by spatula to a 4 mm magic angle spinning (MAS) NMR rotor with ~40 μL rotor volume.

Previous solution NMR studies showed that dissolving HFP in dodecylphosphocholine (DPC) detergent resulted in helical structure.[11] 200 μM DPC and 2 μM HFP solutions were combined and vortexed for one hour. This solution was then frozen at –80 °C in the NMR probe while spinning.

Setup Compounds

Uniformly labeled N-Acetyl-leucine (U-NAL) (figure 6) served as a general setup compound for the SSNMR experiments. Synthesis began with the addition of uniformly ^{13}C, ^{15}N labeled leucine (24.8 mg) to 0.5 mL glacial acetic acid and heating to 100 ^{o}C while stirring. After addition of 1-^{13}C-acetic anhydride (38 μL), the solution was cooled to 80 °C and water (1 mL) was added to react with any excess acetic anhydride. The U-NAL product was washed with cyclohexane, which was subsequently removed under vacuum. Residual solvents were removed with the following sequential steps : (1) water aspirator vacuum until weight loss was no longer detected; (2) drying in a vacuum dessicator; and (3) dissolution in water followed by lyophilization.[12] ^{1}H and ^{13}C LSNMR were used to confirm the U-NAL synthesis.

U-NAL was diluted in unlabeled NAL (ICN, Auroa,OH) by dissolving U-NAL (16.5 mg) and unlabeled NAL (89.4 mg) into ~ 5 ml of water under gentle heating. After cooling, the solution was filtered using a 0.22 μm sterile syringe filter (Millipore, Bedford).[13] Crystals were formed upon slow evaporation of the water.

A modified lyophilized "I4" peptide (AEAAAKEALAKEAAAKAW) was used as an additional setup compound for 2D ^{15}N-^{13}C correlation spectroscopy.[14] The peptide was synthesized and purified as previously described for the HFP and IFPs and contained uniform ^{13}C, ^{15}N labeling at A8 and L9.

Magic Angle Spinning (MAS)

In solids, there is negligible molecular tumbling and the NMR signals are broadened by anisotropic effects. These effects can be reduced and the lines narrowed by magic angle spinning (MAS), whereby the sample is rotated at kHz frequencies about an

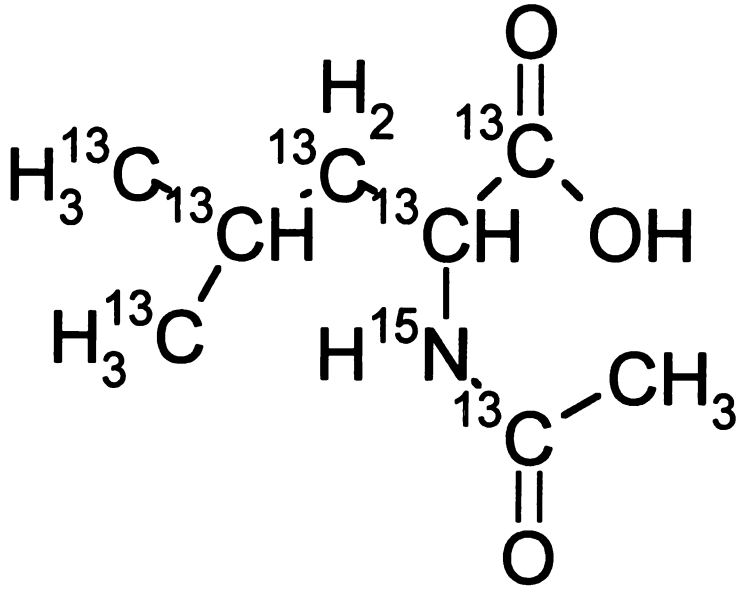

Figure 6. Chemical structure of U-N-Acetyl-leucine showing ^{13}C and ^{15}N labeling.

axis tilted at 54.7° relative to the external magnetic field direction. The MAS spectrum contains signals at the isotropic chemical shifts, i.e. the shifts, which would be observed in a typical liquid state spectrum. If the spinning frequency is slow enough, additional signals are observed which are separated from the isotropic peaks by integral multiples of the spinning frequency and are known as spinning sidebands.

^{13}C CP MAS Experiments

Transfer or "Cross polarization" (CP) of magnetization from protons to ^{13}C is a SSNMR technique which increases ^{13}C signals in 1D as well as multidimensional NMR experiments. CP is accomplished by simultaneous RF radiation of both the ^{1}H and ^{13}C nuclei such that both isotopes precess at the same frequency. Magnetization transfer is mediated by heteronuclear dipolar coupling. Figure 7 shows the typical pulse sequence for a 1D ^{13}C CP experiment including acquisition.

Filtering Methods

In peptide/membrane samples containing specifically ^{13}C labeled peptide, ^{1}H-^{13}C cross-polarized (CP) ^{13}C NMR spectra typically have very large lipid, cholesterol, and peptide natural abundance signals. Two approaches were taken to filter out the natural abundance signals. For 1D spectra, a rotational-echo double- resonance (REDOR) NMR filtering sequence was applied and the resulting spectra were dominated by labeled backbone ^{13}C with directly bonded ^{15}N.[15, 16] For example, for the HFP-U3 sample, a clean spectrum was observed of the Phe-8, Leu-9, and Gly-10 C_α and the Phe-8 and Leu-9 CO carbons. In the second filtering approach, 2D ^{13}C-^{13}C correlation spectra were obtained on both the HFP-U3 and HFP-U12 sample and off-diagonal cross peaks were

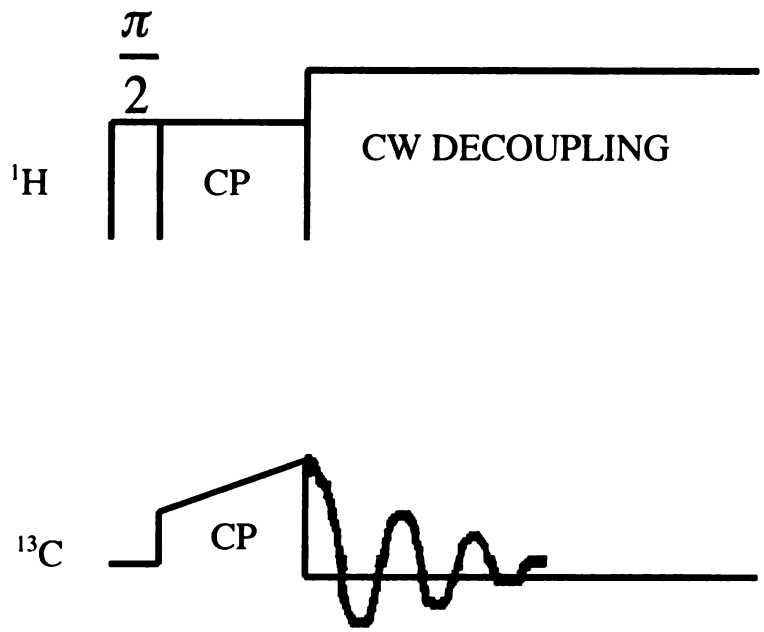

Figure 7. ^{13}C CP MAS sequence. Magnetization was transferred from protons to ^{13}C during CP. ^{1}H continuous wave decoupling was applied during acquisition.

only detected between labeled ^{13}C which are separated by one or a few bonds; i.e. in a strong ^{13}C-^{13}C dipole coupling network.

The REDOR technique relies on the difference of two spectra, one with the REDOR sequence (Figure 8), and one with a REDOR sequence without ^{15}N π pulses. With ^{15}N pulses (S_1 spectrum), there is heteronuclear ^{13}C-^{15}N dipolar coupling and the signals of ^{13}C directly bonded to ^{15}N are reduced. Without ^{15}N pulses (S_0 spectrum), there is no ^{13}C-^{15}N dipolar coupling and the signals of all ^{13}C nuclei are equally detected. Thus, the $S_0 - S_1$ difference spectrum yields only the signals of ^{13}C directly bonded to ^{15}N.

NMR Spectroscopy – Experimental Details

Most NMR spectra were taken on a 9.4 T spectrometer (Varian Infinity Plus, Palo Alto, CA) using a triple resonance MAS probe designed for a 4 mm or 6 mm diameter rotor. The temperature was monitored by a thermocouple located about 1" from the rotor and in the flow of the cooling nitrogen gas. The actual temperature of the sample is likely warmer than the measured temperature because of frictional heating from the sample spinning and from heating due to the radiofrequency(RF) fields. In the NMR probe circuit, the RF fields are highly attenuated at the ends of the coil and it was experimentally observed that nearly the entire NMR signal comes form the central 2/3 of the sample volume specified by the manufacturer. Hence, in the 6 mm rotor, longer spacers were used to restrict samples to this central 2/3 volume (~160 μl). For the 4 mm rotor, the total possible rotor sample volume was also restricted to 2/3 volume (~40 μl).

The ^{13}C detection channel was tuned to 100.8 or 100.2 MHz, the decoupling channel was tuned to 400.8 or 398.6 MHz and the third channel ^{15}N was tuned to 40.6 or 40.4 MHz. For the 1D REDOR experiments, ^{13}C chemical shift referencing was done

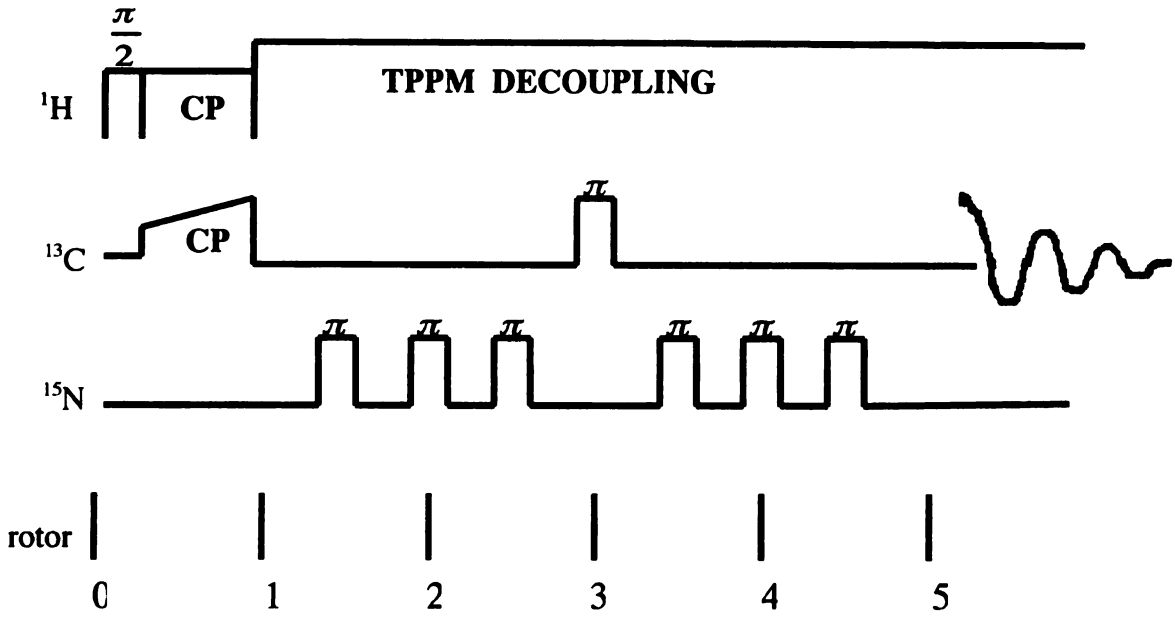

Figure 8. 1D ^{13}C REDOR pulse sequence. CP transferred proton magnetization to ^{13}C. ^{13}C magnetization is dephased (reduced) by ^{13}C-^{15}N dipolar coupling mediated by two equally spaced ^{15}N 180° pulses per rotor period. A ^{13}C 180° pulse in the middle of the dephasing period refocuses the ^{13}C chemical shift.

using the methylene resonance of solid adamantane at 38.5 ppm.[17] For the 2D experiments, the ^{13}C chemical shift referencing was done with the methylene resonance of solid adamantane at 40.5 ppm and ^{15}N channel was referenced indirectly using conversion factors from ratios of NMR frequencies.[18] The zero frequency for ^{13}C was found by referencing to adamantane and the ^{15}N zero frequency was calculated by multiplying the ^{13}C zero frequency by 10.129118/25.1449530.[18] The ^{13}C and ^{15}N referencing correlates with that used in NMR of soluble proteins. The sample temperature was –50 °C and the MAS frequency was 6800±2 Hz for the 2D $^{13}C/^{13}C$ correlation experiments and 7000±2 Hz for the 2D $^{15}N/^{13}C$ correlation experiments. The MAS frequency was 8000±2 Hz for the 1D REDOR experiments.

1D REDOR Experimental Details

For the REDOR experiments, generation of ^{13}C transverse magnetization was followed by a REDOR dephasing period and then direct ^{13}C detection. For the HFP-U3 sample, the ^{13}C transmitter was set to 155 ppm at –50 °C and to 100 ppm at 20 °C. ^{13}C transverse magnetization was generated using ^{1}H-^{13}C CP with a 53–57 kHz ^{13}C ramp and 1.8 ms contact time at –50 °C and 1 ms contact time at 20 °C. The dephasing period was set to 8 rotor periods (1 ms) and contained a single 55 kHz ^{13}C refocusing π pulse at the center of this period. For the S_1 acquisition, 45 kHz ^{15}N π pulses were applied at the middle and end of every rotor cycle during the dephasing period except for the fourth and eighth cycles. The S_0 acquisition did not contain these ^{15}N π pulses. In the dephasing period, pulse timing was not actively synchronized to the rotor position. Two-pulse phase modulation (TPPM) ^{1}H decoupling at 100 kHz was applied during both dephasing and detection with 5.4 μs pulse length and 90° and 105° phases.[19] To obtain optimal

compensation of B_0, B_1, and MAS frequency drifts, S_0 and S_1 free induction decays (FIDs) were acquired alternately. The recycle delay was 2 s at –50 °C and 1.3 s at 20 °C.

A Z-filter sequence was used to set the ^{13}C π pulse length and contained the following sequential elements: ^{1}H-^{13}C CP; ^{13}C $\pi/2$; 10 ms; ^{13}C π; detection. ^{1}H decoupling was applied during pulses and detection. The ^{15}N π pulse length was set by minimization of S_1 signals for the model compound and the TPPM pulse length was set by maximization of the S_0 signal for the model compound.

For each S_1 transient, XY-8 phase cycling was applied to the ^{15}N π pulses.[20, 21] Individual S_0 or S_1 transients were coadded with the following phase cycling scheme: ^{1}H $\pi/2$, x, -x, x, -x; ^{13}C CP and ^{13}C π, -y, -y, x, x; receiver, x, -x, y, -y. After completion of data acquisition, the sum of S_1 FIDs was subtracted from the sum of S_0 FIDs. Spectral processing was done on the difference FID with a DC offset correction, 25 Hz Gaussian line broadening, Fourier transform, and baseline correction.

2D ^{13}C-^{13}C Experimental Details

The 2D ^{13}C-^{13}C correlation spectra were obtained with a double resonance ^{1}H /^{13}C probe configuration because ^{13}C signal-to-noise is ~ 1.5 times higher than in the ^{1}H/^{13}C/^{15}N configuration. Correlations were generated by the Proton Driven Spin Diffusion (PDSD) pulse sequence: CP – t_1 – $\pi/2$ – τ – $\pi/2$ – t_2 (figure 9) where CP corresponds to ^{1}H-^{13}C cross-polarization, t_1 was the evolution period, the first $\pi/2$ pulse rotated ^{13}C transverse magnetization to the longitudinal axis, τ was a spin diffusion period during which ^{13}C longitudinal magnetization was transferred between ^{13}C nuclei, the second $\pi/2$ pulse rotated ^{13}C longitudinal magnetization to the transverse plane, and t_2

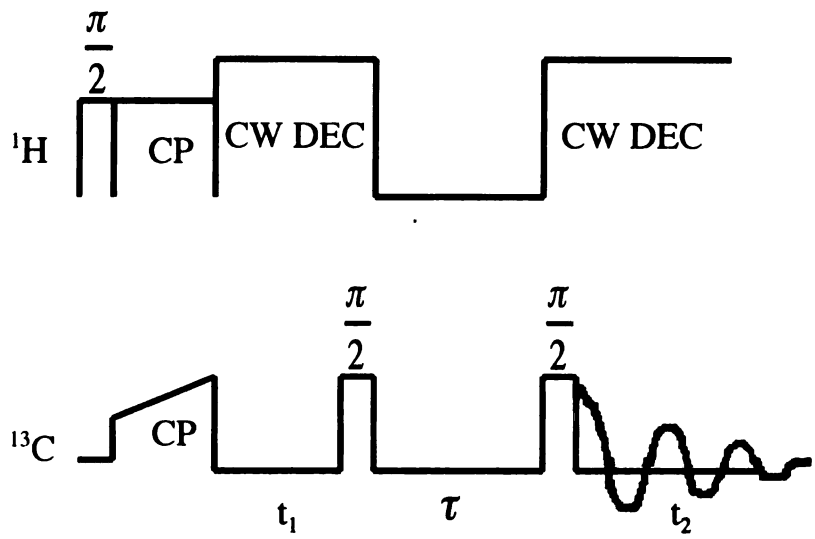

Figure 9. 2D ^{13}C-^{13}C correlation PDSD sequence. Magnetization was transferred from ^{1}H to ^{13}C during CP. Continuous wave (CW) decoupling is applied after CP on the protons during t_1 and t_2, but not during τ. t_1 was the evolution time, τ was the magnetization exchange time, and t_2 was the acquisition time.

was the detection period.[22] Continuous wave (CW) ^{1}H decoupling at 100 kHz was applied during the pulse, t_1, and t_2 periods, but not during τ. In a second data set, longitudinal transfer of ^{13}C magnetization during τ was achieved with the radiofrequency-driven dipolar recoupling (RFDR) method (figure 10).[23, 24] In this approach, a ^{13}C π pulse was applied at the end of the rotor cycles 1,3,5,...,31 during τ. CW ^{1}H decoupling at 100 kHz was also applied during τ. The τ period contained a total of 32 rotor cycles. NAL was used to optimize all of the ^{1}H and ^{13}C rf fields. The $\pi/2$ was set by first finding the π pulse using a CP z-filter sequence.[25]

The following parameters were common for RFDR and PDSD data sets: 44-64 kHz ramp on the ^{13}C CP rf field; 62.5 kHz ^{1}H CP rf field; 2 ms CP contact time; 50 kHz ^{13}C $\pi/2$ pulse rf field; 25 μs t_1 dwell time; 20 μs t_2 dwell time; and 1 s recycle delay. Hypercomplex data were obtained by acquiring two individual FIDs for each t_1 point with either a ^{13}C $(\pi/2)_x$ or $(\pi/2)_y$ pulse at the end of the t_1 evolution period. For the first of these t_1 FIDs, individual transients were coadded with the following phase cycling scheme: first ^{13}C $\pi/2$ pulse, x, -x, x, -x, x, -x, x, -x; second ^{13}C $\pi/2$ pulse, x, x, y, y, -x, -x, -y, -y; receiver, y, -y, -x, x, -y, y, x, -x. For the other t_1 FID, the first ^{13}C $\pi/2$ pulse followed y, -y, y, -y, y, -y, y, -y cycling. HFP-U3 and HFP-U12 PDSD data were acquired in ~ 108 hours with 200 t_1 points, 1024 t_2 points, and 1024 transients per FID, and the RFDR data were acquired in ~60 hours with 200 t_1 points, 1024 t_2 points, and 512 transients per FID. Dimer A-E samples 10 ms PSDS data were each collected in ~ 58 hours and the 1 s data were each collected in ~ 114 hours. The parameters for the IFP PDSD experiments were similar except for a 41-59 kHz ramped ^{13}C CP rf field, 128 t_1 points, and ~ 104 hour acquisition time. All data sets were processed according to the

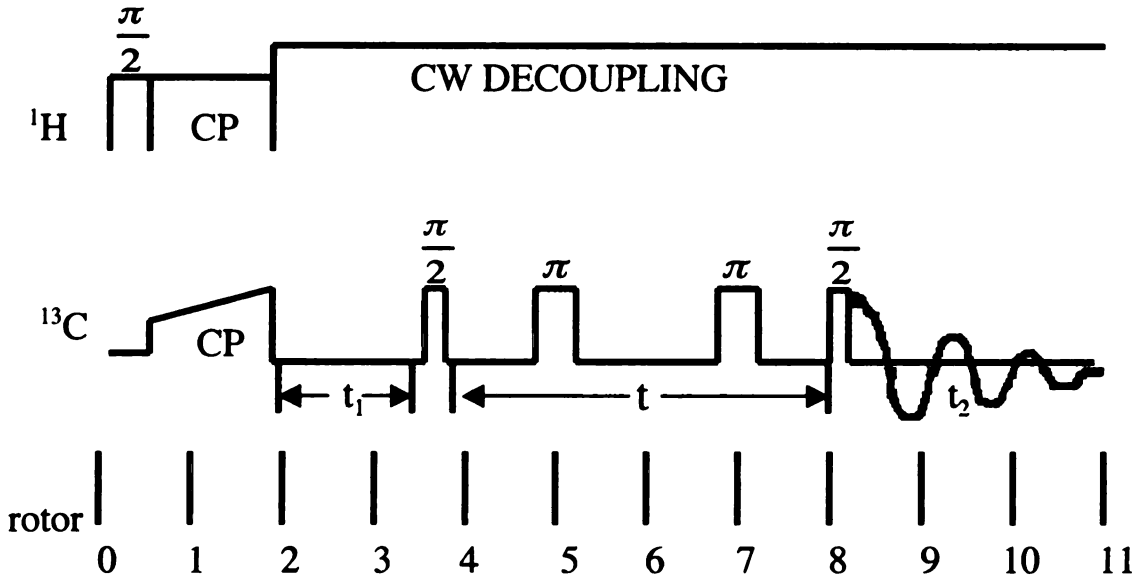

Figure 10. 2D ^{13}C-^{13}C correlation RFDR sequence. CP transferred magnetization from ^{1}H to ^{13}C and magnetization evolved during t_1. The τ exchange period consists of ^{13}C π pulses every other rotor period. Acquisition was done during t_2.

method of States using nmrPipe software.[26, 27] Processing included zero-filling, Gaussian line broadening, and baseline correction.

The 700 MHz spectrum of the HFP-U3 sample was obtained using a Bruker Avance spectrometer (Billerica,MA) and a triple resonance $^{1}H/^{13}C/^{15}N$ MAS probe equipped for use with 4 mm diameter rotors. The acquisition parameters included: 10 kHz MAS frequency; 67 kHz ^{13}C CP rf field; 77 kHz ^{1}H CP rf field; 2 ms CP contact time; 110 MHz SPINAL-64 ^{1}H decoupling[28]; 64 t_1 points with 28.4 μs dwell time; τ=100 ms; 444 t_2 points with 28.4 μs dwell time; 1 s recycle delay; 512 transients per FID; and ~1 day total acquisition time.

1D ^{15}N-^{13}C Correlation Experiments

The 1D ^{15}N-^{13}C correlation spectra were obtained at –50 °C and 6.8 kHz MAS with the pulse sequence: CP1- τ - CP2 – acquisition where CP1 was the ^{1}H-^{15}N cross polarization, τ was 1 μs, and CP2 was ^{15}N-^{13}C cross polarization (figure 11). The ^{15}N transmitter was set to 115 ppm and ^{15}N transverse polarization was generated by ^{1}H-^{15}N CP with a ^{15}N ramp of 30-49 kHz and a 4.0 ms contact time. 100 kHz CW ^{1}H decoupling was used during τ, CP2, and acquisition. Polarization was transferred from ^{15}N to ^{13}C during CP2 using a ^{15}N ramp of 19-30 kHz and 1.5 ms contact time. When the ^{13}C transmitter was set to 155 ppm, the CP2 transfer was selective for CO and when the ^{13}C transmitter was set to 60 ppm, the CP2 transfer was selective for C_α. The ^{13}C CP2 field was 25 KHz for the selective CO transfer and 24.8 kHz for the selective C_α transfer.

Figure 12 (bottom) displays a ^{13}C CP MAS spectrum of the model compound. The spectrum was taken at –50 °C using 6.8 kHz MAS and processed using 10 Hz Gaussian line broadening. Two carbonyl peaks are resolved at 177.2 ppm and 175.4 ppm

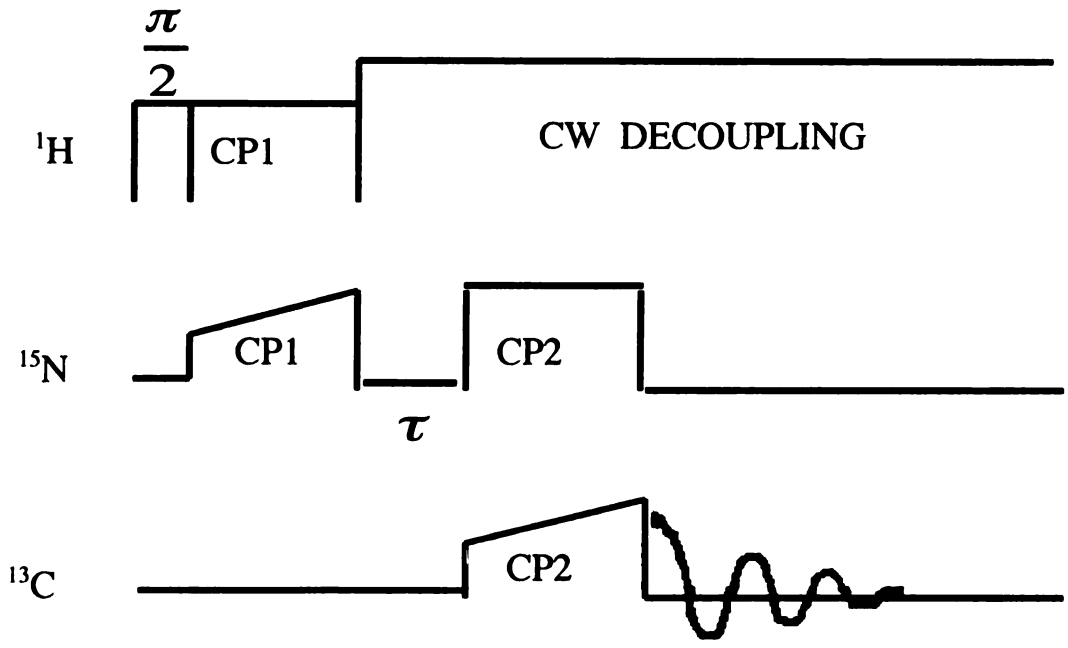

Figure 11. 1D ^{15}N-^{13}C correlation sequence. CP1 transfers magnetization from protons to ^{15}N. CP2 transfers magnetization from ^{15}N to ^{13}C followed by ^{13}C detection.

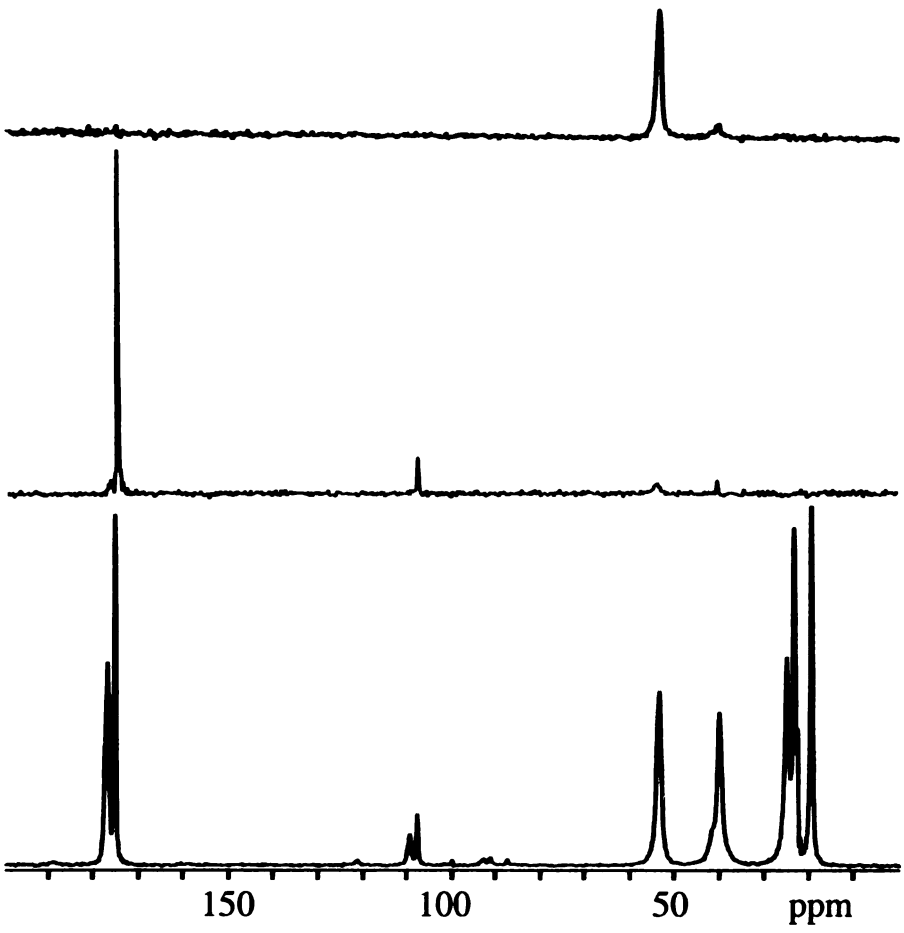

Figure 12. Crystalline N-Acetyl-Leucine model compound uniformly $^{13}C/^{15}N$ labeled. The spectra were obtained at –50 °C, MAS frequency of 6.8 kHz, 32 scans signal averaging and processed using 10 Hz of Gaussian line broadening. Using ^{13}C CP MAS, all labeled carbons were observed (bottom). 1D ^{1}H-^{15}N-^{13}C selective CP spectrum showed only one dominate signal that was from the carbonyl directly bonded to ^{15}N (middle). The ^{1}H-^{15}N-^{13}C selective CP sequence also allows signal suppression of the ^{13}CO and observation of only the $^{13}C\alpha$ signal (Top).

where the upfield shift is due to the carbonyl carbon directly bonded to the ^{15}N and the downfield shift is due to the carbonyl bonded to the oxygen. Five peaks are observed in the aliphatic region of the spectrum and had chemical shifts of 53.8, 40.5, 25.5, 23.9, and 20.0 ppm. The signals arose from the C_α, C_β,C_γ,C_δ, and the methyl carbon respectively. Integrated intensities from the CO directly bonded to the ^{15}N and the alpha carbon were used to determine the efficiency of the selective 1D ^{15}N-^{13}C experiments.

Figure 12 (middle) displays a selective ^{15}N-^{13}C correlation spectrum. A single peak was observed at 175.4 ppm, which corresponds to the chemical shift of the CO carbon directly bonded to the ^{15}N. For selective CP from ^{15}N to the alpha carbon, a single peak at 53.8 ppm was the primary observed peak (figure 12 top). The chemical shifts of both selective experiments correspond to chemical shifts in the ^{13}C CP MAS experiment. The integrated intensities of CO and C_α peaks were measured for both the ^{15}N-^{13}C selective CP and ^{13}C CP MAS experiments to determine the efficiencies of the selective CP experiments. Both efficiencies were quite similar with 30% for C_α and 33% for CO. The observed efficiencies suggest that it is reasonable to apply these experiments to peptide/lipid samples.

U-N-Acetyl-leucine has been very useful as a model compound to determine the feasibility of the ^{15}N-^{13}C correlation experiments on biologically relevant samples. An efficiency of ~30% for both CO and C_α selective experiments was observed and suggests that with sufficient signal averaging time, ^{15}N-^{13}C experiments could be applied to membrane-associated fusion peptide samples.

2D ^{15}N-^{13}C Experimental Details

The 2D ^{15}N-^{13}C correlation experiments were acquired with the probe in triple resonance $^{1}H/^{13}C/^{15}N$ configuration. The correlations were generated with the double cross polarization sequence: CP1 – t_1 – CP2 – t_2 (figure 13) where CP1 corresponds to ^{1}H to ^{15}N cross-polarization, t_1 was the evolution period, CP2 corresponds to selective ^{15}N-^{13}CO (NCO) or ^{15}N-$^{13}C_{\alpha}$ (NCA) cross-polarization, and t_2 was the detection period.[29] Two Pulse Phase Modulation (TPPM) ^{1}H decoupling at 100 kHz was applied during the t_2 period, and CW decoupling was applied during the CP2 and t_1 periods.[30, 31] The ^{1}H, ^{13}C, and ^{15}N rf fields were first optimized with U-NAL and ^{15}N and ^{13}C fields during the CP2 step were then further optimized with the I4 peptide.

For each sample, a NCO and a NCA spectrum were acquired. NCO acquisition parameters were: 36-47 kHz ramp on the ^{15}N CP1 rf field; 57 kHz ^{1}H CP1 rf field; 1.1 ms CP1 contact time; 25 kHz ^{15}N CP2 rf field; 28 kHz ^{13}C CP2 rf field with the ^{13}C transmitter at ~155 ppm; 1.3 ms CP2 contact time; 250 μs t_1 dwell time; 20 μs t_2 dwell time; and 1 s recycle delay. Hypercomplex data were collected by acquiring two individual FIDs for each t_1 point with either $^{15}N(CP2)_x$ or $^{15}N(CP2)_y$ phases. The following phase cycling scheme was used: ^{1}H $\pi/2$ x, x, x, x, -x, -x, -x, -x ; ^{15}N CP1 x, x, x, x, x, x, x, x ; ^{1}H CP1 y, y, y, y, y, y, y, y; ^{15}N CP2, x, x, x, x, x, x, x, x; ^{13}C CP2, y, -x, -y, x, y, -x, -y, x; receiver, y, -x, -y, x, -y, x, y, -x. For the other t_1 FID, the ^{15}N CP2 phase followed y, y, y, y, y, y, y, y. The NCO data were acquired with 41 t_1 points, and 1024 t_2 points. The data were acquired in 2D blocks with each block ~1 day acquisition time and the final data set was the sum of several blocks. The NCA parameters were similar to the NCO parameters except for a 2.3 ms CP2 contact time, 29 kHz ^{13}C CP2 rf field, and a ^{13}C

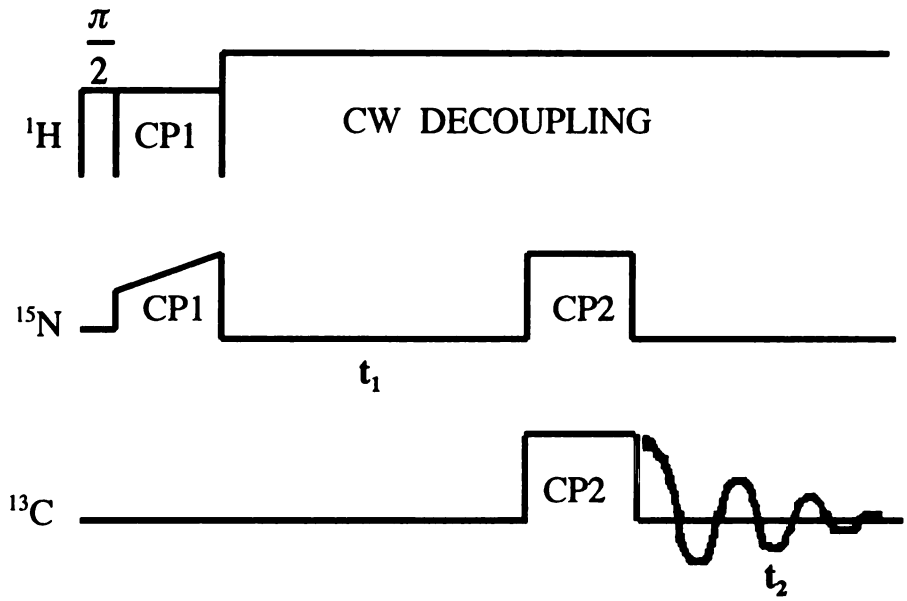

Figure 13. 2D ^{15}N-^{13}C correlation sequence. CP1 transferred magnetization from protons to ^{15}N, which then evolved during t_1. CP2 transferred magnetization from ^{15}N to ^{13}C and was detected during t_2.

transmitter of ~ 35 ppm. Data for NCO and NCA experiments were processed using nmrPipe in the same manner as the ^{13}C-^{13}C PDSD experiments.

Sedimentation Equilibrium

Sedimentation equilibrium experiments at room temperature where performed on an analytical ultracentrifuge (Beckman XL-1, Palo Alto, CA) using a An-60 Ti rotor. The experiments were carried out in absorbance mode at 280 nm. Samples were loaded into a two channel aluminum centerpiece with quartz windows and equilibrated at 48,000 rpm. The data were fitted to a single molar mass (M) using:

$$(A/A_0) = \exp[M(1-\nu\rho)(r^2-r_0^2)(\omega^2/2RT)] \quad (1)$$

where A and A_0 are the experimental absorbancies at the radius r and reference radius r_0, respectively, ν is the partial specific volume of the peptide, ρ is the buffer density, ω is the angular velocity, R is the ideal gas constant, and T is the temperature.[32] This equation assumes no baseline offset and a single value of M meaning a single self-association state for all peptides in solution. The values of ν for each peptide were calculated from the mass average of the partial specific volumes of the individual amino acids.[33] The value of ρ was set to 1.0 g/mL. This data was fitted using Origin 4.1 software.

References

1. Chang, C.D., et al., *Preparation and Properties of N-Alpha-9-Fluorenylmethyloxycarbonylamino Acids Bearing Tert-Butyl Side- Chain Protection.* International Journal of Peptide and Protein Research, 1980. 15(1): p. 59-66.

2. Lapatsanis, L., et al., *Synthesis of N-2,2,2-(Trichloroethoxycarbonyl)-L-Amino Acids and N-(9-Fluorenylmethoxycarbonyl)-L-Amino Acids Involving Succinimidoxy Anion As a Leaving Group in Amino-Acid Protection.* Synthesis-Stuttgart, 1983. 8: p. 671-673.

3. Weissenhorn, W., et al., *Atomic structure of the ectodomain from HIV-1 gp41.* Nature, 1997. 387(6631): p. 426-30.

4. Caffrey, M., et al., *Three-dimensional solution structure of the 44 kDa ectodomain of SIV gp41.* Embo J, 1998. 17(16): p. 4572-84.

5. Munoz-Barroso, I., et al., *Dilation of the human immunodeficiency virus-1 envelope glycoprotein fusion pore revealed by the inhibitory action of a synthetic peptide from gp41.* J Cell Biol, 1998. 140(2): p. 315-23.

6. Eckert, D.M. and P.S. Kim, *Mechanisms of viral membrane fusion and its inhibition.* Annu Rev Biochem, 2001. 70: p. 777-810.

7. Han, X. and L.K. Tamm, *A host-guest system to study structure-function relationships of membrane fusion peptides.* Proceedings of the National Academy of Sciences of the United States of America, 2000. 97(24): p. 13097-13102.

8. Aloia, R.C., H. Tian, and F.C. Jensen, *Lipid composition and fluidity of the human immunodeficiency virus envelope and host cell plasma membranes.* Proc Natl Acad Sci U S A, 1993. 90(11): p. 5181-5.

9. Macosko, J.C., C.H. Kim, and Y.K. Shin, *The membrane topology of the fusion peptide region of influenza hemagglutinin determined by spin-labeling EPR.* J Mol Biol, 1997. 267(5): p. 1139-48.

10. Han, X., et al., *Membrane structure and fusion-triggering conformational change of the fusion domain from influenza hemagglutinin.* Nat Struct Biol, 2001. 8(8): p. 715-20.

11. Chang, D.K., S.F. Cheng, and W.J. Chien, *The amino-terminal fusion domain peptide of human immunodeficiency virus type 1 gp41 inserts into the sodium dodecyl sulfate micelle primarily as a helix with a conserved glycine at the micelle-water interface.* J Virol, 1997. 71(9): p. 6593-602.

12. Williamson, K.L., *Macroscale and Microscale Organic Experiments. second ed.* 1994, Lexington,Massachusetts,Toronto: Heath and Company. 632-635.

13. Baldus, M., *Personal Conmmunication.*

14. Long, H.W. and R. Tycko, *Biopolymer conformational distributions from solid-state NMR: alpha-helix and 3(10)-helix contents of a helical peptide.* Journal of the American Chemical Society, 1998. 120(28): p. 7039-7048.

15. Yang, J., et al., *Application of REDOR Subtraction for Filtered MAS Observation of Labeled Backbone Carbons of Membrane-Bound Fusion Peptides.* Journal of Magnetic Resonance, 2002. 159(2): p. 101-110.

16. Gullion, T., *Introduction to rotational-echo, double-resonance NMR.* Concepts in Magnetic Resonance, 1998. 10(5): p. 277-289.

17. Morcombe, C.R. and K.W. Zilm, *Chemical shift referencing in MAS solid state NMR.* Journal of Magnetic Resonance, 2003. 162: p. 479-486.

18. Markley John L., B.A., Arata Yoji, Hilbers C.W., Kaptein Robert, Sykes Brian D., Wright Peter E., Wuthrich Kurt, *Recommendations for the presentation of NMR Structures of Proteins and Nucleic Acids.* International Union of Pure and Applied Chemistry, 1998. 70(1): p. 117-142.

19. Bennett, A.E., et al., *Heteronuclear Decoupling in Rotating Solids.* Journal of Chemical Physics, 1995. 103(16): p. 6951-6958.

20. Gullion, T., D.B. Baker, and M.S. Conradi, *New, Compensated Carr-Purcell Sequences.* Journal of Magnetic Resonance, 1990. 89(3): p. 479-484.

21. Gullion, T. and J. Schaefer, *Elimination of Resonance Offset Effects in Rotational-Echo, Double-Resonance Nmr.* Journal of Magnetic Resonance, 1991. 92(2): p. 439-442.

22. Tycko, R., D.P. Weliky, and A.E. Berger, *Investigation of molecular structure in solids by two- dimensional NMR exchange spectroscopy with magic angle spinning.* Journal of Chemical Physics, 1996. 105(18): p. 7915-7930.

23. Bennett, A.E., et al., *Chemical-Shift Correlation Spectroscopy in Rotating Solids - Radio Frequency-Driven Dipolar Recoupling and Longitudinal Exchange.* Journal of Chemical Physics, 1992. 96(11): p. 8624-8627.

24. Bennett, A.E., et al., *Homonuclear radio frequency-driven recoupling in rotating solids.* Journal of Chemical Physics, 1998. 108(22): p. 9463-9479.

25. Bodner, M.L., et al., *Temperature Dependence and Resonance Assignment of 13C NMR Spectra of Selectively and Uniformly Labeled Fusion Peptides Associated with Membranes.* Magnetic Resonance in Chemistry, 2004. 42: p. 187-194.

26. States, D.J., R.A. Haberkorn, and D.J. Ruben, *A Two-Dimensional Nuclear Overhauser Experiment With Pure Absorption Phase in 4 Quadrants.* Journal of Magnetic Resonance, 1982. 48(2): p. 286-292.

27. Delaglio, F., et al., *NMRPipe: a multidimensional spectral processing system based on UNIX pipes [see comments].* J Biomol NMR, 1995. 6(3): p. 277-93.

28. Brauniger, T., P. Wormald, and P. Hodgkinson, *Improved Proton Decoupling in NMR Spectroscopy of Crystalline Solids Using the SPINAL-64 Sequence.* Monatshefte fur Chemie, 2002. 113: p. 1549-1554.

29. Rienstra, C.M., et al., *2D and 3D N-15-C-13-C-13 NMR chemical shift correlation spectroscopy of solids: Assignment of MAS spectra of peptides.* Journal of the American Chemical Society, 2000. 122(44): p. 10979-10990.

30. Petkova, A.T., et al., *Backbone and side chain assignment strategies for multiply labeled membrane peptides and proteins in the solid state.* Journal of Magnetic Resonance, 2003. 160(1): p. 1-12.

31. Pauli, J., et al., *Backbone and side-chain C-13 and N-15 signal assignments of the alpha-spectrin SH3 domain by magic angle spinning solid-state NMR at 17.6 tesla.* Chembiochem, 2001. 2(4): p. 272-281.

32. Cantor, C.R. and P.R. Shimmel, *Biophysical Chemistry Part II: Techniques for the study of biological structure and function.* 1980, New York: W. H. Freeman.

33. Laue, T.M., et al., *Computer-aided interpretation of analytical sedimentation data for proteins*, in *Analytical Ultracentrifugation in Biochemistry and Polymer Science*, S.E. Harding, A.J. Rowe, and J.C. Horton, Editors. 1992, Royal Society of Chemistry: Cambridge. p. 90-125.

Chapter 3

1D HIV Fusion Peptide Studies

In MAS solid state NMR spectra of membrane-bound peptides and proteins, signals from specifically labeled nuclei can provide important information about the local structure and structural homogeneity.[1-4] However, for ^{13}C, these labeled nuclei signals are usually poorly resolved from large natural abundance signals of lipid and protein. To filter out these natural abundance signals, REDOR difference spectroscopy was investigated. REDOR difference spectroscopy was shown to be an easy method to implement because it only requires one sample and uses a fairly simple pulse sequence.

Utility of REDOR Filtering

For the NMR sample HFP-U3 associated with the LM3 lipid/cholesterol mixture at peptide:lipid mol ratio ~0.04, Figure 14 displays the REDOR S_o and difference spectra. In the S_o spectrum, there is significant natural abundance signal from the lipid and peptide. The difference spectrum was taken with a 1.6 ms dephasing time and cleanly shows the signals of backbone carbons directly bonded to labeled ^{15}N. The isotropic C_α, carbonyl, and M = +1, -1 , and –2 spinning sidebands of the carbonyls are apparent. In the filtered spectrum, the isotropic Phe-8 and Leu-9 carbonyl signals at 172 ppm are unresolved whereas the 40-55 ppm Phe-8, Leu-9, and Gly-10 C_α signals were all resolved. On the basis of the characteristic chemical shifts of residue-types, we can tentatively assign the 42.5 ppm signal to Gly-10 C_α.[5]

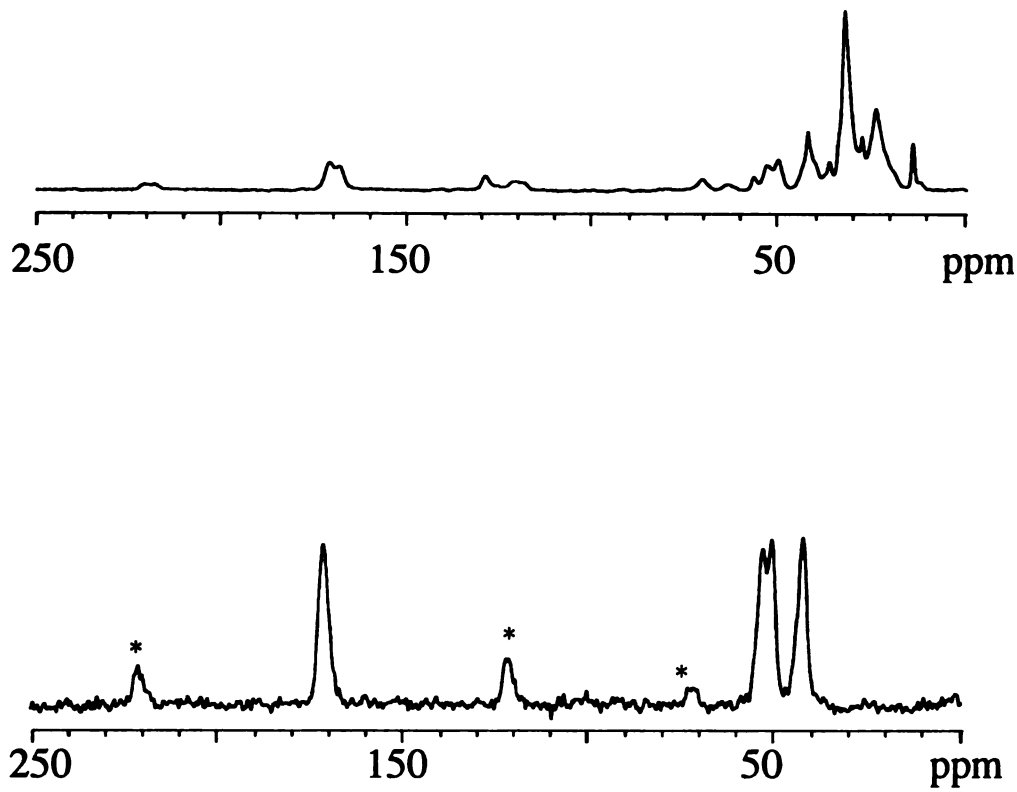

Figure 14. ^{13}C solid-state NMR spectra of HFP-U3 peptide associated with LM3 lipid mixture at –50°C. (top) Unfiltered REDOR spectrum where signal from both the lipids and peptide are observed. (bottom) Filtered spectrum obtained from the difference of S_0-S_1 FIDs. For both spectra, 10496 transients were taken, the spinning speed was 8 kHz and 50 Hz Gaussian line broadening was applied. Because of the short 1.6 ms dephasing time only the backbone carbonyl and C_α signals from Phe-8, Leu-9, and Gly-10 are observed. * = Carbonyl spinning sidebands

In this case, the difference spectrum is also useful for assessing linewidths and indirectly, the feasibility of doing a full assignment of this peptide with multidimensional NMR methods. The linewidths are a few times larger than those observed in larger U-^{13}C, ^{15}N crystalline peptides and proteins, but the recent successes in assignment of these crystalline systems suggest that a fairly long sequence in the membrane-associated fusion peptide can be assigned, followed by a full structure determination.[1, 6-10]

Figure 15 displays the REDOR difference spectrum of HFP-U12 associated with LM3 at peptide: lipid mol ratio of ~ 0.04. The REDOR difference spectrum was taken with a 1 ms dephasing time and shows the signals of backbone carbons directly bonded to labeled ^{15}N. The isotropic carbonyl signals from the labeled residues at 172.1 ppm and 168.9 ppm are unresolved. This is also true of the C_α region of the spectrum where there are three peaks at 42.7 pm, 49.1 ppm, and 50.8 ppm. Because of the linewidths, it appears from the REDOR difference spectrum that the full assignment of this peptide will be quiet challenging even with the use of multidimensional NMR methods.

Comparison of HFP Spectra in Detergent and Membranes

In Figure 16, HFP-U3 was associated with frozen detergent at –80 °C (top) and frozen LM3 membranes at –50 °C (bottom). In both the carbonyl and C_α regions of the spectra, there are significant differences in chemical shifts which indicate a change from helical structure in detergent to non-helical structure in LM3. In the C_α region, signals are expected from the Phe-8, Leu-9, Gly-10 nuclei, and there are three clear peaks in both the DPC and the LM3 samples. Although site-specific assignment is not definitive in this one-dimensional spectrum, a tentative assignment can be made on the basis of characteristic chemical shifts of particular amino acids. In particular, the C_α shifts for

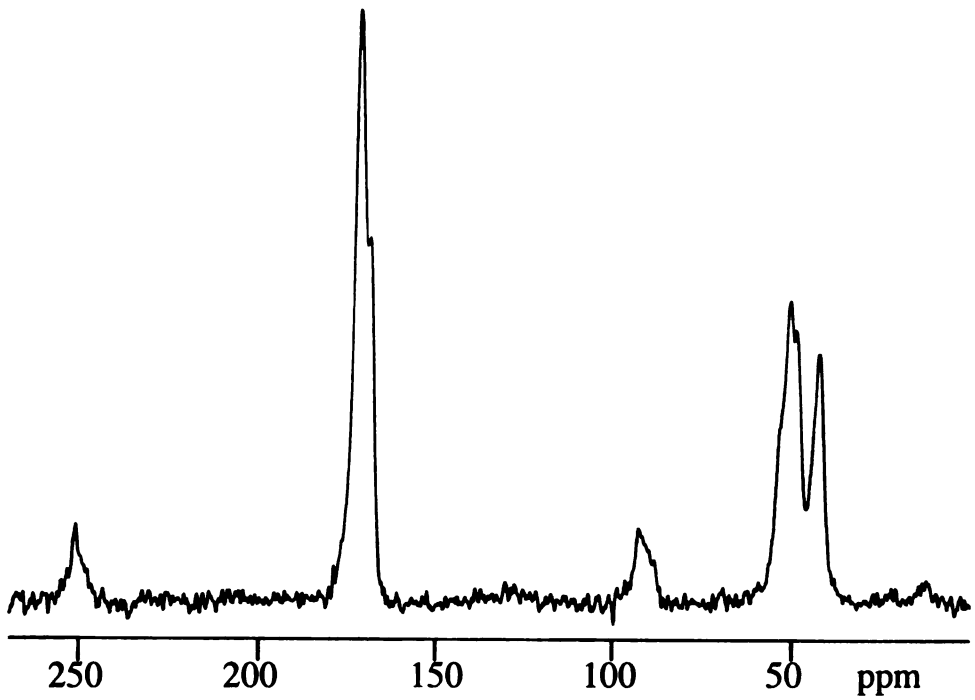

Figure 15. ^{13}C solid state NMR spectrum of HFP–U12 dimer associated with LM3 at –50°C. Due to a 1 ms REDOR filter time only the backbone carbonyl and C_α signals are observed. Other experimental conditions were: 13056 transients; 4 mm rotor diameter; 8 kHz MAS frequency; and 50 Hz line broadening.

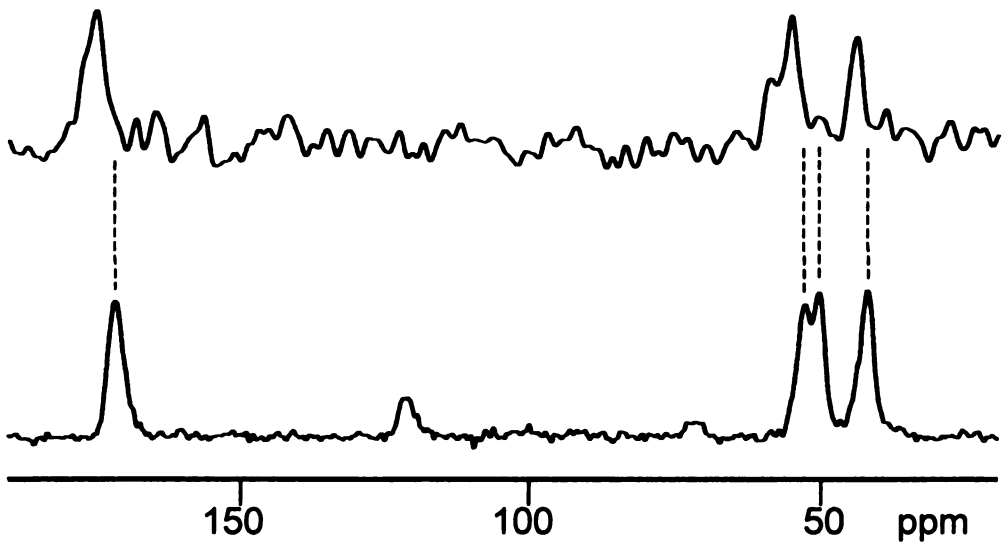

Figure 16. ^{13}C solid state NMR spectra of HFP-U3 associated with DPC at –80°C (top) and LM3 lipid mixture at –50°C (bottom). The peptide had uniform ^{13}C , ^{15}N labeling at the Phe-8, Leu-9, and Gly-10 residues. Because of the 1ms REDOR filter, the spectra are dominated by backbone carbonyl signals from Phe-8 and Leu-9 and backbone C_α signals from Phe-8, Leu-9, and Gly-10. For each spectrum, the spinning speed was 8 kHz and 50 Hz gaussian line broadening was applied. 50000 and 10800 transients were taken for the top and bottom spectrum respectively. The large differences between chemical shifts in (top) and (bottom) spectra are consistent with a change from helical structure in detergent to non-helical structure in LM3.

Phe, Leu, and Gly in random coil structures are 57.4 ppm, 53.6 ppm, and 43.5 ppm, respectively.[11] When this ordering is used to assign C_α peaks in the spectra, the measured shifts for the DPC and LM3 samples lie downfield and upfield of the random coil values, which is consistent with a change for this part of HFP from helical structure in detergent to non-helical structure in LM3. Thus, it appears that there can be significantly different structures in detergent and membranes.

Temperature Dependence of Spectra

Although physiological fusion occurs at 37 °C, NMR sensitivity is much better at lower temperature and spectra are often obtained at these temperatures. It is therefore important to determine whether lower temperature changes peptide structure. Figure 17 displays the C_α region of the REDOR filtered spectrum of the HIV-1 fusion peptide sample at (top) –50 °C and (bottom) 20 °C. Because of the 1 ms REDOR filter, the displayed spectral regions are dominated by backbone C_α signals from Phe-8, Leu-9, and Gly-10. Corresponding peak chemical shifts agree to within 0.5 ppm at the two temperatures, indicating that the lower temperature does not induce a large peptide structural change. The carbonyl region was similarly invariant to temperature. The linewidths were smaller at 20 °C than at –50 °C. For example, for the Gly-10 peak centered at 43.0 ppm, the full-width at half-maximum (FWHM) linwidths is ~ 2.6 ppm at –50 °C and is ~ 1.9 ppm at 20 °C. In addition, the integrated signal-to-noise per ^{13}C per transient at 20 °C is approximately 1/3 of its value at –50 °C. For hydrated membrane samples, it is reasonable that motion could increase significantly between –50 °C and 20 °C and this greater motion could explain these experimental observations. For example, increased motion could reduce inhomogeneous broadening and result in smaller

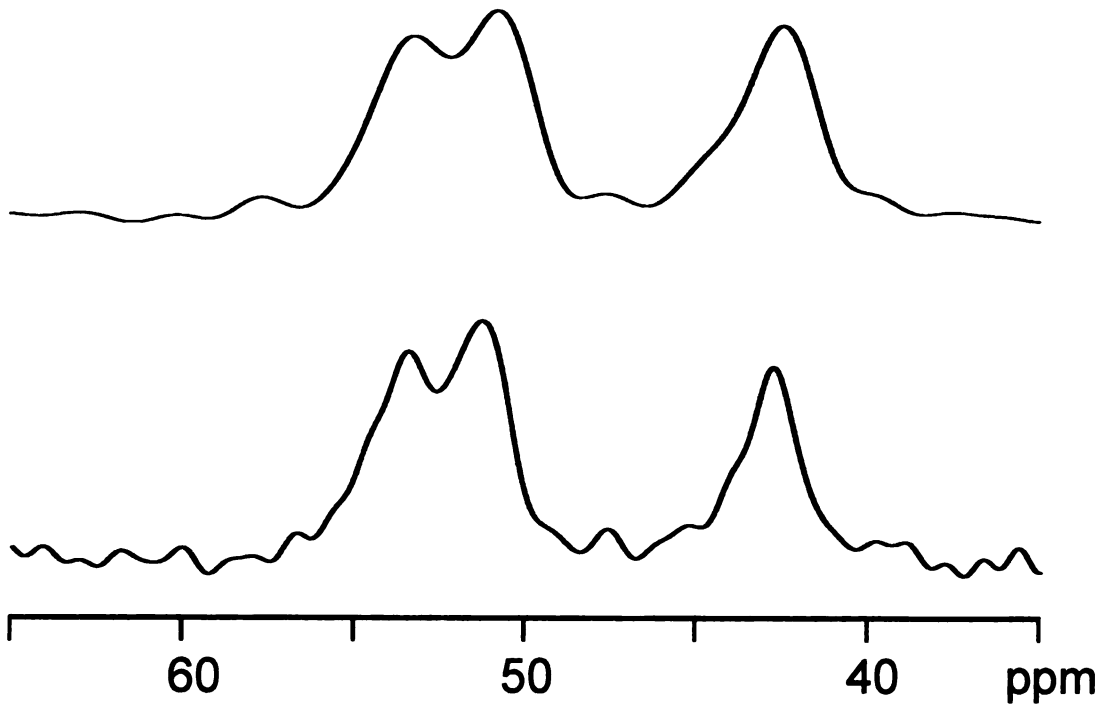

Figure 17. ^{13}C solid state NMR spectra of HFP-U3 associated with LM3 lipid mixture at –50 °C (top) and 20 °C. For both spectrum, the spinning speed was 8 kHz and 50 Hz Gaussian line broadening was applied. The chemical shifts in the spectra are consistent with non-helical structure at both –50 °C and 20 °C. However, the –50 °C spectrum has about three times more integrated signal per scan than the 20 °C spectrum, which can be explained by greater motion at 20 °C. Spectrum (a) was derived from the S_o-S_1 difference FID and a total of 10496 S_o and 10496 S_1 transients. Spectrum (b) was similarly obtained with 82048 S_o and 82048 S_1 transients.

linewidths. In addition, motion could attenuate dipolar couplings and decrease the efficiency of the ^{1}H-^{13}C cross-polarization (CP) and REDOR dephasing and result in lower REDOR-filtered ^{13}C signal per transient.

Conclusions

The REDOR filtering technique proved to be extremely useful in removing the natural abundance signal from the lipids in the sample as well as the unlabeled residues. This technique was also helpful in assessing linewidths and the feasibility of completing a full assignment using 2D methods. HFP-U3 shifts were observed using REDOR filter in both DPC and LM3. It was shown using known correlations between chemical shifts and secondary structure that the peptide is helical in DPC and non-helical in LM3.

Viral/target cell membrane fusion occurs at 37 °C, but for membrane-associated HIV-FP samples, the signal-to-noise per peptide ^{13}C per transient is about three times higher at –50 °C. In order to take advantage of the higher signal to noise at low temperatures, it is important to demonstrate the biological relevance of the cold samples and to therefore investigate whether cooling changes the peptide structure. The chemical shifts are similar at 20 °C and at –50 °C, which suggest that cooling does not change the average peptide structure. The temperature dependence of intensities and linewidths do suggest that motion at 20 °C is attenuated at –50 °C, which is a physically reasonable result for hydrated membrane samples.

References

1. Smith, S.O., C.S. Smith, and B.J. Bormann, *Strong hydrogen bonding interactions involving a buried glutamic acid in the transmembrane sequence of the neu/erbB-2 receptor.* Nat Struct Biol, 1996. 3(3): p. 252-8.

2. Wang, J., Y.S. Balazs, and L.K. Thompson, *Solid-state REDOR NMR distance measurements at the ligand site of a bacterial chemotaxis membrane receptor.* Biochemistry, 1997. 36(7): p. 1699-703.

3. Yang, J., C.M. Gabrys, and D.P. Weliky, *Solid-State Nuclear Magnetic Resonance Evidence for an Extended beta Strand Conformation of the Membrane-Bound HIV-1 Fusion Peptide.* Biochemistry, 2001. 40(27): p. 8126-37.

4. Yang, J., et al., *Solid state NMR measurements of conformation and conformational distributions in the membrane-bound HIV-1 fusion peptide.* J Mol Graph Model, 2001. 19(1): p. 129-35.

5. Evans, J.N.S., *Biomolecular NMR Spectroscopy.* 1995, New York: Oxford.

6. Rienstra, C.M., et al., *2D and 3D N-15-C-13-C-13 NMR chemical shift correlation spectroscopy of solids: Assignment of MAS spectra of peptides.* Journal of the American Chemical Society, 2000. 122(44): p. 10979-10990.

7. McDermott, A., et al., *Partial NMR assignments for uniformly (C-13, N-15)-enriched BPTI in the solid state.* Journal of Biomolecular Nmr, 2000. 16(3): p. 209-219.

8. Detken, A., et al., *Methods for sequential resonance assignment in solid, uniformly C-13, N-15 labelled peptides: Quantification and application to antamanide.* Journal of Biomolecular Nmr, 2001. 20(3): p. 203-221.

9. Jaroniec, C.P., et al., *Frequency selective heteronuclear dipolar recoupling in rotating solids: Accurate C-13-N-15 distance measurements in uniformly C-13,N-15-labeled peptides.* Journal of the American Chemical Society, 2001. 123(15): p. 3507-3519.

10. Straus, S.K., T. Bremi, and R.R. Ernst, *Side-chain conformation and dynamics in a solid peptide: CP-MAS NMR study of valine rotamers and methyl-group relaxation in fully C-13-labelled antamanide.* Journal of Biomolecular Nmr, 1997. 10(2): p. 119-128.

11. Wishart, D.S., et al., *H-1, C-13 and N-15 Random Coil Nmr Chemical-Shifts of the Common Amino-Acids .1. Investigations of Nearest-Neighbor Effects.* Journal of Biomolecular Nmr, 1995. 5(1): p. 67-81.

Chapter 4

2D HIV Fusion Peptide Studies

Introduction

In recent years, the problem of structure determination in uniformly labeled ^{13}C and ^{15}N biological solid samples has attracted a considerable amount of interest. Partial and complete assignment of uniformly labeled samples has been done using 2D $^{13}C/^{13}C$ and $^{15}N/^{13}C$ experiments.[1-5] For sequential assignment, it is particularly interesting to selectively transfer polarization from the backbone ^{15}N to either a directly bonded $^{13}C_{\alpha}$ or to a directly bonded ^{13}CO and to therefore correlate nuclei within a residue i or between adjacent i and i-1 residues.

2D Correlation Spectra

Figure 18 displays a 2D $^{13}C/^{13}C$ correlation spectrum for the HFP-U3/LM3 sample. The displayed spectra were generated from –50 °C data and the correlations were a result of magnetization exchange driven by 10 ms proton-driven spin diffusion (PDSD). A 2D correlation spectrum with similar appearance (figure 19) was obtained from data for which the magnetization exchange was generated by a 4 ms radiofrequency-driven dipolar recoupling (RFDR) sequence.[6, 7] Measurement of the crosspeak chemical shifts made possible a full resonance assignment of all the labeled ^{13}C in the peptide.

In the PDSD and RFDR spectra, (1) only intra-residue crosspeaks were definitively observed and (2) relatively strong crosspeaks were observed between ^{13}C

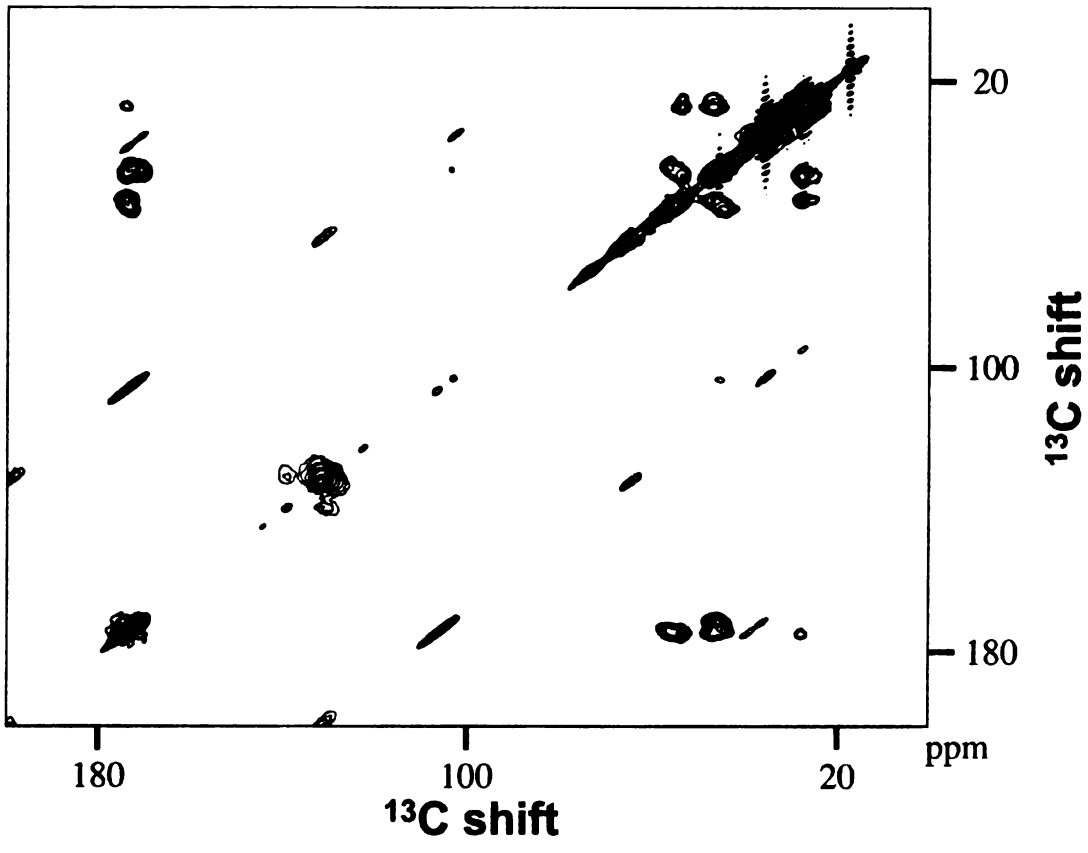

Figure 18. 2D ^{13}C-^{13}C contour plot spectrum of HFP-U3 associated with LM3 membranes. The peptide:lipid mol ratio was ~0.04 with ~0.8 μmol HFP-U3. The sample pH was 7.0 and the sample volume in the 4 mm rotor was ~30 μl. The data were collected with proton-driven spin diffusion with 10 ms exchange time and signal averaging time of ~4.5 days. The MAS frequency was 6.8 kHz. The spectrum was processed with 80 Hz Gaussian line broadening in each dimension.

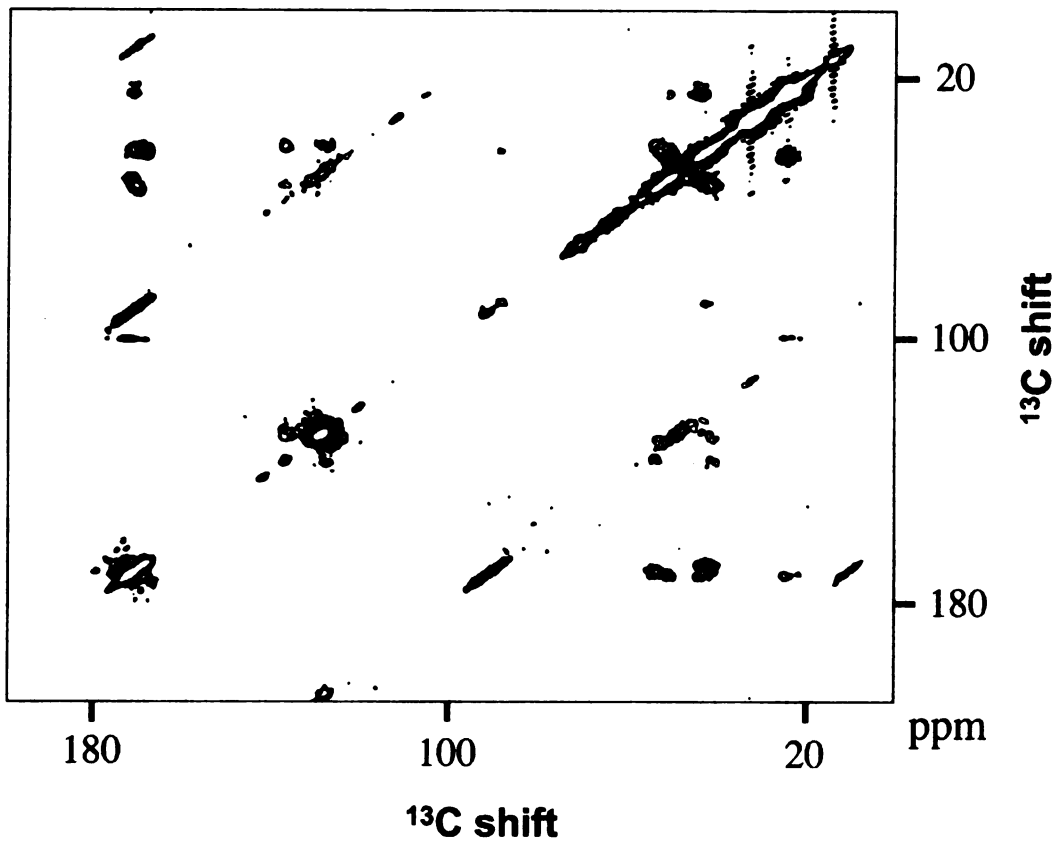

Figure 19. 2D ^{13}C- ^{13}C contour plot spectrum of HFP-U3 associated with hydrated LM3. The peptide to lipid molar ratio was ~0.04 with ~ 0.8 μmol HFP-U3. The buffer was at pH 7.0, and the sample volume in the 4 mm rotor was ~30 μl. This data were collected with radio frequency driven recoupling with a 4 ms exchange time. The MAS frequency was 8 kHz. The spectrum was processed with 80 Hz Gaussian line broadening in each dimension.

separated by several bonds (e.g. Leu-9 CO/C_γ). These observations are consistent with the results of other groups using these experiments with short mixing times on U-^{13}C, ^{15}N labeled peptides and proteins.[2, 3, 7, 8] Both PDSD and RFDR are relatively broad-banded exchange sequences mediated by ^{13}C-^{13}C dipolar coupling. For two ^{13}C separated by distance r, the exchange rate will have an approximate r^{-6} dependence, and direct exchange between ^{13}C separated by two bonds or three bonds would respectively occur at ~ 5% or 2 % of the rate of exchange between ^{13}C separated by one bond. Thus, it is more likely that a two-bond or three-bond cross peak is due to multiple steps of exchange between directly bonded ^{13}C rather than a single step exchange process. With the assumption that there is a single rate constant for the directly bonded ^{13}C exchange, at short times the ratio of intensities of the two bond/one bond cross peaks will be about the same as the ratio of three bond/two bond cross peaks and the ratio of four bond/three bond cross peaks. This model is qualitatively supported by the relative intensities of the Leu-9 CO/Cα, CO/Cβ, CO/Cγ, CO/Cδ, cross peaks (10:6:2:1) and all of the (n+1)/n-bond cross peak intensity ratios are within a range of 0.3 – 0.6. Inter-residue cross peaks are likely not observed in these short mixing time spectra because the ^{15}N interrupts the direct ^{13}C bond network. Inter-residue cross peaks are apparent in a 2D PDSD spectrum with a longer 100 ms mixing time (figure 20), in accord with the experience of other investigators.[8]

Figure 21 displays 2D NCO and NCA correlation spectra for the HFP-U3 sample. In these spectra, crosspeaks between directly bonded ^{15}N-^{13}CO and ^{15}N-$^{13}C\alpha$ nuclei are observed. The combination of the ^{13}C-^{13}C and ^{15}N-^{13}C spectra makes possible a nearly unambiguous assignment of the ^{13}C and ^{15}N nuclei in the three residues, as is listed in

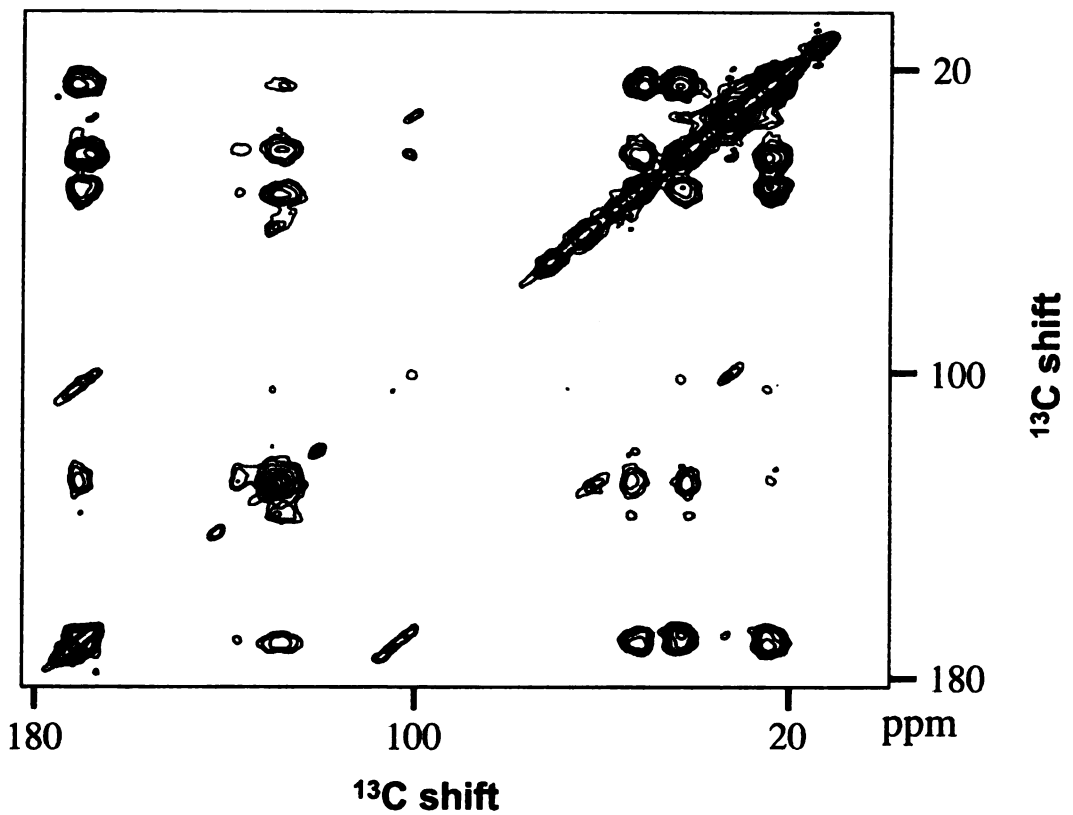

Figure 20. 2D ^{13}C-^{13}C contour plot spectrum of HFP-U3 associated with LM3 lipid mixture at –50 °C. The 2D data was obtained with a proton-driven spin difussion sequence using a 100 ms exchange time. The crosspeaks between Phe ar. 2-6 and Leu C_γ are observed because of the longer exchange time. The MAS frequency was 6.8 kHz and the spectrum processed with 100 Hz Gaussian line broadening in both dimensions.

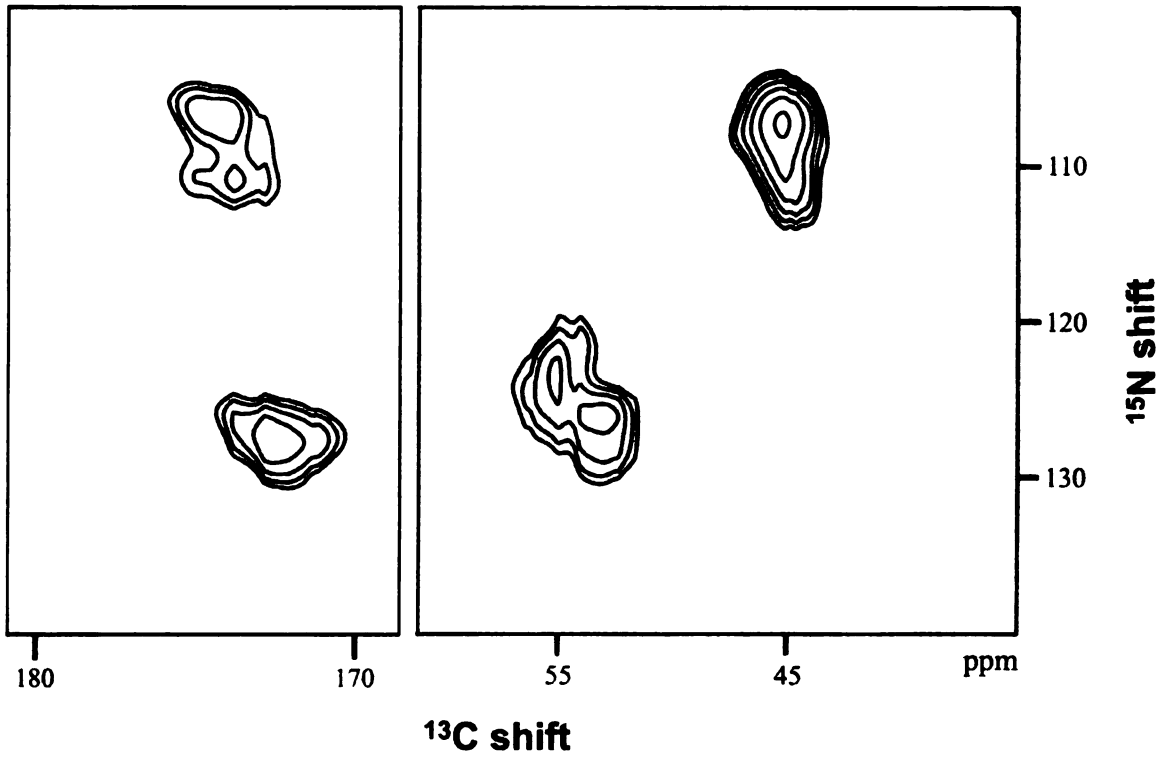

Figure 21. 2D NCO (left) and NCA (right) spectra of HFP-U3 associated with LM3 membranes using the same sample as in Figure 18. The MAS frequency was 7.0 kHz and the total signal averaging time for each spectrum was ~3 days. The spectra were processed with 100 Hz Gaussian line broadening in the ^{15}N dimension and 150 Hz Gaussian line broadening in the ^{13}C dimension. The NCO spectrum correlates $^{15}N_i/^{13}CO_{i-1}$ nuclei and the NCA spectrum correlates $^{15}N_i/^{13}C\alpha_i$ nuclei.

Table1. The assignment relies on comparison of the $^{15}N/^{13}C$ and intra-residue $^{13}C/^{13}C$ crosspeak shifts with characteristic ^{13}C and ^{15}N shifts of each residue type. The ^{13}C sidechain and Gly ^{13}CO shifts were obtained from analysis of the ^{13}C-^{13}C spectra, the Leu ^{13}CO, Gly $^{13}C\alpha$, and ^{15}N shifts were obtained from analysis of the NCO and NCA spectra, and the Phe $^{13}C\alpha$, Phe ^{13}CO, and Leu $^{13}C\alpha$ shifts were the average of the shifts obtained from analysis of the ^{13}C-^{13}C and the ^{15}N-^{13}C spectra. For a given nucleus, the typical variation in shift between different spectra is ~0.1 ppm and the largest variation is 0.5 ppm.

Figure 22 presents the difference between experimental ^{13}C shifts and characteristic helical or β strand shifts.[9] The experimental chemical shifts appear to be more consistent with β strand conformation. An interesting feature of the NCA and NCO spectra is the observation of two Gly-10 ^{15}N chemical shifts which correlate to two Leu ^{13}CO and two Gly $^{13}C\alpha$ shifts. One possible assignment of the shift doubling is distinct populations of parallel and antiparallel strand arrangements. This hypothesis is consistent with a previous REDOR study showing a mixture of parallel and antiparallel strand arrangements.[10]

The success of the complete assignment of the HFP-U3 uniformly labeled peptide associated with LM3 prompted the addition of more uniformly labeled amino acid residues to the sequence. HFP-U12 peptide was synthesized and cross-linked with twelve sequential uniformly ^{13}C and ^{15}N labeled residues between Gly-5 and Gly-16.

Figure 23 displays a 2D ^{13}C-^{13}C correlation spectrum of the HFP-U12 dimer associated with LM3. The displayed spectra were obtained from –50 °C data and the observed crosspeaks were a result of magnetization exchange driven by 10 ms PDSD

Table 1. ^{13}C and ^{15}N chemical shift assignments for HFP-U3 associated with LM3.

	Cα	Cβ	Cγ	Cδ	C_1	C_{2-6}	CO	N
Phe-8	55.4	43.6			139.3	131.2	172.9	123.5
Leu-9	53.2	46.4	27.3	24.5			174.3 173.8	126.7
Gly-10	45.2 44.6						171.1	107.1 110.8

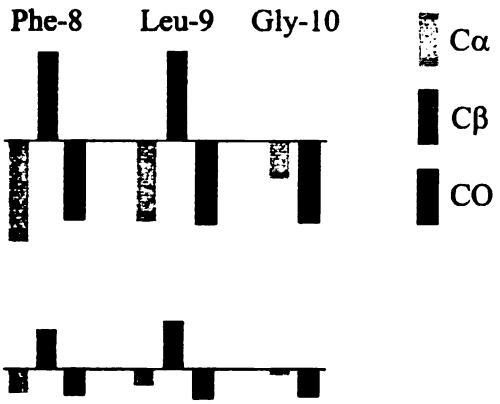

Figure 22. Differences between experimental ^{13}C chemical shifts and characteristic helical (top) or β strand (bottom) ^{13}C shifts for HFP-U3 associated with LM3 membranes. The vertical scale is 10 ppm/inch and each bar in the legend represents 3 ppm. The horizontal lines represent 0 ppm shift difference. In cases of two experimental shifts for a single nucleus, the bar height was calculated using the average shift. There appears to be better agreement with the β strand shifts.

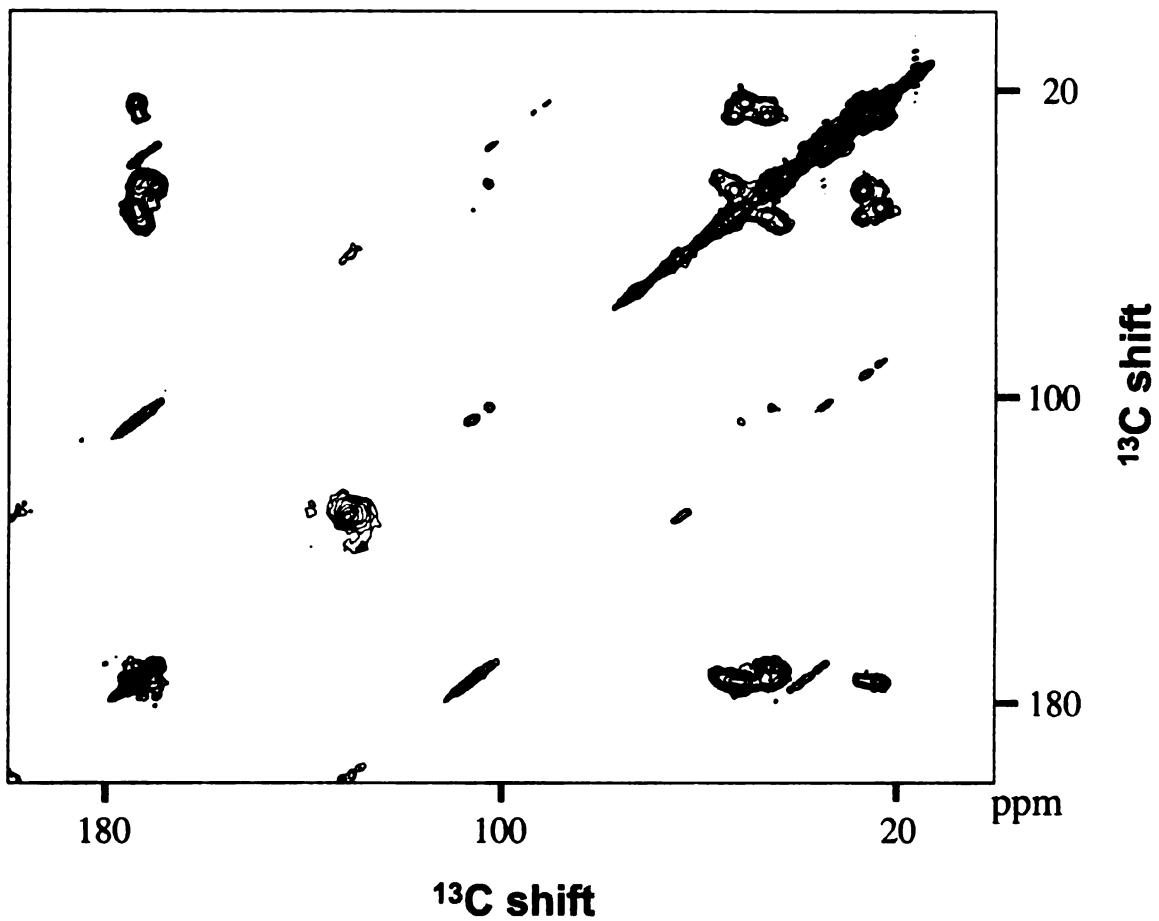

Figure 23. 2D ^{13}C-^{13}C contour plot spectrum of HFP-U12 associated with LM3 membranes. The peptide:lipid mol ratio was ~0.02, the sample pH was 7.0, and the sample volume in the 4 mm rotor was ~30 μl with ~0.4 μmol HFP-U12. The data were collected with proton-driven spin diffusion with 10 ms exchange time and signal averaging time of ~4.5 days. The MAS frequency was 6.8 kHz. The spectrum was processed with 100 Hz Gaussian line broadening in each dimension.

exchange time. Figure 24 displays a 2D ^{13}C-^{13}C correlation spectrum of the HFP-U12 dimer associated with LM3. This spectrum shows crosspeaks similar to those observed in Figure 23.

Figure 25 displays 2D NCO (left) and NCA (right) correlation spectra for the HFP-U12/LM3 sample. The NCO spectrum displays two groups of crosspeaks. The group with upfield ^{15}N shifts corresponds to the L9/G10, L12/G14, and A15/G16 crosspeaks and shows a doubling of the ^{15}N Gly shift as was observed in the HFP-U3 sample. The group with downfield ^{15}N shifts is a superposition of crosspeaks from the other eight $^{13}CO/^{15}N$ pairs in the peptide. There are peaks with ^{13}CO shifts at ~174.7, 173.9, 172.6, and 170.8 ppm which respectively correlate with the Ala, Leu, Phe, and Gly ^{13}CO shifts observed in the ^{13}C-^{13}C spectra of the sample. The respective ^{15}N shifts are 121.8, 125.1 122.9, and 120.7 ppm. Consideration of these ^{13}CO and ^{15}N shifts and the sequential $^{13}CO/^{15}N$ pairs in this region suggests the following ^{15}N assignments: 125.1 ppm – F8; 122.9 ppm – L9, L12; 121.8 ppm – L7, A15; and 120.7 ppm – F11, A14. In the NCA spectrum, there are two groups of crosspeaks which can be generally assigned to Gly (upper right) and non-Gly (lower left) residues. In Table 2, all of the ^{13}C shifts except for Gly $^{13}C\alpha$ are derived from analysis of the 2D ^{13}C-^{13}C spectra, while the Gly $^{13}C\alpha$ and all of the ^{15}N shifts are derived from the analysis of the NCO and NCA spectra.

Figure 26 displays differences between the experimental ^{13}C shifts of the HFP-U12 sample and characteristic helical or β strand ^{13}C shifts.[9] There is a better agreement with the β strand shifts.

Figure 27 displays comparative 2D ^{13}C-^{13}C spectra of HFP-U3/LM3 samples taken on a 400 MHz (left) or 700 MHz (right) spectrometer. Both spectra were processed

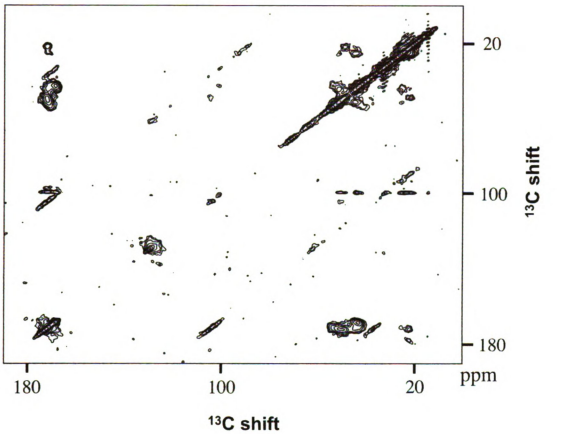

Figure 24. 2D ^{13}C- ^{13}C contour plot spectrum of HFP-U12 associated with hydrated LM3 membranes. The peptide to lipid molar ratio was ~0.02, the buffer pH was 7.0 and the sample volume in the 4 mm rotor was ~30 μl, with ~0.4 μmol HFP-U12. The RFDR spectrum was collected with a 4 ms exchange time and signal averaging time of ~4.5 days. The spectrum was processed with 100 Hz Gaussian line broadening in each dimension.

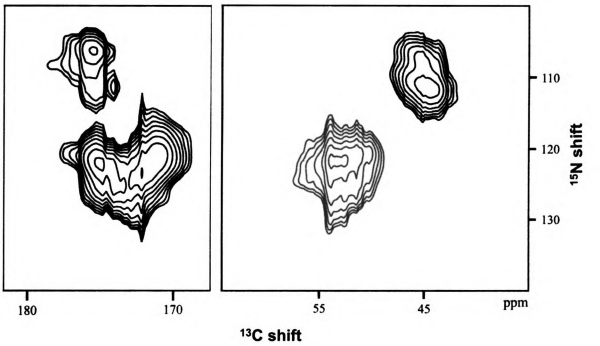

Figure 25. 2D NCO (left) and NCA (right) spectra of HFP-U12 associated with LM3 membranes using the same sample as in Figure 23. The MAS frequency was 7.0 kHz. Signal averaging times were ~5 and ~4 days for the NCO and NCA spectra, respectively. Spectra were processed using 100 Hz Gaussian line broadening in the ^{15}N dimension and 150 Hz Gaussian line broadening in the ^{13}C dimension. In the two spectra, the regions with upfield ^{15}N shifts include peaks which correlate with ^{15}N from Gly residues and the regions with downfield ^{15}N shifts include peaks which correlate with ^{15}N from non-Gly residues.

Table 2. ^{13}C and ^{15}N chemical shift assignments for HFP-U12 associated with LM3.

	Cα	Cβ	Cγ	Cδ	C_1	C_{2-6}	CO	N
Phe	55.8	44.0			138.7	130.6	173.2	125.1(F8),120.7(F11)
Leu	53.0	46.5	27.2	23.8			173.7	121.8(L7), 122.9(L9,L12)
Ala	51.1	23.8					175.2	120.7(A6,A14), 121.8(A15)
Gly	45.2 44.6						170.6	107.0 111.4

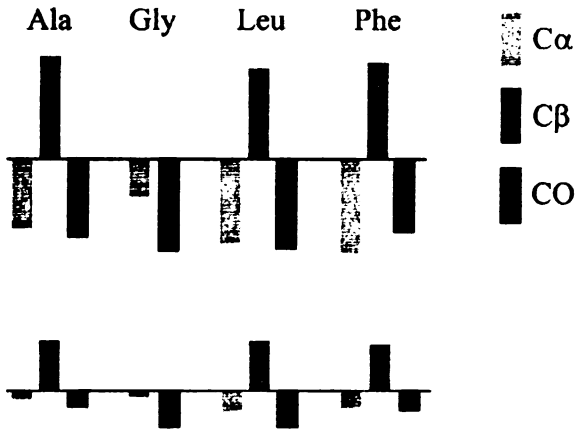

Figure 26. Differences between experimental ^{13}C chemical shifts and characteristic helical (top) or β strand (bottom) ^{13}C shifts for HFP-U12 associated with LM3. The vertical scale is 10 ppm/inch and each bar in the legend represents 3 ppm. The horizontal lines represent 0 ppm shift difference. In cases of two experimental shifts for a single nucleus, the bar height was calculated using the average shift. There appears to be better agreement with the β strand shifts.

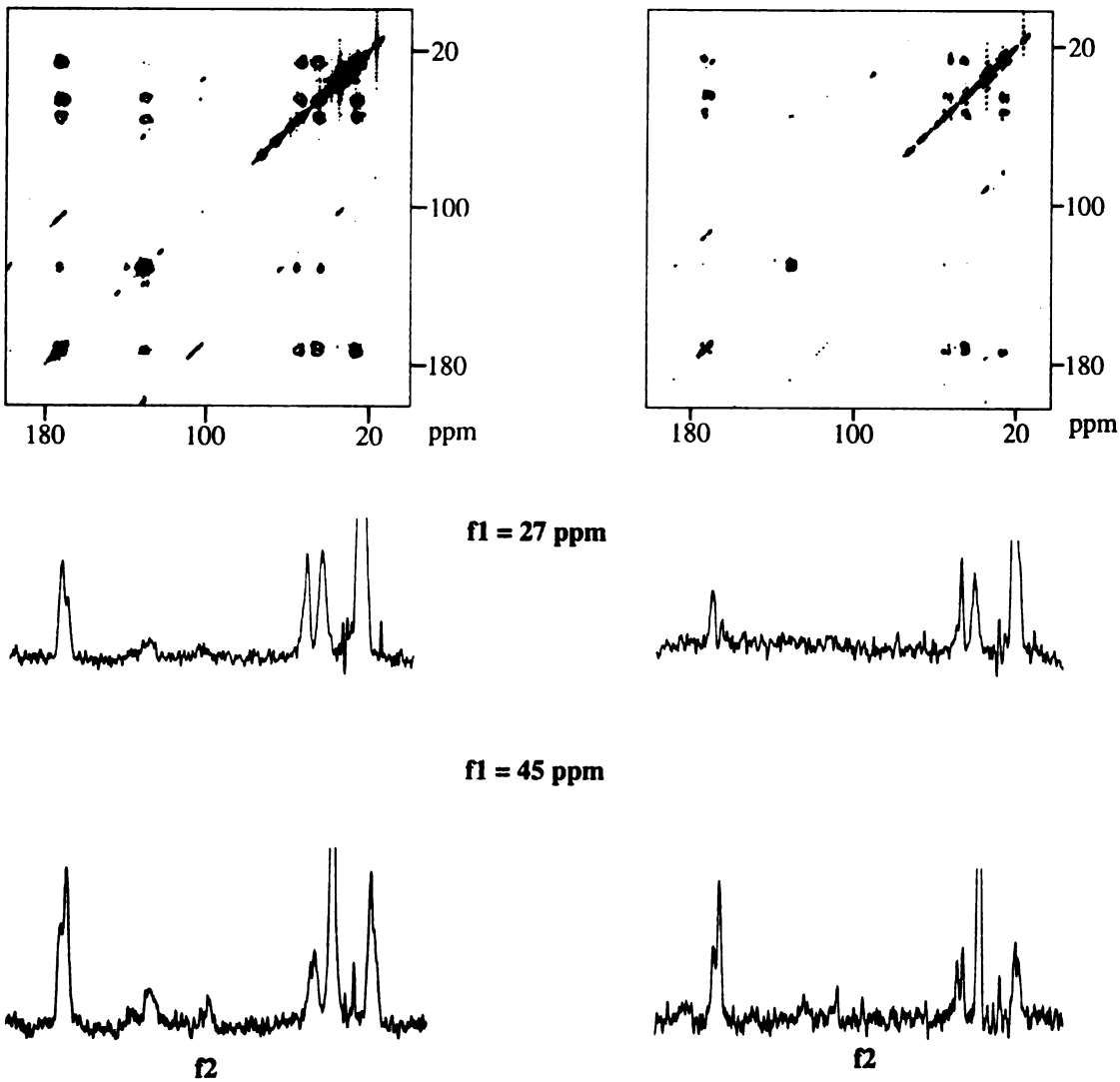

Figure 27. 2D ^{13}C-^{13}C contour plot spectra of HFP-U3 associated with LM3 membranes obtained with either a 400 MHz (left) or 700 MHz (right) spectrometer. The 1D spectra display slices in the f_2 dimension for f_1=27 ppm and f_1=45 ppm. The peptide:lipid mol ratio was ~0.04 with ~0.8 μmol HFP-U3. The 400 MHz spectrum was obtained using PDSD sequence with 6.8 kHz MAS frequency and with ~5 days signal averaging time and was processed with 60 Hz Gaussian line broadening in each dimension. The 700 MHz spectrum was obtained using PDSD sequence with 10 kHz MAS frequency and with ~1 day signal averaging time and was processed with 100 Hz Gaussian line broadening in each dimension. Relative to 400 MHz, the ppm linewidths at 700 MHz are narrower by a factor of ~0.6.

with ~0.6 ppm Gaussian line broadening in each dimension, and relative to 400 MHz, the ppm linewidths of the 700 MHz spectrum are narrower by a factor of ~0.6. For the Leu-9 $^{13}C\beta/^{13}C\alpha$ and $^{13}C\gamma/^{13}C\alpha$ crosspeaks in the 700 MHz spectrum, the Leu-9 $^{13}C\alpha$ linewidth in the f_2 dimension is ~1.4 ppm. Although the reduction in linewidth with increased field is not yet well-understood, one contribution is attenuation of the ^{13}C-^{13}C J and dipolar couplings at the higher field. Because of this favorable linewidth effect, assignment of membrane-associated FPs with U-^{13}C, ^{15}N labeling will likely be more straightforward at higher field.

Assignments and secondary structure

The HFP-U3 sample is an example of scatter-uniform FP labeling where only one residue type is uniformly labeled over the entire peptide. Nearly unambiguous assignment was possible from 2D ^{13}C-^{13}C and ^{15}N-^{13}C spectra at 400 MHz. The HFP-U12 is an example of more extensive FP labeling and only residue-type assignment was possible. The chemical shifts suggest that the HFP-U12 sample had predominant β strand conformation over the labeled residues. Unambiguous assignment has been achieved for U-^{13}C, ^{15}N labeled microcrystalline proteins of 50-110 residues and the difficulties for the membrane-associated FPs are larger linewidths (by a factor of ~25 in 2D crosspeak area) and lower dispersion because of a single secondary structure rather than mixed secondary structure. In this regard, the FP samples are similar to β-amyloid for which scatter-uniform labeling was necessary for a complete unambiguous assignment. The 700 MHz spectrum suggests that experiments at higher field may lead to improved resolution for FP samples.

In both the HFP-U3 and HFP-U12 NCA spectra, each Gly $^{15}N/^{13}C\alpha$ region appears to be a combination of two peaks, which have ^{15}N shifts of ~107 and ~111 ppm. However, in the HFP-U3 spectrum, the 107 ppm peak is larger while in the HFP-U12 spectrum, the 111 ppm peak is larger. Quantitatively, the 107/111 ppm intensity ratio is ~0.8 and ~1.4 in the HFP-U3 and HFP-U12 spectra respectively. One hypothesis for this different intensity ratio is different ratios of parallel and antiparallel strand arrangements. The cysteine crosslinking in HFP-U12 might favor parallel strand arrangement as opposed to the mixed parallel/antiparallel arrangement known for HFP-U3. A parallel arrangement could lead to alignment of apolar regions on adjacent strands. The resulting large apolar volume could induce a larger local perturbation to membranes and be a structural basis for the experimentally higher fusion rate of crosslinked HFP's.

Conclusions

2D $^{13}C/^{13}C$ and $^{13}C/^{15}N$ correlation spectra of the HFP-U3/LM3 sample were used to give insight into the secondary structure over the three uniformly labeled residues in the peptide chain. The chemical shifts were determined using a number of sequences including: PDSD, RFDR, NCA, NCO. The differences between the measured ^{13}C shifts and the known shifts for characteristic helix and β strand were used to determine the secondary structure. The differences between the shifts were smallest for the β strand structure, which suggests that the structure over the labeled residues is β strand.

2D $^{13}C/^{13}C$ and $^{13}C/^{15}N$ correlation spectra of the HFP-U12 dimer associated with LM3 showed that only a residue type chemical shift assignment could be made at 400 MHz. The measured chemical shifts were subtracted from the known shifts for helix and β strand and smaller differences were observed for β-strand values. Spectra could be

better resolved at higher field because of the narrower resonances arising from attenuation of the ^{13}C-^{13}C J- and dipolar couplings. This phenomenon has been shown using the HFP-U3 sample at 700 MHz where the linewidths were narrower by a factor of ~ 0.6. In addition, sensitivity should be improved at higher field and will be beneficial for sequential assignment based on 3D experiments.

References

1. Rienstra, C.M., et al., *2D and 3D N-15-C-13-C-13 NMR chemical shift correlation spectroscopy of solids: Assignment of MAS spectra of peptides.* Journal of the American Chemical Society, 2000. **122**(44): p. 10979-10990.

2. McDermott, A., et al., *Partial NMR assignments for uniformly (C-13, N-15)-enriched BPTI in the solid state.* Journal of Biomolecular Nmr, 2000. **16**(3): p. 209-219.

3. Pauli, J., et al., *Backbone and side-chain C-13 and N-15 signal assignments of the alpha-spectrin SH3 domain by magic angle spinning solid-state NMR at 17.6 tesla.* Chembiochem, 2001. **2**(4): p. 272-281.

4. Castellani, F., et al., *Structure of a protein determined by solid-state magic-angle-spinning NMR spectroscopy.* Nature, 2002. **420**(6911): p. 98-102.

5. Detken, A., et al., *Methods for sequential resonance assignment in solid, uniformly C-13, N-15 labelled peptides: Quantification and application to antamanide.* Journal of Biomolecular Nmr, 2001. **20**(3): p. 203-221.

6. Bennett, A.E., et al., *Chemical-Shift Correlation Spectroscopy in Rotating Solids - Radio Frequency-Driven Dipolar Recoupling and Longitudinal Exchange.* Journal of Chemical Physics, 1992. **96**(11): p. 8624-8627.

7. Bennett, A.E., et al., *Homonuclear radio frequency-driven recoupling in rotating solids.* Journal of Chemical Physics, 1998. **108**(22): p. 9463-9479.

8. Straus, S.K., T. Bremi, and R.R. Ernst, *Side-chain conformation and dynamics in a solid peptide: CP-MAS NMR study of valine rotamers and methyl-group relaxation in fully C-13-labelled antamanide.* Journal of Biomolecular Nmr, 1997. **10**(2): p. 119-128.

9. Zhang, H.Y., S. Neal, and D.S. Wishart, *RefDB: A database of uniformly referenced protein chemical shifts.* Journal of Biomolecular Nmr, 2003. **25**(3): p. 173-195.

10. Yang, J. and D.P. Weliky, *Solid State Nuclear Magnetic Resonance Evidence for Parallel and Antiparallel Strand Arrangements in the Membrane-Associated HIV-1 Fusion Peptide.* Biochemistry, 2003. **42**: p. 11879-11890.

Chapter 5

Scatter Uniform Labeling in the HIV Fusion Peptide

Introduction

SSNMR studies of peptides and proteins with uniform ^{13}C, ^{15}N labeling can provide substantial structural information for development of detailed structural models. This type of SSNMR approach was recently applied to β-amyloid peptide fibrils by Tycko and co-workers and led to an experimentally-based coil-strand-turn-strand structure.[1] Due to the amino acid multiplicity and broad linewidthes, scatter-uniform rather than complete-uniform labeling maybe necessary for the unambiguous CS assignment of individual residues with 2D SSNMR. In scatter-uniform labeling, only one residue of each amino acid type is U-^{13}C, ^{15}N-labeled and the distinct ^{13}C-^{13}C correlations of each amino acid type make unambiguous CS assignment fairly straightforward. ^{13}C-^{13}C correlation spectra will be used to determine ^{13}C CSs at the labeled residues and will be input into the TALOS program which will provide best fit values for the secondary structure (ϕ,ψ) angles.[2]

Sedimentation Equilibrium

Figure 28 displays the results of the sedimentation equilibrium experiment at 20 °C for the HFP-DimerC sample with a concentration of 50 μM in 5 mM HEPES buffer at pH 7.4. The rotor speed was 48000 rpm. The top panel shows that the differences between the experimental and fitted absorbances were small (< 0.04) and random as a function of r, which indicates that a single-species model is reasonable. The bottom

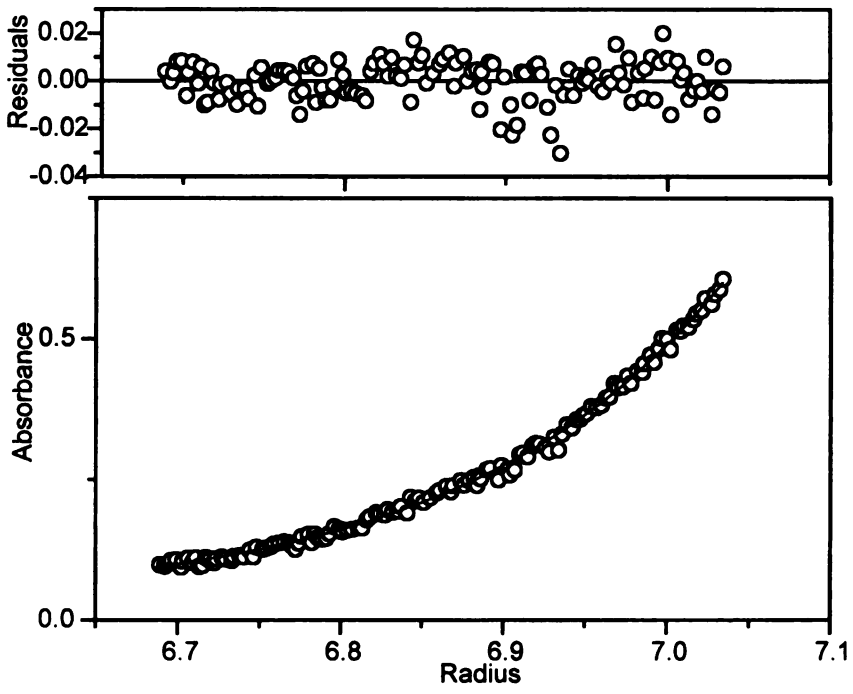

Figure 28. Sedimentation equilibrium experiments of 50 mM HFP-DimerC. The main panel shows the absorbance at 280 nm as a function of the centrifugal radius after reaching equilibrium. The best fit to the model for a single species was obtained with a molecular weight of ~ 3690 which is shown as a solid line through the experimental data. The upper panel shows the residuals between the data and the fit.

panel displays the 280 nm absorbance as a function of centrifugal radius with a partial specific volume of 0.7610 ml/g and a solvent density of 1.0 g/ml. The optimal fit of the data was determined by a non-linear least squared method with a molecular weight of ~ 3690 g/mol. The molecular weight is larger than the monomeric molecular weight of 3203.8 g/mol, but smaller than the dimeric molecular weight of 6407.6 g/mol. A molecular weight of 3690 g/mol suggests that the HFP-DimerC fusion peptide is a mixture of both monomer and dimer. In previous work with HFP dimer at a 45000 rpm a molecular mass of 4800 g/mol was observed.[3] The actual molecular mass of the HFP dimer was 6364 g/mol. Using the same sample but spinning at 3200 rpm a molecular mass of ~ 5700 g/mol was observed for the dimer, which was in better agreement with the correct value.[3]

2D Correlation Spectra

Figures 29 and 30 display 2D ^{13}C-^{13}C correlation spectra for the HFP-DimerA sample, with magnetization exchange driven by 10 and 100 ms PDSD respectively. Only intra-residue crosspeaks were observed in Figures 29 and 30 whereas sequential inter-residue crosspeaks were observed in 100 ms PDSD spectra of previous samples. In HFP-U3 and HFP-U12, samples the uniformly labeled residues were next to each another in the sequence. In the five HFP-Dimer samples, the uniformly labeled residues were further away from one another. The 10 ms PDSD 2D ^{13}C-^{13}C correlation spectrum displayed in figure 31 for the HFP-DimerB sample also shows only intra-residue crosspeaks. Figure 32 shows the 100 ms PDSD 2D ^{13}C-^{13}C correlation spectrum where only intra-residue crosspeaks were observed. Not all of the expected crosspeaks were observed for the Phe residue in the 10 ms correlation spectrum. The crosspeaks between

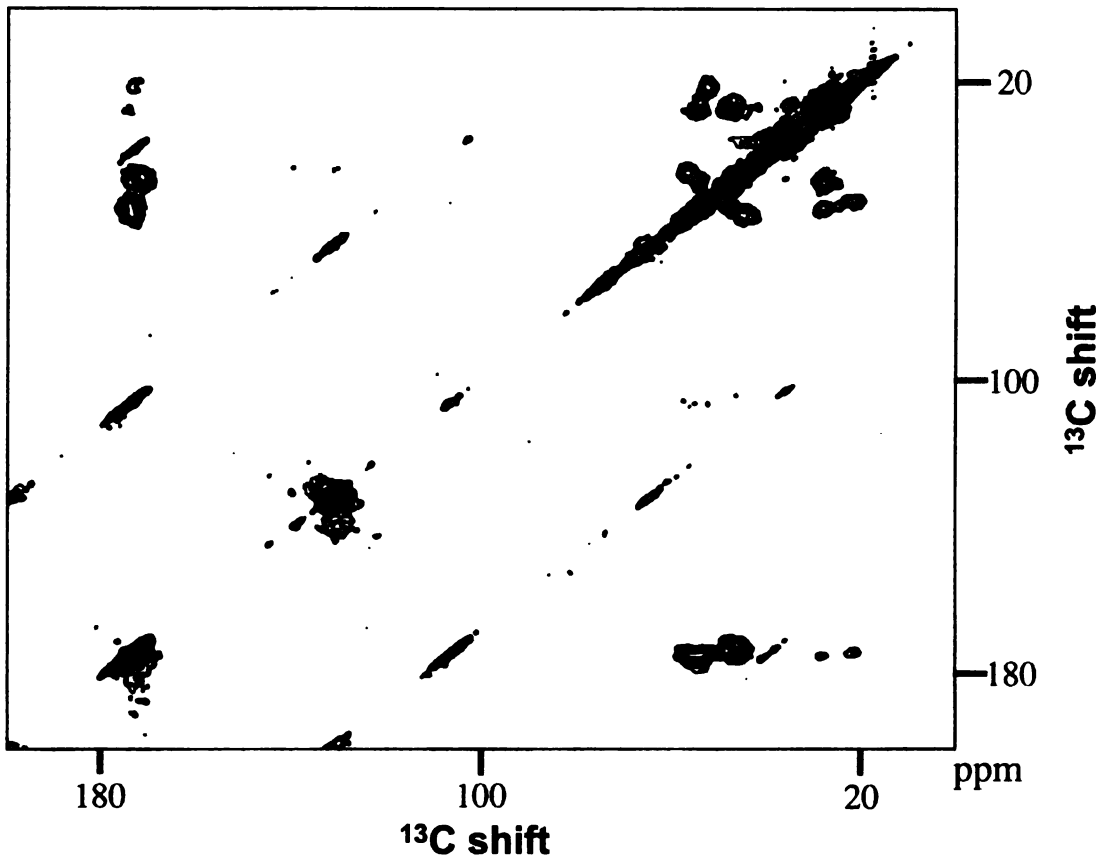

Figure 29. 2D ^{13}C- ^{13}C contour plot spectrum of HFP Dimer A associated with hydrated LM3. The peptide to lipid molar ratio was ~0.04 with ~ 0.8 mmol HFP Dimer A. Uniformly labeled residues were at: Ala-1, Gly-3, Phe-8, and Leu-12.The buffer was at pH 7.0, and the sample volume in the 4 mm rotor was ~30 ml. Data were collected with proton-driven spin diffusion with a 10 ms exchange time and total signal averaging time of ~57 hrs. The MAS frequency was 6.8 kHz. The spectrum was processed with 100 Hz Gaussian line broadening in each dimension.

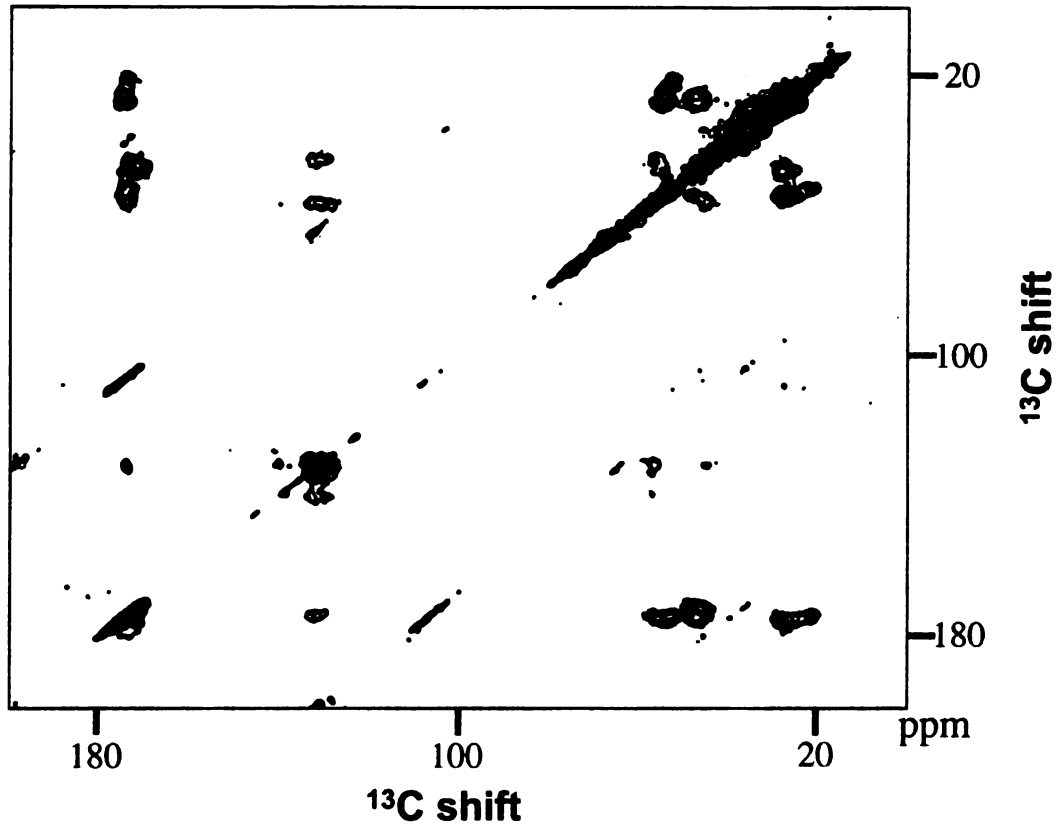

Figure 30. 2D ^{13}C- ^{13}C contour plot spectrum of HFP Dimer A associated with hydrated LM3. The peptide to lipid molar ratio was ~0.04 with ~ 0.8 mmol HFP Dimer A. The buffer was at pH 7.0, and the sample volume in the 4 mm rotor was ~30 ml. Data were collected with proton-driven spin diffusion with a 100 ms exchange time and total signal averaging time of ~62 hrs. The MAS frequency was 6.8 kHz. The spectrum was processed with 100 Hz Gaussian line broadening in each dimension.

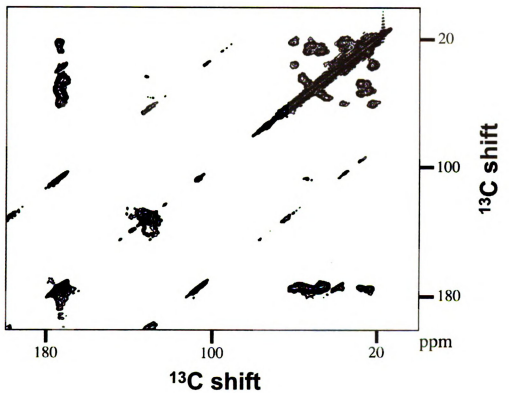

Figure 31. 2D ^{13}C- ^{13}C contour plot spectrum of HFP Dimer B associated with hydrated LM3. The peptide to lipid molar ratio was ~0.04 with ~ 0.8 mmol HFP Dimer B. Uniformly labeled residues were at: Val-2, Leu-7, Phe-11, Ala-14, and Gly-16. The buffer was at pH 7.0, and the sample volume in the 4 mm rotor was ~30 ml. Data were collected with proton-driven spin diffusion with a 10 ms exchange time and total signal averaging time of ~57 hrs. The MAS frequency was 6.8 kHz. The spectrum was processed with 100 Hz Gaussian line broadening in each dimension.

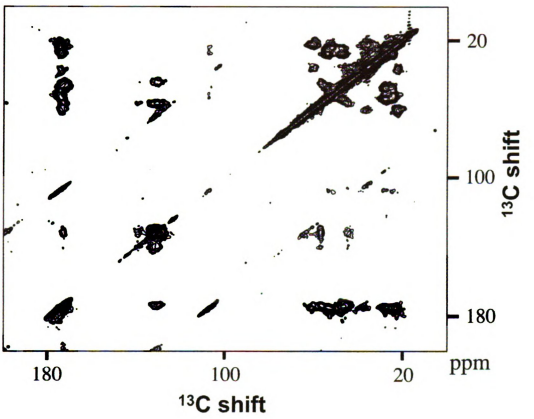

Figure 32. 2D ^{13}C- ^{13}C contour plot spectrum of HFP Dimer B associated with hydrated LM3. The peptide to lipid molar ratio was ~0.04 with ~ 0.8 mmol HFP Dimer B. The buffer was at pH 7.0, and the sample volume in the 4 mm rotor was ~30 ml. Data were collected with proton-driven spin diffusion with a 100 ms exchange time and total signal averaging time of ~62 hrs. The MAS frequency was 6.8 kHz. The spectrum was processed with 100 Hz Gaussian line broadening in each dimension.

^{13}C in the phenyl ring and ^{13}CO, $^{13}C\alpha$, and $^{13}C\beta$ were absent from the spectra. Crosspeaks were observed between the ^{13}C in the ring and $^{13}C\alpha$ and $^{13}C\beta$ in Figure 32.

2D ^{13}C-^{13}C correlation spectra are shown in figures 33, figure 34, and figure 35 for the three remaining HFP samples. From this collection of data, a ^{13}C assignment can be made for resides 1-16, and residue 21 as shown in table 3. Figure 36 displays a graphical representation of the difference between the experimental chemical shifts and the characteristic helical or β strand ^{13}C shifts.[4] The best agreement was observed for the β strand ^{13}C shifts.

Figure 34 displays the 10 ms PDSD correlation spectrum for Dimer D associated with LM3. In this spectrum, crosspeaks are observed between Gly-10 Cα and the spinning side band of Gly-10 ^{13}CO. This sample also shows crosspeaks between Ala-6 $^{13}C\alpha$ and $^{13}C\beta$ to the spinning side band of Ala-6 ^{13}CO. For this spectrum, the two spin systems are isolated from one another and only intra-residue crosspeaks were observed. When the spin system is at equilibrium, the crosspeaks are of equal integrated intensity compared to the isotropic peaks along the diagonal. HFP-U3 was also labeled at Gly-10 along with Leu-8 and Phe-9 where the ratio of Gly-10 $^{13}CO/^{13}C\alpha$ to $^{13}C\alpha/^{13}C\alpha$ was 0.232. In Dimer D the ratio is 0.414; thus, it appears as though the Ala-6/Gly-10 spin system is closer to equilibrium. The $^{13}CO/^{13}C\alpha$ to $^{13}C\alpha/^{13}C\alpha$ ratio is even higher for Ala-6 at 0.5241 in the Dimer D sample. For HFP-U3, the uniformly labeled residues are next to each other and the magnetization can move between the residues.

Figure 37 displays a 10 ms PDSD correlation spectrum of the setup sample UNAL. Crosspeaks are observed from $^{13}C\alpha$ to $^{13}C\beta$, $^{13}C\gamma$, $^{13}C\delta$, ^{13}CO upfield, ^{13}CO downfield, and the ssb for both ^{13}CO shifts. The downfield ^{13}CO was directly

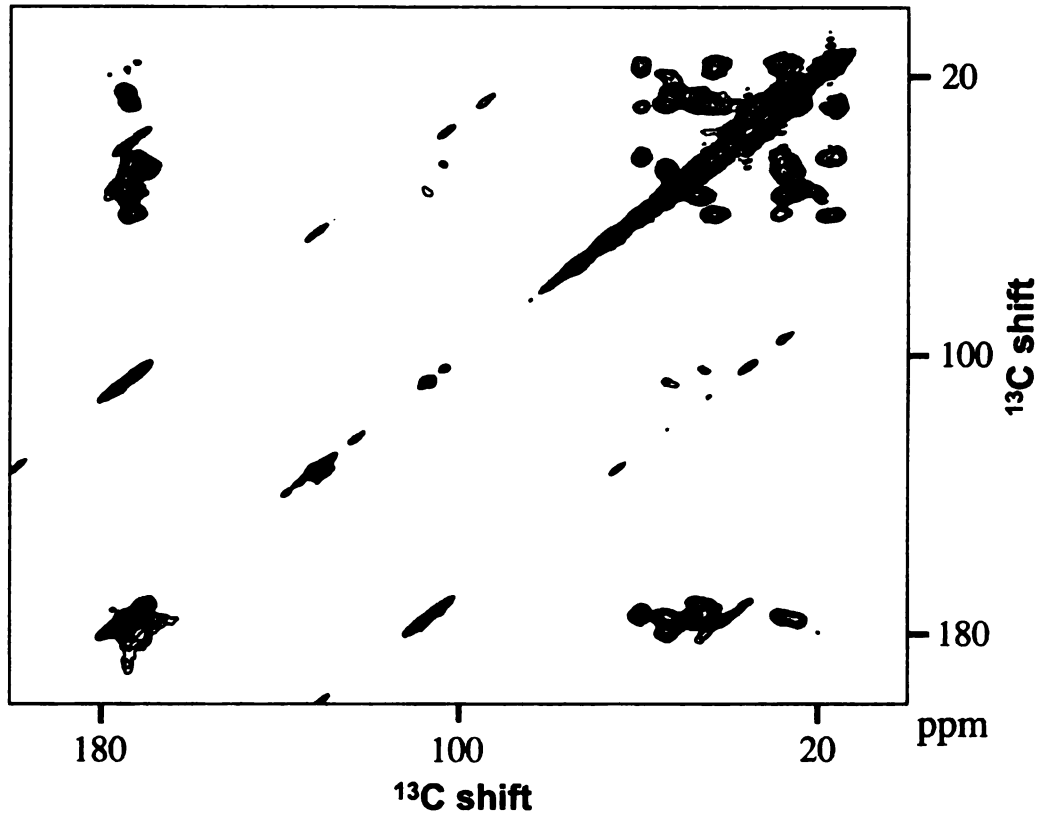

Figure 33. 2D ^{13}C- ^{13}C contour plot spectrum of HFP Dimer C associated with hydrated LM3. The peptide to lipid molar ratio was ~0.04 with ~ 0.8 mmol HFP Dimer C. Uniformly labeled residues were at: Ile-4, Leu-9, Gly-13, and Ala-15. The buffer was at pH 7.0, and the sample volume in the 4 mm rotor was ~30 ml. Data were collected with proton-driven spin diffusion with a 10 ms exchange time and total signal averaging time of ~115 hrs. The MAS frequency was 6.8 kHz. The spectrum was processed with 100 Hz Gaussian line broadening in each dimension.

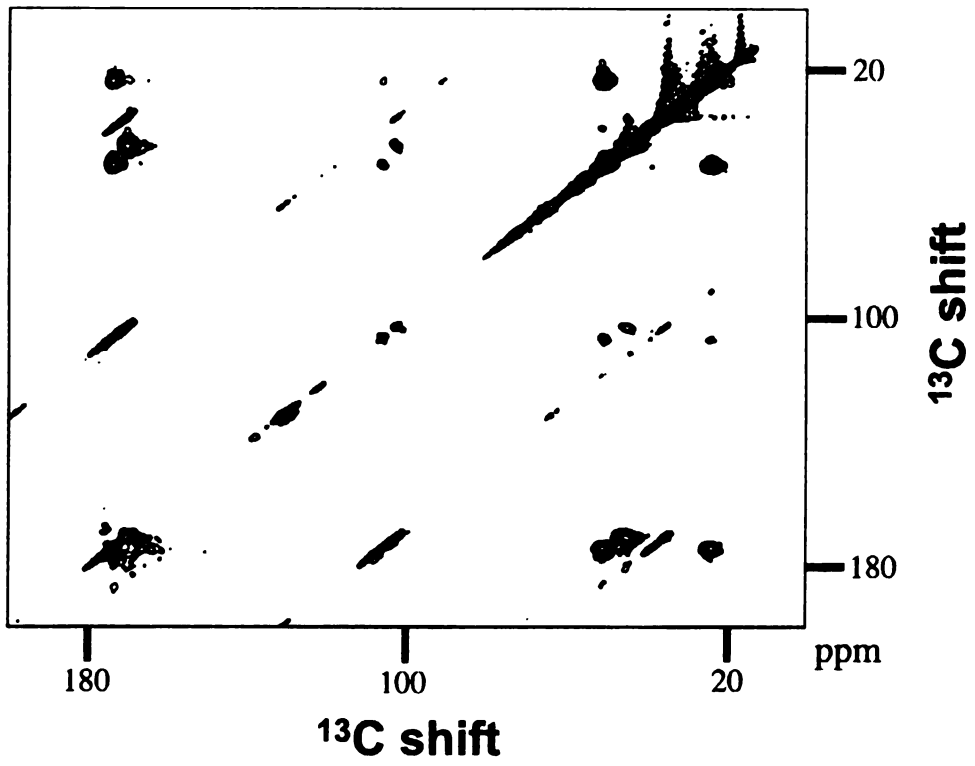

Figure 34. 2D ^{13}C- ^{13}C contour plot spectrum of HFP Dimer D associated with hydrated LM3. The peptide to lipid molar ratio was ~0.04 with ~ 0.8 mmol HFP Dimer D. Uniformly labeled residues were at Ala-6 and Gly-10. The buffer was at pH 7.0, and the sample volume in the 4 mm rotor was ~30 ml. Data were collected with proton-driven spin diffusion with a 10 ms exchange time and total signal averaging time of ~57 hrs. The MAS frequency was 6.8 kHz. The spectrum was processed with 100 Hz Gaussian line broadening in each dimension.

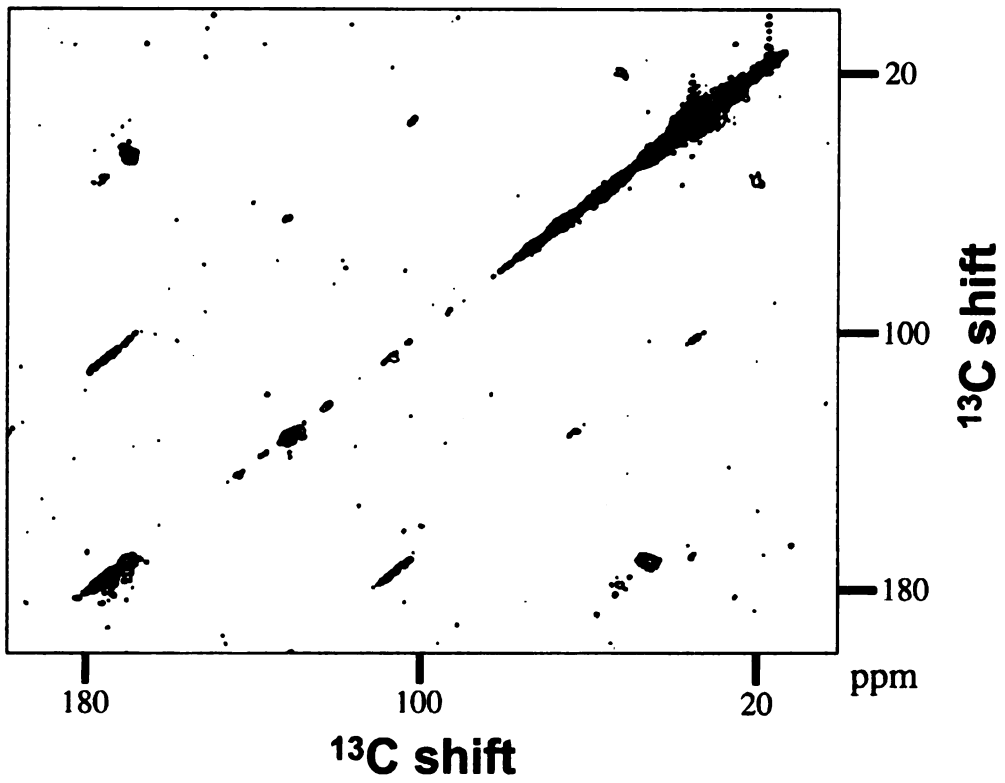

Figure 35. 2D ^{13}C- ^{13}C contour plot spectrum of HFP Dimer E associated with hydrated LM3. The peptide to lipid molar ratio was ~0.04 with ~ 0.8 mmol HFP Dimer E. Uniform labeled residues were at Gly-5 and Ala-21. The buffer was at pH 7.0, and the sample volume in the 4 mm rotor was ~30 ml. Data were collected with proton-driven spin diffusion with a 10 ms exchange time and total signal averaging time of ~114 hrs. The MAS frequency was 6.8 kHz. The spectrum was processed with 100 Hz Gaussian line broadening in each dimension.

Table 3. ^{13}C chemical shift assignments for SUL-HFPs associated with LM3.

Residue	Cα	Cβ	Cγ	Cε	Cδ	C1	C2-6	CO
Ala-1	52.0	21.3						173.5
Val-2	60.5	36.2	22.3					174.7
Gly-3	45.5							171.5
Ile-4	59.6	42.9	28.7	18.8	15.8			174.5
Gly-5	45.6							170.3
Ala-6	51.0	23.9						174.2
Leu-7	53.8	47.5	27.8		24.4			174.2
Phe-8	56.0	44.3				139.7	131.1	173.8
Leu-9	53.6	47.1	27.6		19.9			174.7
Gly-10	44.8							170.7
Phe-11	56.5	44.6				140.0	131.2	173.3
Leu-12	53.7	47.1	27.6					174.4
Gly-13	45.6							171.4
Ala-14	51.8	24.3						174.9
Ala-15	52.0	24.6						175.6
Gly-16	45.5							172.4
Ala-21	52.3	18.9						176.7

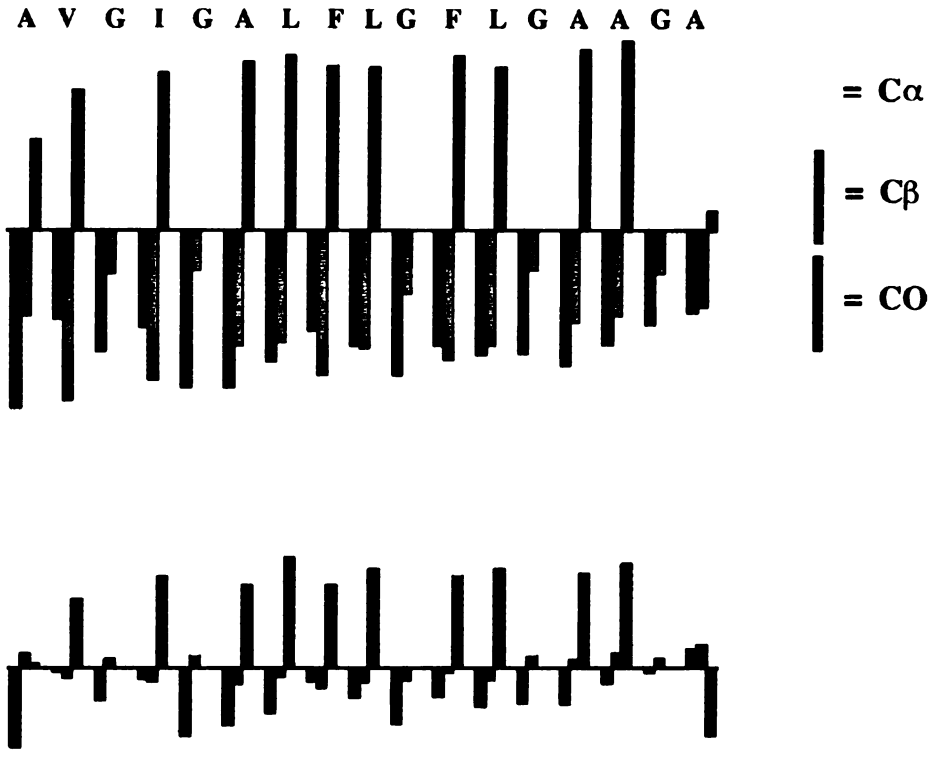

Figure 36. Differences between experimental ^{13}C chemical shifts and characteristic helical (top) or β strand (bottom) ^{13}C shifts for SUL-HFPs associated with LM3 membranes. Each bar in the legend represents 3 ppm. There appears to be better agreement with the β strand shifts.

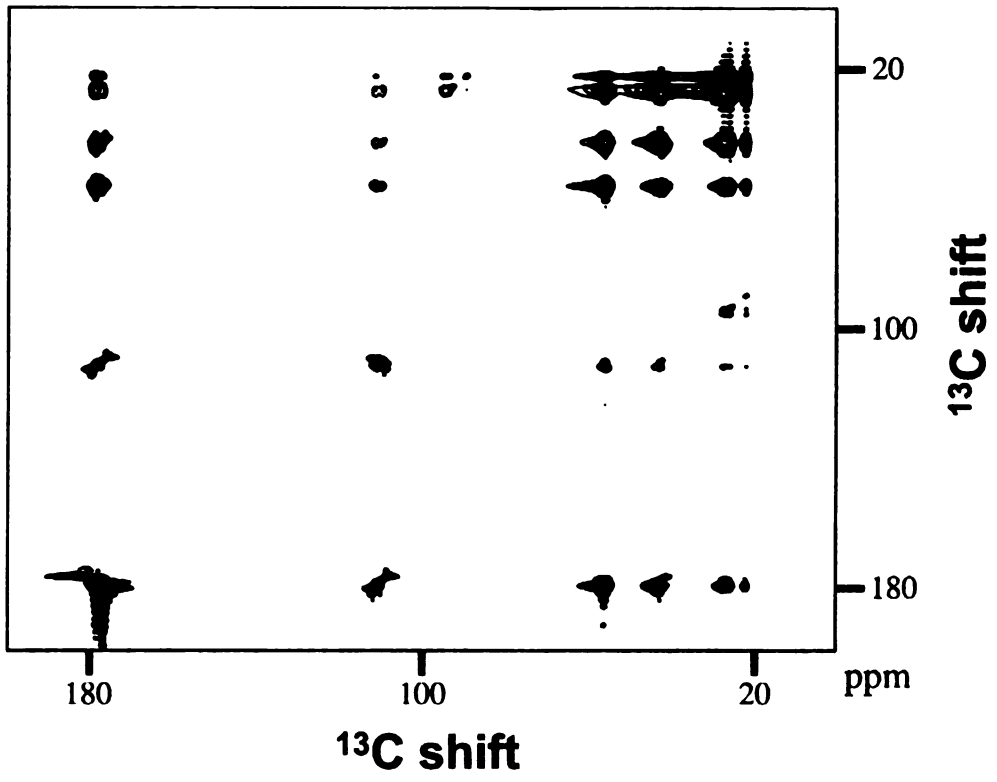

Figure 37. 2D ^{13}C- ^{13}C contour plot spectrum of UNAL. Data were collected with proton-driven spin diffusion with a 10 ms exchange time and total signal averaging time of ~ 54 mins. The MAS frequency was 6.8 kHz and the spectrum was processed with 50 Hz Gaussian line broadening in each dimension.

bonded to the oxygen and the upfield ^{13}CO is directly bonded to the ^{15}N. The ratios of ^{13}CO downfield/$^{13}C\alpha$ to $^{13}C\alpha/^{13}C\alpha$ and ^{13}CO upfield/$^{13}C\alpha$ to $^{13}C\alpha/^{13}C\alpha$ were 0.590 and 0.280 respectively. Compared to the $^{13}CO/^{13}C\alpha$ for Gly-10 and Ala-6, it appears as though the experiment was highly efficient. This high efficiency aids in the observation of the crosspeaks between $^{13}C\alpha$ and the ^{13}CO spinning side bands.

The observed ratios for the upfield and downfield ^{13}CO crosspeaks are very different due to the bonding network. The upfield ^{13}CO is directly bonded to the ^{15}N, so in order for magnetization to exchange between the $^{13}C\alpha$ and ^{13}CO, magnetization has to go through two ^{13}C-^{15}N bonds. Correlation between the upfield ^{13}CO and $^{13}C\alpha$ was only through the ^{13}C-^{13}C bond. The most plausible explanation was that the ^{13}C-^{13}C longitudinal exchange was a resonant process while the ^{13}C-^{15}N exchange was a non-resonant process.

Figure 35 displays the 2D PDSD correlation experiment for Dimer E associated with LM3, which was uniform ^{13}C, ^{15}N labeled at Gly-5 and Ala-21. The ^{13}CO shift for Ala-21 was 176.7 ppm. Previous work reports the ^{13}CO chemical shift for Ala-21 as ~ 177.3 ppm[5] which was corrected for the difference in referencing. This showed a difference of 1.7 ppm compared to the value reported here. An interesting observation in the 2D spectrum is the attenuation of the Ala-21 crosspeak signal intensity compared to the Gly-5 intensity by a factor of ~ 3.4. An explanation of the attenuation of the Ala signal is increased motion at that residue. Motion could attenuate dipolar couplings and decrease the efficiency of ^{1}H-^{13}C cross-polarization (CP) and decrease the efficiency of exchange in the PDSD sequence. This is consistent with a model of insertion of the N-terminal and central residues of the peptide into the membrane and the C-terminus

outside the membrane. In this model, there is greater structure for the residues within the membrane than outside the membrane. This is reasonable because outside of the membrane the peptide is in aqueous buffer and has greater mobility.

The TALOS computer program was used to determine the backbone ψ and ϕ angles over the uniformly labeled residues.[2] This program uses a database which contains $^{13}C\alpha$, $^{13}C\beta$,^{13}CO, ^{15}N, and $^{1}H\alpha$ chemical shifts for a number of proteins where the high resolution X-ray structure and a nearly complete NMR resonance assignment is known. Using a triplet of adjacent residues, experimental chemical shifts were compared to shifts of triplet residues of proteins in the database. TALOS produces the 10 triplets that have the closest chemical shifts and amino acid sequence to the sequence of interest. The ψ and ϕ backbone angles are reported for the center residue in the triplet. The conformation of the first and last residues in the peptide sequence cannot be determined by TALOS. 3% of the predictions given by TALOS for all 20 proteins in the database were wrong.[2]

The $^{13}C\alpha$, $^{13}C\beta$, and ^{13}CO chemical shifts reported in Table 3 were entered into the TALOS program. Table 4 shows the average and standard deviation for both ψ and ϕ angles reported from the analysis. For all residues except the Gly and Ala-21 residues, ten triplets were used to determine the average ψ and ϕ angles. Seven triplets were used in the average of G3, G5, G10, G13, and A21. G16 had only five triplets used in the average and standard deviation. The program excluded values from calculation of the reported average of a single prediction falls well outside the Ramachandran region where the remaining values are located.[2] The low number of reported triplets that were within the Ramachandran region for the Gly and Ala-21 residues adds some ambiguity to the

reported values. β strand conformation was consistent with the ψ and ϕ backbone angles reported in Table 4.

Relatively short exchange time PDSD spectra give insight into secondary structure, but little information is gained about higher order structure such as tertiary or quaternary structure. Tycko found that long exchange time (500 ms to 1500 ms) PDSD spectra provided information about contacts between the side chains and gave insight into the quaternary structure of the β-Amyloid fibrils. The long exchange time spectra can be used to probe ^{13}C-^{13}C distances of ~ 6 angstroms.[6] These type of spectra could be useful in studying the HFPs in membranes because from the crosspeaks insight can be gained about the tertiary or quaternary structure.

Figure 38 displays the 2D PDSD correlation spectrum for Dimer C associated with LM3 using an exchange time of 500 ms. In this spectrum, crosspeaks are only observed within one residue and no inter-residue crosspeaks are observed. Increasing the allowed exchange time might allow crosspeaks to be observed between residues that are quite far apart in the sequence but close in the strucutre. Increasing the exchange time would possibly allow for long-range exchange between residues.

2D PDSD correlation experiments using a 1 s exchange time were carried out on all five SUL samples. Figure 39, 40, 41, 42, 43 display the 1 s PDSD correlation spectra for Dimer A, Dimer B, Dimer C, Dimer D, and Dimer E, respectively. Four out of the five samples only show intra-residue crosspeaks. The one exception was Dimer D where crosspeaks were observed between Ala-6 and Gly-10. All possible crosspeaks between the two residues were observed. Figure 44 displays a 1 s 2D PDSD correlation spectrum of LM3 only. This spectrum shows no observable crosspeaks thus proving that the

Table 4. Residue-specific Phi and Psi angles for SUL-HFPs associated with LM3, predicted from ^{13}C chemical shifts in Table 3.

Residue	ϕ	ψ
V2	-130±9	143±15
G3	-146±16	152±31
I4	-135±14	154±16
G5	-149±13	159±21
A6	-136±14	150±15
L7	-133±16	143±11
F8	-127±15	143±14
L9	-142±11	147±18
G10	-150±12	160±21
F11	-137±10	152±13
L12	-143±10	148±18
G13	-149±13	159±21
A14	-141±9	149±13
A15	-145±8	149±12
G16	-130±26	154±16
A21	-76±9	146±9

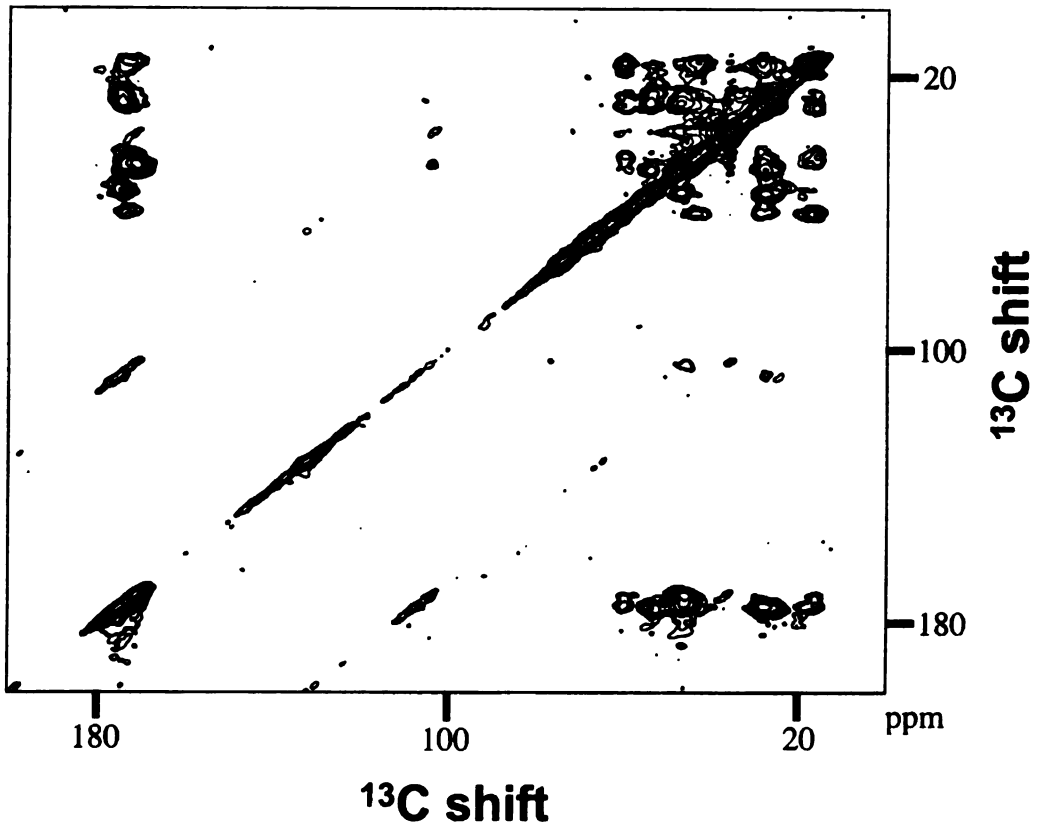

Figure 38 2D ^{13}C- ^{13}C contour plot spectrum of HFP Dimer C associated with hydrated LM3. The peptide to lipid molar ratio was ~0.04 with ~ 0.8 mmol HFP Dimer C. The buffer was at pH 7.0, and the sample volume in the 4 mm rotor was ~30 ml. Data were collected with proton-driven spin diffusion with a 500 ms exchange time and total signal averaging time of ~85 hrs. The MAS frequency was 6.8 kHz. The spectrum was processed with 100 Hz Gaussian line broadening in each dimension.

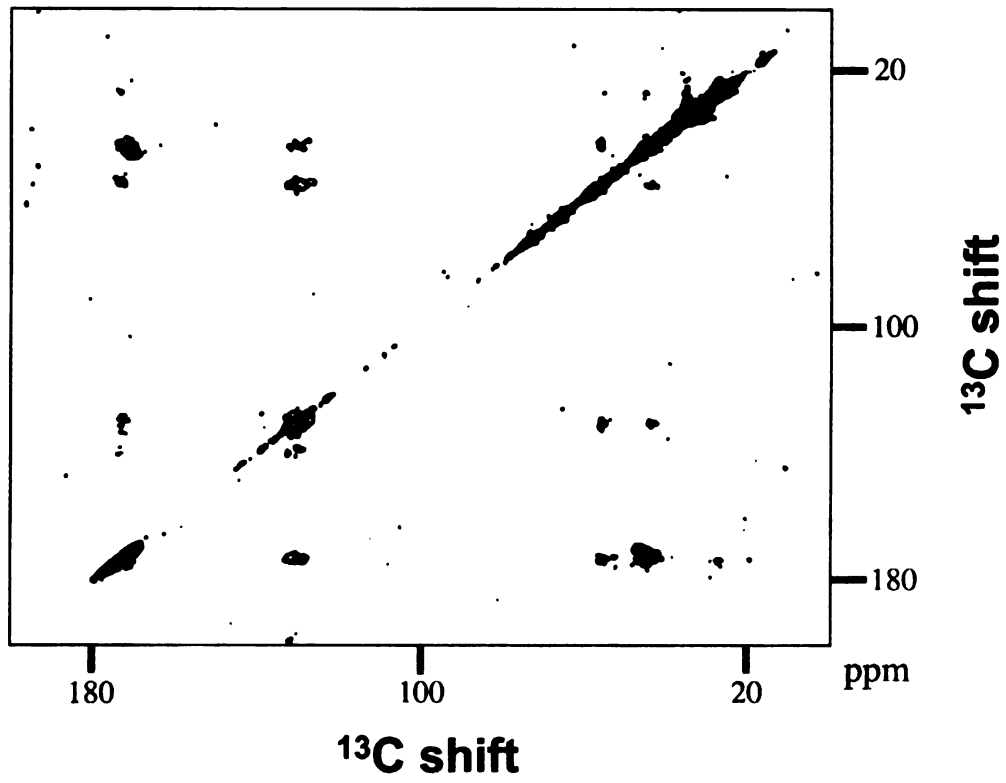

Figure 39. 2D ^{13}C- ^{13}C contour plot spectrum of HFP Dimer A associated with hydrated LM3. The peptide to lipid molar ratio was ~0.04 with ~ 0.8 mmol HFP Dimer A. The buffer was at pH 7.0, and the sample volume in the 4 mm rotor was ~30 ml. Data were collected with proton-driven spin diffusion with a 1 s exchange time and total signal averaging time of ~114 hrs. The MAS frequency was 6.8 kHz. The spectrum was processed with 100 Hz Gaussian line broadening in each dimension.

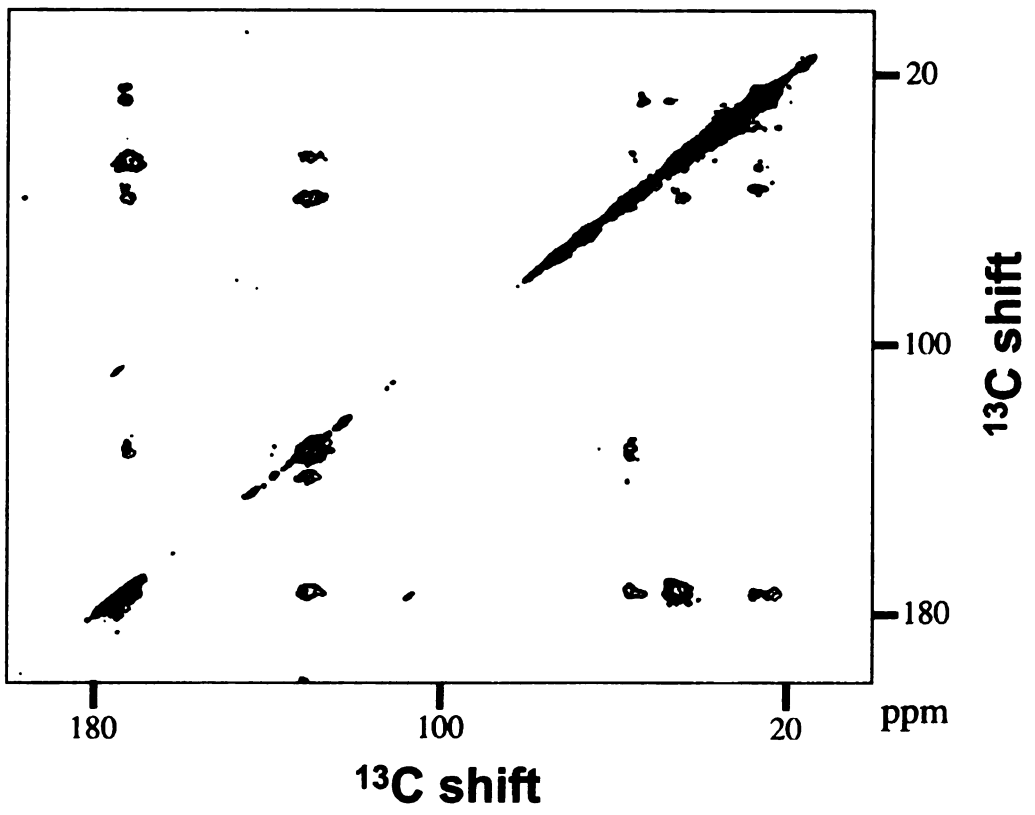

Figure 40. 2D ^{13}C- ^{13}C contour plot spectrum of HFP Dimer B associated with hydrated LM3. The peptide to lipid molar ratio was ~0.04 with ~ 0.8 mmol HFP Dimer B. The buffer was at pH 7.0, and the sample volume in the 4 mm rotor was ~30 ml. Data were collected with proton-driven spin diffusion with a 1 s exchange time and total signal averaging time of ~114 hrs. The MAS frequency was 6.8 kHz. The spectrum was processed with 100 Hz Gaussian line broadening in each dimension.

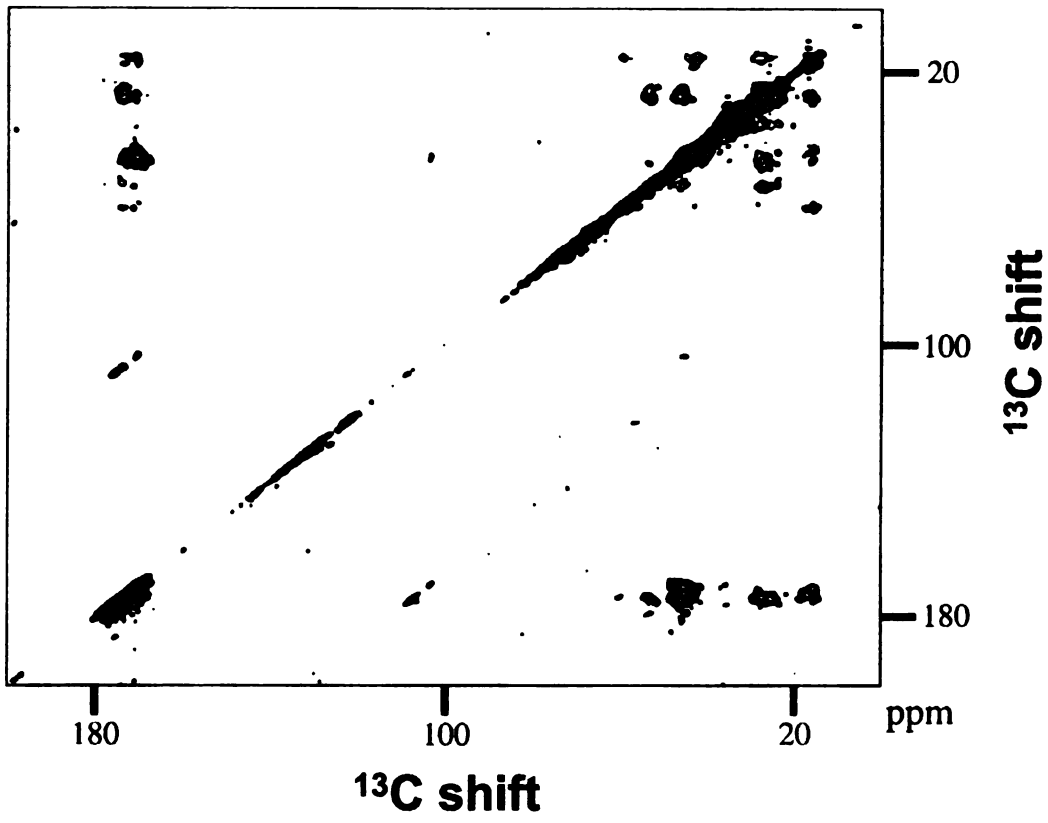

Figure 41. 2D ^{13}C- ^{13}C contour plot spectrum of HFP Dimer C associated with hydrated LM3. The peptide to lipid molar ratio was ~0.04 with ~ 0.8 mmol HFP Dimer C. The buffer was at pH 7.0, and the sample volume in the 4 mm rotor was ~30 ml. Data were collected with proton-driven spin diffusion with a 1 s exchange time and total signal averaging time of ~114 hrs. The MAS frequency was 6.8 kHz. The spectrum was processed with 100 Hz Gaussian line broadening in each dimension.

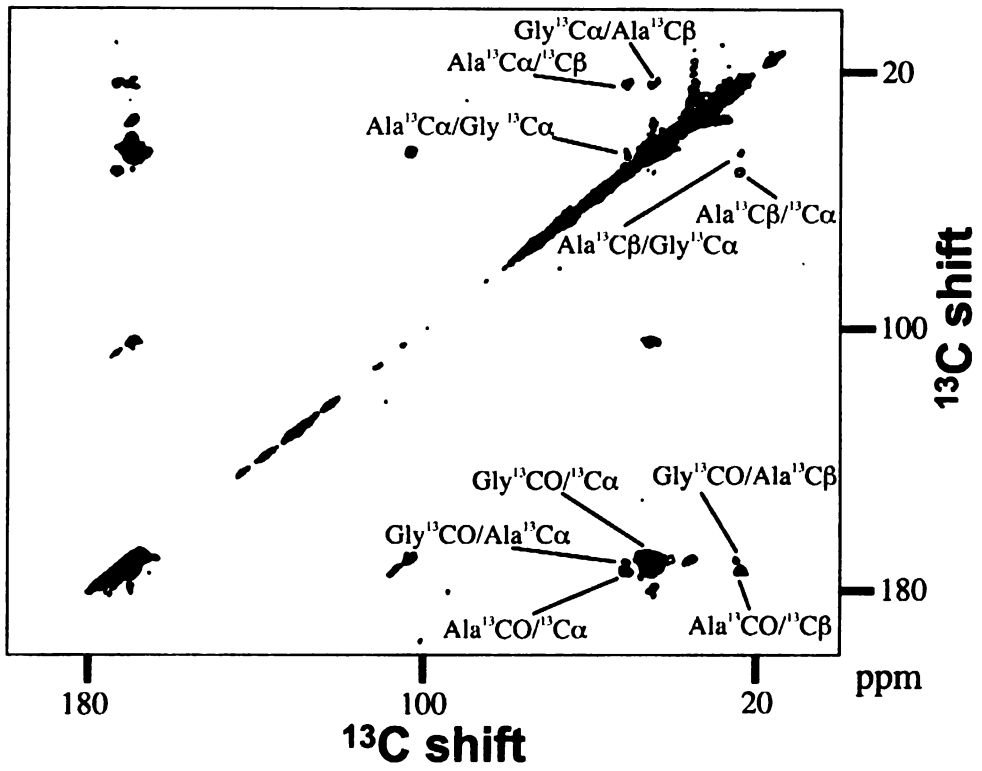

Figure 42. 2D ^{13}C- ^{13}C contour plot spectrum of HFP Dimer D associated with hydrated LM3. The peptide to lipid molar ratio was ~0.04 with ~ 0.8 mmol HFP Dimer D. The buffer was at pH 7.0, and the sample volume in the 4 mm rotor was ~30 ml. This data was collected with proton-driven spin diffusion with a 1 s exchange time and total signal averaging time of ~114 hrs. The MAS frequency was 6.8 kHz. The spectrum was processed with 100 Hz Gaussian line broadening in each dimension.

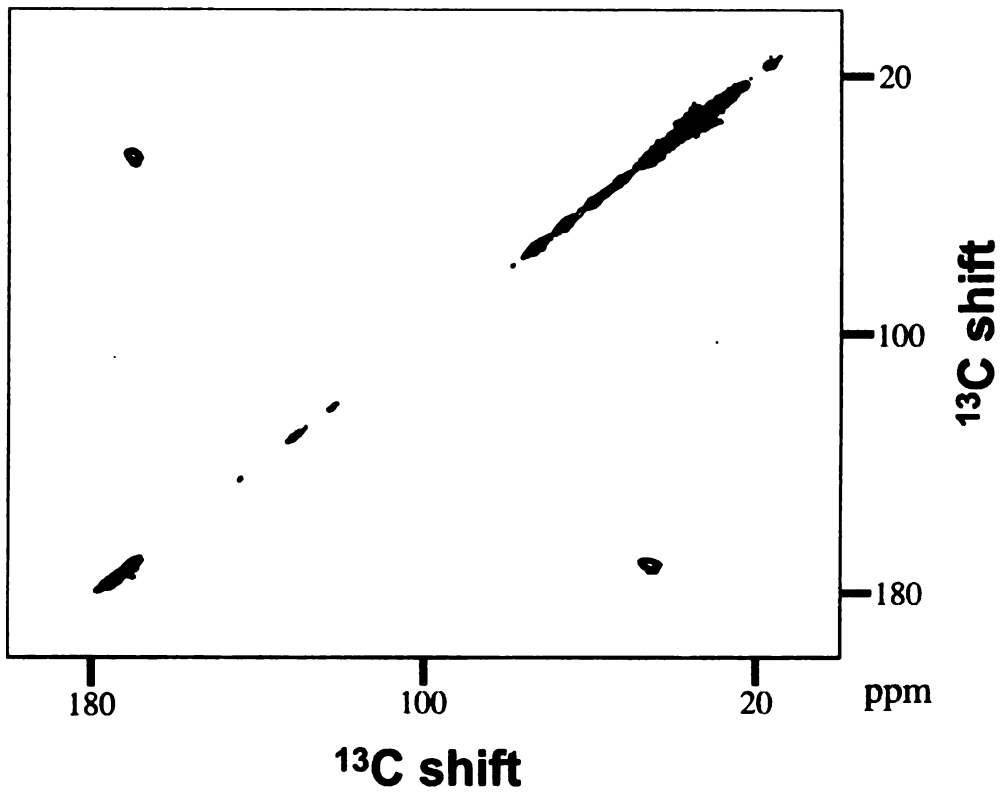

Figure 43. 2D ^{13}C- ^{13}C contour plot spectrum of HFP Dimer E associated with hydrated LM3. The peptide to lipid molar ratio was ~0.04 with ~ 0.8 mmol HFP Dimer E. The buffer was at pH 7.0, and the sample volume in the 4 mm rotor was ~30 ml. Data were collected with proton-driven spin diffusion with a 1 s exchange time and total signal averaging time of ~114 hrs. The MAS frequency was 6.8 kHz. The spectrum was processed with 100 Hz Gaussian line broadening in each dimension.

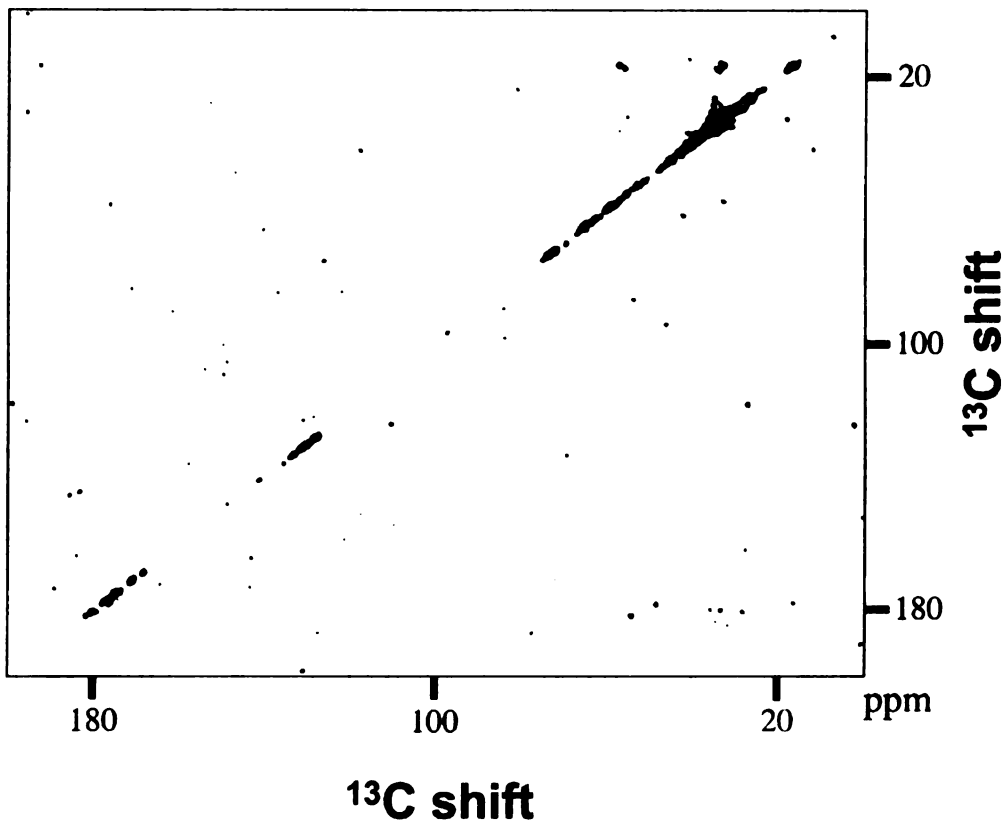

Figure 44. 2D ^{13}C- ^{13}C contour plot spectrum of hydrated LM3 lipids. Data were collected with proton-driven spin diffusion with a 1 s exchange time and total signal averaging time of ~114 hrs. The MAS frequency was 6.8 kHz. The spectrum was processed with 100 Hz Gaussian line broadening in each dimension.

crosspeaks in the Dimer D sample are due to the peptide and are not due to the lipid or cholesterol.

The crosspeaks observed in Dimer D suggest that the two residues are no more than 6 angstroms apart. The distance down the backbone from Ala-6 ^{13}CO to Gly-10 $^{13}C\alpha$ was ~ 13.2 angstroms which was out of the range of this experiment. Using the distance constraints of the experiment, the only way these two residues can be within 6 angstroms of one another was if the β strands are arranged in an anti-parallel manner (Figure 45).

Conclusions

The use of selective uniform labeling has been successful in the unambiguous assignment of all ^{13}C in residues 1-16 and residue 21. SUL required more samples because only one residue of each amino acid type was labeled and also took more spectrometer time but resulted in an unambiguous chemical shift assignment. The alternative in the past has been only labeling one ^{13}C per sample, which in a peptide of this length would not be reasonable to gain a complete ^{13}C chemical shift assignment. Chemical shift differences between the experimental chemical shifts and the known values for both helical and β-strand conformations showed a better agreement with β–strand conformation. TALOS was used to calculate the ψ and ϕ angles, which also show agreement for the β-strand conformation. Crosspeaks observed in the Dimer D sample at long exchange time gave insight into strand arrangement. Using the crosspeaks from the Dimer D sample an anti-parallel strand arrangement was determined to be the most reasonable explanation of the data.

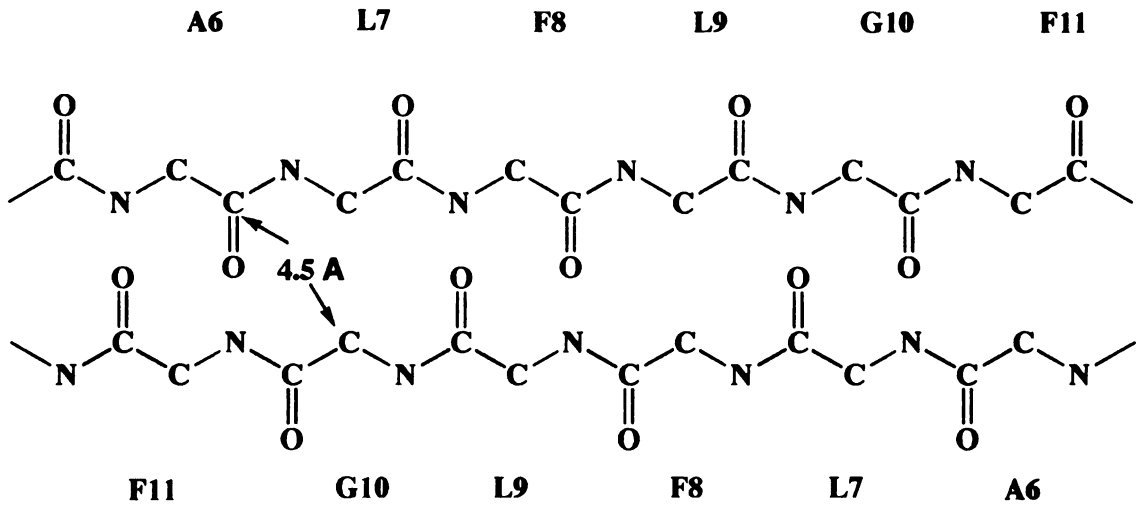

Figure 45 Anti-parallel strand arrangement for HFP.

References

1. Petkova, A.T., et al., *A structural model for Alzheimer's beta-amyloid fibrils based on experimental constraints from solid state NMR.* Proceedings of the National Academy of Sciences of the United States of America, 2002. **99**(26): p. 16742-16747.

2. Cornilescu, G., F. Delaglio, and A. Bax, *Protein backbone angle restraints from searching a database for chemical shift and sequence homology.* J Biomol NMR, 1999. **13**(3): p. 289-302.

3. Yang, R., *Synthesis, Enhanced Fusogenicity, and Solid State NMR Measurements of Oligomeric HIV-1 Fusion Peptide Constructs*, in *Department of Chemistry.* 2005, Michigan State University: East Lansing. p. 158.

4. Zhang, H.Y., S. Neal, and D.S. Wishart, *RefDB: A database of uniformly referenced protein chemical shifts.* Journal of Biomolecular Nmr, 2003. **25**(3): p. 173-195.

5. Yang, J., C.M. Gabrys, and D.P. Weliky, *Solid-State Nuclear Magnetic Resonance Evidence for an Extended beta Strand Conformation of the Membrane-Bound HIV-1 Fusion Peptide.* Biochemistry, 2001. **40**(27): p. 8126-37.

6. Petkova, A.T., W.-M. Yau, and R. Tycko, *Experimental Constraints on Quaternary Structure in Alzheimer's Beta-Amyloid Fibrils.* Biochemistry, 2006. **45**(2): p. 498-512.

Chapter 6

2D Influenza Fusion Peptide Studies

Introduction

Understanding the structure of the fusion peptide in the membrane will help to solve the viral fusion problem. A better understanding of the mechanism of viral fusion can lead to therapeutic treatments designed to inhibit viral fusion. Viral fusion in influenza is induced by a simple change in pH rather than binding to a host cell, and thus influenza has served as the most studied system for fusion research. Studies of pH-dependent influenza fusion and fusion protein structures probe the relationship between structure and function.

A crystal structure of the low-pH activated HA_2 domain exists for residues 34-176, but atomic resolution structural data for the membrane-bound form of the N-terminus fusion peptide of HA_2 is absent.[1, 2] The insertion angle of the peptide has also been studied by FTIR and the peptide has been reported to insert at various angles ranging from parallel to oblique relative to the membrane normal, depending upon the sample and sample preparation conditions.[3] ATR-FTIR of the fusion peptide, and of fusion-active fusion peptide analogues, in both hydrated and dry egg phosphatidylcholine membranes at neutral and acidic pH, have shown insertion angles between 45 and 70 degrees relative to the membrane normal.[4-6] Circular Dichroism spectroscopy has suggested that the influenza fusion peptide is inserted into micelles predominately as a helix at the pH of fusion.[7] A solution NMR structure of the fusion peptide in both sodium dodecyl sulfate (SDS) and DPC micelles has been determined, and shows

predominately helical structure.[8, 9] There is also evidence for helical structure for the fusion peptide in lipid vesicles.[10] EPR studies revealed a helical structure with a maximum insertion depth of 15 angstroms from the lipid phosphate group and a helix tilt angle of ~65° from the membrane normal at both neutral and acidic pH.[11]

Sedimentation Equilibrium

Figure 46 displays the results of the sedimentation equilibrium experiment at 20 °C for the IFP-U10 sample with a concentration of 50 μM in 5 mM HEPES/ 10 mM MES buffer at pH 7. The rotor speed was 48000 rpm. The top panel shows that the difference between the experimental and fitted absorbance were small (< 0.02) and random as a function of r, which indicates that a single-species model is reasonable. The bottom panel displays the 280 nm absorbance as a function of centrifugal radius with a partial specific volume of 0.7928 ml/g and a solvent density of 1.0 g/ml. The optimal fit of the data was determined by a non-linear least squared method with a molecular weight of ~ 5200 g/mol. This molecular weight is nearly double the monomeric molecular weight of 2739 g/mol. A molecular weight of 5200 suggests that the IFP-U10 fusion peptide is not monomeric is solution but could be a small oligomer. A lower than expected absorbance was observed on the bottom panel of figure 46. The expected absorbance using Beer's Law was 0.3, but the observed absorbance was 0.12 which was ~ a third less than expected. This phenomenon could be explained by pelleting of some of the sample.

The same sedimentation equilibrium experiment was also performed with the same parameters except that the pH was dropped to 5 (data not shown). No reasonable

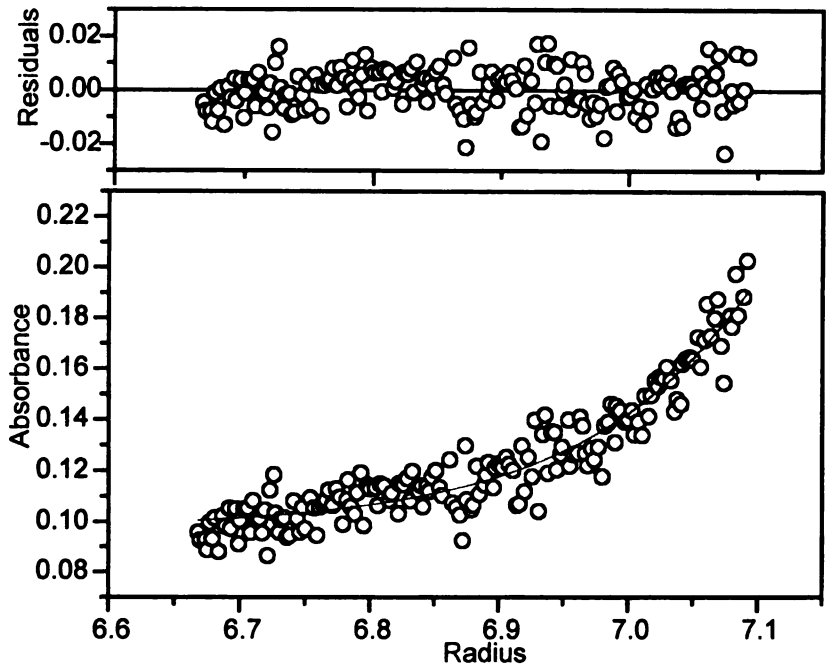

Figure 46. Sedimentation equilibrium experiments of 50 μM IFP-U10. The main panel shows the absorbance at 280 nm as a function of the centrifugal radius after reaching equilibrium. The best fit to the model for a single species was obtained with a molecular weight of ~ 5198 g/mol which is shown as a solid line through the experimental data. The upper panel shows the residuals between the data and the fit.

absorbance was observed due to the sample pelleting. Peptide pelleting was evidence of large oligomers for IFP-U10 fusion peptide.

At pH 7.4 the peptide was dimeric, but when the pH is lowered to 5.0 large oligomers were observed. This suggests that the large oligomers are necessary for fusion to occur.

2D Correlation Spectra

Figure 47a displays a 2D ^{13}C-^{13}C correlation spectrum of IFP-U10 associated with PC/PG membranes. Spectral overlap was such that only residue-type assignment was possible as listed in Table 5.

As displayed in Figure 47b, three Gly $^{13}C\alpha/^{13}CO$ crosspeaks are observed. Peak A has $^{13}C\alpha$ and ^{13}CO shifts closer to those expected in helical conformation, peak B has $^{13}C\alpha$ and ^{13}CO shifts closer to those expected in β strand conformation, and peak C has a $^{13}C\alpha$ shift closer to helical conformation and a ^{13}CO shift closer to β strand conformation. The ratio of intensities of crosspeaks A:B:C is ~ 2:1:1. For Ala, there are two $^{13}C\alpha/^{13}CO$ (cf. Fig 47b), two $^{13}C\beta/^{13}C\alpha$, and two $^{13}CO/^{13}C\beta$ crosspeaks. For each set of crosspeaks, one correlates with helical conformation and the other correlates better with β strand conformation. The ratio between the two sets of crosspeaks helical: β stand was ~ 4. For the Ile, Leu, and Phe residues, only one crosspeak for each correlation type (e.g. $^{13}C\alpha/^{13}CO$) was clearly detected. More definitive (beyond residue-type) assignment was not obtained from analysis of the ^{13}C–^{13}C spectrum with τ= 100 ms because of overlap between interresidue crosspeaks.

The presence of multiple Gly $^{13}CO/^{13}C\alpha$ crosspeaks and similar multiple Ala crosspeaks in spectra of the IFP-U10 sample suggest that there are multiple

a

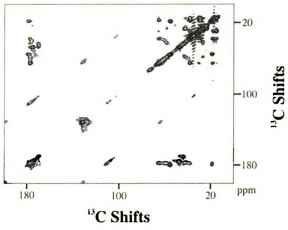

b

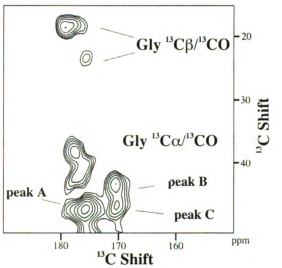

Figure 47. 2D ^{13}C-^{13}C contour plot spectrum of IFP-U10 associated with PC/PG membranes. The peptide:lipid mol ratio was ~0.02, the sample pH was 5.0, and the sample volume in the 4 mm rotor was ~30 µl with ~0.4 µmol of IFP-U10. The data were collected with proton-driven spin diffusion with a 10 ms exchange time and total signal averaging time of ~3 days. The MAS frequency was 6.8 kHz. Spectra were processed with 150 Hz Gaussian line broadening in each dimension.

conformations and are consistent with IR spectra indicating populations of helical and β strand structure in PC/PG-associated IFPs. The Gly $^{13}CO/^{13}C\alpha$ "peak C" in Figure 47b is particularly intriguing because the $^{13}C\alpha$ shift is more characteristic of helical conformation while the ^{13}CO shift is more characteristic of β strand conformation. Studies on scatter-uniform labeled samples will be necessary to distinguish whether peak C is due to a single Gly residue or is diagnostic of a particular conformation at multiple Gly residues.

Previous work on selectively Leu-2 ^{13}CO/Phe-3 ^{15}N labeled IFP associated with PC/PG membranes yielded a Leu-2 ^{13}CO shift of 177.7 ppm.[12] This is close to the 177.5 ppm shift determined from analysis of the Figure 47 spectra and provides evidence that the spectrum was assigned correctly.

Figure 48 displays 2D NCO (left) and NCA (right) correlation spectra of the IFP-U10 sample. In the NCO spectrum, there are distinct crosspeaks with ^{13}CO shifts at 177.9 and 176.0 ppm and respective ^{15}N shifts of 119.4 and 123.5 ppm. Using ^{13}CO shifts derived from the ^{13}C-^{13}C spectra and knowledge that Gly ^{15}N shifts are in the 100-115 ppm range, it appears that the L2/F3, I6/A7, and F9/I10 sequential pairs could contribute to the first crosspeak and that the G1/L2, G4/A5, and G8/F9 sequential pairs could contribute to the second crosspeak. In the NCA spectrum, there are two crosspeaks with $^{13}C\alpha$ shifts of 55.1 ppm and 47.1 ppm and corresponding ^{15}N shifts of 121.3 ppm and 105.5 ppm. Using $^{13}C\alpha$ shifts derived from the ^{13}C-^{13}C spectra and knowledge of Gly ^{15}N shifts, the most reasonable assignment of the crosspeaks are Ala and Gly, respectively. In Table 5, the ^{13}C shifts were derived from analysis of the ^{13}C-^{13}C spectra and the Gly and Ala ^{15}N shifts were obtained from the analysis of the NCA spectrum. In addition to

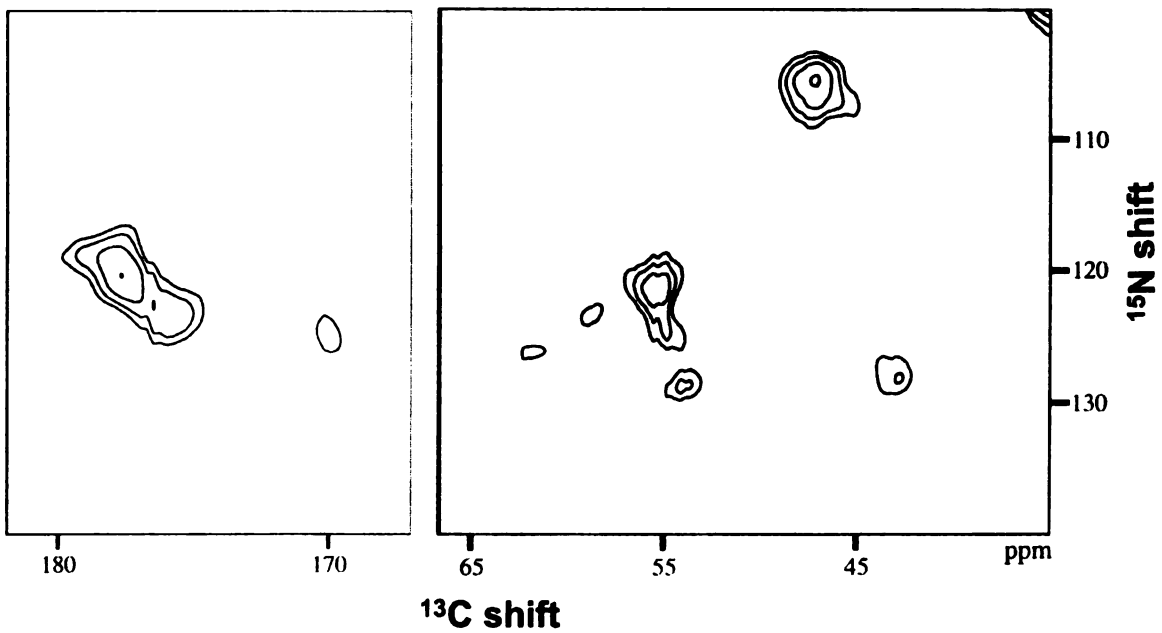

Figure 48. 2D NCO (left) and NCA (right) spectra of IFP-U10 associated with PC/PG membranes using the same sample as in Figure 7. The MAS frequency was 7 kHz. Signal averaging times were ~10 and ~4 days for NCO and NCA spectra, respectively. Both spectra were processed using 100 Hz Gaussian line broadening in the ^{15}N dimension and 150 Hz Gaussian line broadening in the ^{13}C dimension.

Table 5. ^{13}C and ^{15}N chemical shift assignments for IFP-U10 associated with PC/PG.

	Cα	Cβ	Cγ	Cδ	Cε	C_{ring}	CO	N
Ala	55.4	18.5					179.6	121.3
	51.6	22.9					175.3	
Phe	61.0	39.1				131.2	178.2	126.2
Ile	65.5	38.1	29.8	14.7	17.8		178.3	
Leu-2	58.5	42.5	26.8	15.5			177.9	123.5
Gly	47.4						176.4	105.5
	43.6						170.4	
	47.1						170.4	105.5

resonance overlap, the IFP-U10 NCO and NCA spectra have low signal-to-noise. It was not possible to make other definitive ^{15}N shift assignments including the ^{15}N shifts which correlate with the minor population β strand ^{13}C shifts.

Figure 49 displays differences between the experimental ^{13}C shifts of the dominant crosspeaks in the IFP-U10 sample and characteristic helical or β strand ^{13}C shifts. There is better agreement with the helical shifts. The assignments of the ^{13}C-^{13}C 10 ms PDSD spectra of the three samples are complete in the sense that all of the defined (i.e. reasonably resolved and signal clearly above the noise) crosspeaks are assigned.

The chemical-shift-based dominant β strand conformation in the HFP samples and helical conformation in the IFP-U10 sample are consistent with previous SSNMR spectra of selectively labeled HFPs and IFPs as well as IR and ESR spectra of the FPs. The earlier SSNMR studies additionally suggest that the absence or presence of cholesterol in the membrane correlates with formation of helical or β strand conformation, respectively. FP-induced fusion activity is observed for vesicles of either composition and suggests that both peptide conformations are fusogenic.

Conclusions

2D correlation spectra of the IFP-U10/ PC/PG sample were used to determine the secondary structure over the ten uniformly labeled residues in the peptide chain. 10 ms and 100ms PDSD sequence was used to determine the chemical shift of each labeled carbon in the sequence. The chemical shift assignment was only a residue-type chemical shift assignment. Experimentally determined chemical shifts were compared to known shifts for helical and β strand conformations. All of the dominant peaks of the labeled residues were closer in chemical shift to the helical structure. Gly and Ala residues

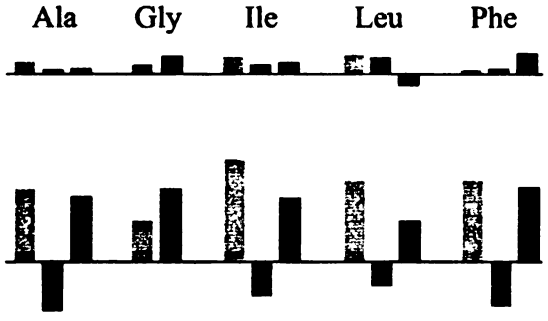

Figure 49. Differences between dominant experimental ^{13}C chemical shifts and characteristic helical (top) or β strand (bottom) ^{13}C shifts for IFP-U10 associated with PC/PG. The light grey, medium grey, and black bars are for C_α, C_β, and CO nuclei, respectively. The vertical scale is 10 ppm/inch. The horizontal lines represent 0 ppm shift difference. There appears to be better agreement with helical shifts.

exhibited both helical and β strand structure, which suggests that there are multiple conformations. Scatter uniform labeling of the peptide sequence would be useful in gaining a residue specific assignment.

References

1. Wilson, I.A., J.J. Skehel, and D.C. Wiley, *Structure of the haemagglutinin membrane glycoprotein of influenza virus at 3 A resolution.* Nature, 1981. 289(5796): p. 366-73.

2. Chen, J., J.J. Skehel, and D.C. Wiley, *N- and C-terminal residues combine in the fusion-pH influenza hemagglutinin HA(2) subunit to form an N cap that terminates the triple-stranded coiled coil.* Proc Natl Acad Sci U S A, 1999. 96(16): p. 8967-72.

3. Gray, C., et al., *Effect of the N-Ternal Glycine on the Secondary Structure, Orientation, and Interaction of the Influenza Hemagglutinin Fusion Peptide with Lipid Bilayers.* BioPhysical Journal, 1996. 70: p. 2275-86.

4. Ishiguro, R., N. Kimura, and S. Takahashi, *Orientation of Fusion-Active Synthetic Peptides in Phospholipid Bilayers: Determination by Fourier Transform Infrared Spectroscopy.* Biochemistry, 1993. 32: p. 9792-97.

5. Ishiguro, R., M. Matsumoto, and S. Takahashi, *Fusogenic Synthetic Peptide with Phospholipid Bilayers: Orientation of the Peptide alpha-Helix and Binding Isoherm.* Biochemistry, 1996. 35: p. 4976-83.

6. Lunenberg, J., et al., *Structure and Topology of the Influenza Virus Fusion Peptide in Lipid Bilayers.* The Journal of Biological Chemistry, 1995. 270(46): p. 27606-14.

7. Chang, D.-K., et al., *The Aminio-terminal Region of the Fusion Peptide of Influenza Virus hemagglutinin HA2 Inserts into Sodium Dodecl Sulfate Micelle with Residues 16-18 at the Aqueous Boundary at Acidic pH.* The Journal of Biological Chemistry, 2000. 275(25): p. 19150-58.

8. Han, X., et al., *Membrane structure and fusion-triggering conformational change of the fusion domain from influenza hemagglutinin.* Nat Struct Biol, 2001. 8(8): p. 715-20.

9. Tamm, L.K., et al., *Strucuture, Dynamics and Function of the outer Membrane Protein A (OmpA) and influenza Hemagglutinin Fusion Domain in Detergent Micelles by Solution NMR.* FEBS Lett, 2003. 555: p. 139-43.

10. Han, X. and L.K. Tamm, *A host-guest system to study structure-function relationships of membrane fusion peptides.* Proceedings of the National Academy of Sciences of the United States of America, 2000. 97(24): p. 13097-13102.

11. Macosko, J.C., C.H. Kim, and Y.K. Shin, *The membrane topology of the fusion peptide region of influenza hemagglutinin determined by spin-labeling EPR.* J Mol Biol, 1997. 267(5): p. 1139-48.

12. Wasniewski, C.M., Parkanzky, Paul D., Bodner, Michele L., Weliky, David P., *Solid-state nuclear magnetic resonance studies of HIV and influenza fusion peptide orientations in membrane bilayers using stacked glass plate samples.* Chemistry and Physics of Lipids, 2004. 132: p. 89-100.

Chapter 7

Summary

1D NMR HIV Fusion Peptides

The REDOR filtering technique proved to be extremely useful in removing the natural abundance signal from the lipids in the sample as well as the unlabeled residues. This technique was also helpful in assessing linewidths and the feasibility of completing a full assignment using 2D methods. HFP-U3 shifts were observed using REDOR filter in both DPC and LM3. It was shown using known correlations between chemical shifts and secondary structure that the peptide is helical in DPC and non-helical in LM3.

Viral/target cell membrane fusion occurs at 37 °C, but for membrane-associated HIV-FP samples, the signal-to-noise per peptide ^{13}C per transient is about three times higher at –50 °C. In order to take advantage of the higher signal to noise at low temperatures, it is important to demonstrate the biological relevance of the cold samples and to therefore investigate whether cooling changes the peptide structure. The chemical shifts are similar at 20 °C and at –50 °C, which suggest that cooling does not change the average peptide structure. The temperature dependence of intensities and linewidths do suggest that motion at 20 °C is attenuated at –50 °C, which is a physically reasonable result for hydrated membrane samples.

2D NMR HIV Fusion Peptide

2D $^{13}C/^{13}C$ and $^{13}C/^{15}N$ correlation spectra of the HFP-U3/LM3 sample were used to give insight into the secondary structure over the three uniformly labeled residues in the peptide chain. The chemical shifts were determined using a number of sequences

including: PDSD, RFDR, NCA, NCO. The differences between the measured ^{13}C shifts and the known shifts for characteristic helix and β strand were used to determine the secondary structure. The differences between the shifts were smallest for the β strand structure, which suggests that the structure over the labeled residues is β strand.

2D $^{13}C/^{13}C$ and $^{13}C/^{15}N$ correlation spectra of the HFP-U12 dimer associated with LM3 showed that only a residue type chemical shift assignment could be made at 400 MHz. The measured chemical shifts were subtracted from the known shifts for helix and β strand and smaller differences were observed for β-strand values. Spectra could be better resolved at higher field because of the narrower resonances arising from attenuation of the ^{13}C-^{13}C J- and dipolar couplings. This phenomenon has been shown using the HFP-U3 sample at 700 MHz where the linewidths were narrower by a factor of ~ 0.6. In addition, sensitivity should be improved at higher field and will be beneficial for sequential assignment based on 3D experiments.

The use of scatter uniform labeling has been successful in the unambiguous assignment of all ^{13}C in residues 1-16 and residue 21. SUL required more samples because only one residue of each amino acid type was labeled and also took more spectrometer time but resulted in an unambiguous chemical shift assignment. The alternative in the past has been only labeling one ^{13}C per sample, which in a peptide of this length would not be reasonable to gain a complete ^{13}C chemical shift assignment. Chemical shift differences between the experimental chemical shifts and the known values for both helical and β-strand conformations showed a better agreement with β–strand conformation. TALOS was used to calculate the ψ and ϕ angles, which also show agreement for the β-strand conformation. Crosspeaks observed in the Dimer D

sample at long exchange time gave insight into strand arrangement. Using the crosspeaks from the Dimer D sample an anti-parallel strand arrangement was determined to be the most reasonable explanation of the data.

IFP Fusion Peptide

2D correlation spectra of the IFP-U10/ PC/PG sample were used to determine the secondary structure over the ten uniformly labeled residues in the peptide chain. 10 ms and 100ms PDSD sequence was used to determine the chemical shift of each labeled carbon in the sequence. The chemical shift assignment was only a residue-type chemical shift assignment. Experimentally determined chemical shifts were compared to known shifts for helical and β strand conformations. All of the dominant peaks of the labeled residues were closer in chemical shift to the helical structure. Gly and Ala residues exhibited both helical and β strand structure, which suggests that there are multiple conformations. Scatter uniform labeling of the peptide sequence would be useful in gaining a residue specific assignment.

Appendix I

Figure 12.

Top: mb4b/data/setup/U-N-Acetyl-Leu/HNC-Calpha-11403

Middle: mb4b/data/setup/U-N-Acetyl-Leu/HNC-CO-11203

Bottom: mb4b/data/setup/U-N-Acetyl-Leu/Ccp-aftersetup-102903

Figure 14. mb4b/data/Lipid_Samples/redor3

Figure 15. mb4b/data/Dimer/UFP-dimer-redor-5103

Figure 16.

Top: mb4b/data/DPC/DPC-U-F8-L9-G10-1002-sum

Bottom: mb4b/data/Lipid_Samples/redor3

Figure17.

Top: mb4b/data/Lipid_Samples/redor3

Bottom: mb4b/data/Lipid_samples/redor6

Figure 18.

Original data: mb4b/data/2D-data/2D-CC/UFP-10mssd-full

Processed data: mb4b/data/2D-data/2D-CC/UFP-10mssd-full

Figure 19.

Original data: mb4c/data/2D-data/combine-RFDR

Processed data: mb4c/2Dprocessing/HFPU3/rfdr.ft2

Figure 20.

Original data: mb4b/data/2D-data/2D-CC/UFP-100ms-6800Hz

Processed data: mb4b/data/2D-data/2D-CC/UFP-100ms-6800Hz

Figure 21.

Left.

Original data: mb4c/data/HFPU3/HNC-HFPU3-CO-sum-9504

Processed data: mb4c/2Dprocessing/HNC-HFPU3-CO-rf.ft2

Right

Original data: mb4c/data/HFPU3/HNC-HFPU3-Ca-sum3-101004

Processed data: mb4c/2Dprocessing/HNC-HFPU3-Ca-rf.ft2

Figure 23.

Original data: mb4b/data/Dimer/Dimer-10mssd-full-51103

Processed data: mb4b/data/Dimer/Dimer-10mssd-full-51103

Figure 24.

Original data: mb4b/data/Dimer/Dimer-rfdr-full-51403

Processed data: mb4c/2Dprocessing/HFPU12/dimerrfdr.ft2

Figure 25.

Left.

Original data: mb4c/data/HFPU12/HNC-HFPU12-CO-sum4-93004

Processed data: mb4c/2Dprocessing/HNC-HFPU12-CO-rf.ft2

Right.

Original data: mb4c/data/HFPU12/HNC-HFPU12-Ca-sum3-101104

Processed data: mb4c/2Dproccessing/HNC-HFPU12-Ca-rf.ft2

Figure 27.

Left

Original data: mb4b/data/2D-data/2D-CC/UFP-100ms-6800Hz

Processed data: mb4b/data/2D-data/2D-CC/UFP-100ms-6800Hz

Right

Original data: mb4b/700data/weliky.SV/33

Processed data: mb4b/data/2D-data/2D-CC/UFP-100ms-6800Hz

Figure 29.

Original data: mb4b/data/New-HFP-Dimer/DimerA-LM3-10ms-7605

Processed data: mb4c/2Dprocessing/DimerA-LM3.ft2

Figure 30.

Original data: mb4b/data/New-HFP-Dimer/DimerA-LM3-100ms-7905

Processed data: mb4c/2Dprocessing/DimerA-LM3-100ms.ft2

Figure 31.

Original data: mb4b/data/New-HFP-Dimer/DimerB-LM3-10ms-71205

Processed data: mb4c/2Dprocessing/DimerB-LM3-10ms.ft2

Figure 32.

Original data: mb4b/data/New-HFP-Dimer/DimerB-LM3-100ms-71505

Processed data: mb4c/2Dprocessing/DimerB-LM3-100ms.ft2

Figure 33.

Original data: mb4b/data/New-HFP-Dimer/DimerC/HFP-DimerC-LM3-52605

mb4b/data/New-HFP-Dimer/DimerC/HFP-DimerC-LM3-2-52605

Processed data: mb4c/2Dprocessing/DimerC-LM3-sum.ft2

Figure 34.

Original data: mb4b/data/DimerD2-12905

Processed data: mb4c/2Dprocessing/DimerD2-10ms.ft2

Figure 35.

Original data: mb4c/data/DimerE2-10ms-sum-2

Processed data: mb4c/2Dprocessing/DimerE2-10ms-sum-2.ft2

Figure 37.

Original data: mb4c/data/NAL-10msPDSD-8905

Processed data: mb4c/2Dprocessing/NAL-10ms-8905-ft2

Figure 38.

Original data: mb4b/data/New-HFP-Dimer/DimerC/DimerC-500ms-LM3-61705

Processed data: mb4c/2Dprocessing/DimerC-500ms-ft2

Figure 39.

Original data: mb4c/data/DimerA-1s-sum

Processed data: mb4c/2Dprocessing/DimerA-1s-sum.ft2

Figure 40.

Original data: mb4c/data/DimerB-1s-sum

Processed data: mb4c/data/DimerB-1s-sum.ft2

Figure 41.

Original data: mb4c/data/DimerC-1s-sum

Processed data: mb4c/2Dprocessing/DimerC-1s-sum.ft2

Figure 42.

Original data: mb4c/data/DimerD2-1s-sum

Processed data: mb4c/2Dprocessing/DimerD2-1s-sum.ft2

Figure 43.

Original data: mb4c/data/DimerE2-1s-sum-2

Processed data: mb4c/2Dprocessing/DimerE2-1s-sum-2.ft2

Figure 44.

Original data: mb4c/data/LM3-sum-1306

Processed data: mb4c/2Dprocessing/LM3-1s-sum.ft2

Figure 45.

Original data: mb4c/data/IFPU10/IFPU10-10ms-sum3-8204

Processed data; mb4c/2Dprocessing/IFPU10-10ms-rf.ft2

Figure 46.

Left.

Original data: mb4c/data/IFPU10/HNC-IFPU10-CO-sum3-9204

Processed data: mb4c/2Dprocessing/HNC-IFPU10-CO-rf-ft2

Right.

Original data: mb4c/data/IFPU10/HNC-IFPU10-Ca-sum7-102404

Processed data: mb4c/2Dprocessing/HNC-IFPU10-Ca-rf.ft2

Appendix II

Figure 7. mb4b/pulse_programs/cpc/cp_ramp

Figure 8. mb4b/pulse_programs/cpc/REDOR_pm_mod

Figure 9. mb4b/pulse_programs/cpc/2Dexchmas_mod

mb4b/macros_acq/run2Dexchmas_mod

mb4c/2Dprocessing/conv.upf and xform.ufp

Figure 10. mb4b/pulse_programs/cpc/2Dexchmas_mod

acquisition macro: run2Dexchmas_mod

processing macros: conv.upf and xform.ufp

Figure 11. mb4b/pulse_programs/cpc/2Dcp3resmod_ramp

Figure 13. mb4b/pulse_programs/cpc/spcpf

mb4b/macros_acq/HNC1

mb4c/2Dprocessing/conv.ufp and xform.ufp